Methods for Control of Liquid Slosh

Grundelius, Mattias

2001

Document Version:
Publisher's PDF, also known as Version of record

Methods for Control of Liquid Slosh

Methods for Control of Liquid Slosh

Mattias Grundelius

Lund 2001

Till Andrea

Department of Automatic Control
Lund Institute of Technology
Box 118
SE-221 00 LUND
Sweden

ISSN 0280–5316
ISRN LUTFD2/TFRT--1062--SE

Printed in Sweden by Bloms i Lund Tryckeri AB.
Lund 2001

Contents

Acknowledgments

I would like to thank colleagues, family and friends for all the help and support I have received during this work. In particular, I would like to thank my supervisors Bo Bernhardsson and Tore Hägglund for valuable input and suggestions as well as constructive criticism, Anders Robertsson for proof reading the manuscript and for his hospitality when I arrived to Lund in 1991, Rolf Braun for his help with the equipment, Leif Andersson and Anders Blomdell for excellent computer support. I also would like to thank Bo Hellberg, Istvan Ulvros and Anders Sundberg at Tetra Pak Research & Development AB for their insight into the practical problems and their comments on my work.

This work has been supported financially by the Swedish National Board for Industrial and Technical development (NUTEK) and the Swedish Agency for Innovation Systems (VINNOVA). The experimental equipment have been supplied by Tetra Pak Research & Development AB, Lund. The support is gratefully acknowledged.

Finally I would like to express my most sincere thanks to my beloved wife Andrea for everything.

Mattias

1

Introduction

This thesis considers a control problem common in industrial packaging machines for fluids. The problem is to move a package filled with liquid from one position to another which is a key operation in the packaging machine. It is essential that such operations can be performed fast and in a well controlled manner.

Acceleration of the package induces motion in the liquid within the package. This is referred to as liquid slosh or liquid vibration. Liquid sloshing is a key factor in the movement problem. It is necessary to perform the movement such that the liquid does not splash out of the package and contaminate the machine or on the sealing areas of the package.

Motion induced sloshing is a classical problem in control theory. It was first encountered in control of guided missiles in the aerospace industry. In this application it was found that sloshing in the fuel tanks could result in instabilities. Similar problems have also been encountered in control of airplanes, see [Graham and Rodriguez, 1952], [Crawley *et al.*, 1989] and [Bryson, 1994]. Liquid sloshing is also a severe problem when transporting liquids both on sea and on land, see [Armenio, 1992] or [Sankar *et al.*, 1992]. Motion of liquid in large storage tanks induced by earthquakes and different methods to dampen the oscillations are given in [Venugopal and Bernstein, 1996].

Lately, movement of open containers containing fluid, e.g. molten metal and various beverages, has been investigated. The main goal is then to move the container as fast as possible without too much slosh, see [Feddema *et al.*, 1997], [Dietze and Schmidt, 1997], [Yano *et al.*, 1999] and [Dubois *et al.*, 1999].

More details are given in this introductory chapter which is organized as follows. In Section 1.1 the operation of the packaging machine is described. Section 1.2 presents the problem formulation considered in this thesis. The motivation for studying this problem is given is Section 1.3. An outline of the thesis is given in Section 1.4.

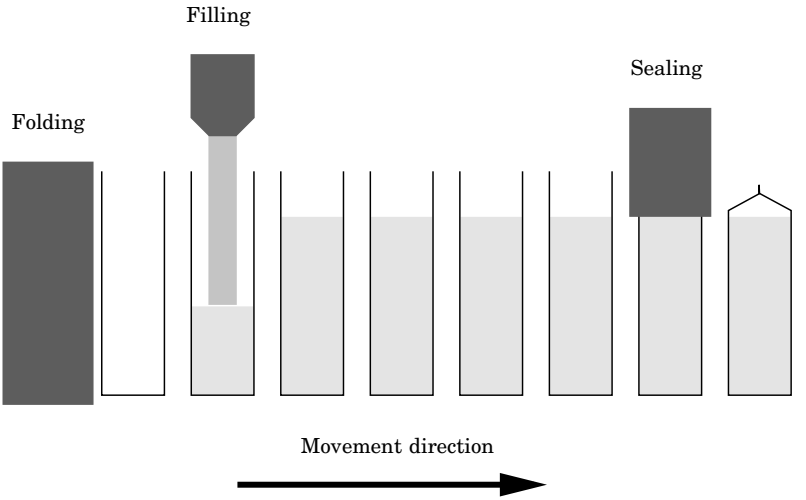

Figure 1.1 Schematic picture of the packaging machine.

1.1 The packaging machine

There exist a large variety of packages machines where the packages are moved horizontally or vertically, along straight or curved paths and in continuous or stepwise operation. The packaging machine studied operates stepwise and the packages are moved horizontally along a straight path.

The operation of a packaging machine studied in this work can be divided into three independent subtasks: folding, filling and sealing. These tasks are performed simultaneously on three packages. A schematic picture of a packaging machine is shown in Figure 1.1.

The folded carton package is placed in a holder which carries the package through the machine. The movement of the package is performed stepwise between the subtasks. The same movement is applied in every step simultaneously on all packages in the machine. The production capacity of the machine is determined by the filling time, which is the slowest of the sub tasks, and the time needed to move the package one step.

The movement of the packages is controlled by a servo system which controls the positions of the packages. A block diagram of the motion control system is shown in Figure 1.2. The movement is specified by the desired acceleration of the package. The desired acceleration is integrated to generate velocity and position references. The positions of the packages are measured using a resolver or encoder.

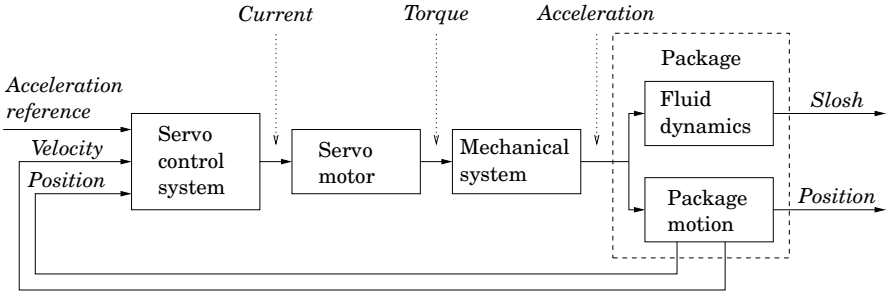

Figure 1.2 Block diagram of the motion control system.

The package contains liquid when it is moved after the filling station. The motion of the package induces motion of the liquid within the package. This is referred to as slosh. The amount of slosh depends on how the package is accelerated and the properties of the liquid. There is for example a large difference between milk and yoghurt.

The machine construction is very stiff and the mass of the liquid is small compared to the rest of the moving parts. Therefore the motion of the liquid does not affect the motion of the packages. If the servo system is well tuned the actual acceleration of the package is very close to the desired acceleration.

1.2 Problem formulation

The aim is to increase the production capacity of the packaging machine. This can be done by either decreasing the filling time and/or the movement time. This thesis considers the problem of decreasing the movement time. The filling time and the movement time is about the same so a 10% decrease in movement time increases the production rate with 5%. Since there is no measurement of the slosh in the packaging machine, open-loop control through the acceleration reference is the only possibility to control the slosh.

The problem is to find an acceleration reference that moves the package a certain distance as fast as possible taking all constraints into consideration. The velocity of the package should be zero in the beginning and in the end of the movement. The major constraint in this problem is the liquid slosh. If there is too much slosh the liquid might contaminate the packaging machine or the sealing areas of the package. If the sealing areas are contaminated the package might not be properly sealed and

possible not airtight.

When the packages are moved, the same acceleration reference is applied at each step. Therefore, the acceleration reference must be such that the slosh constraint is not violated if it is repeated. One way to achieve this is to ensure that the liquid is in the same state at the beginning of each step. The natural choice of initial state is that the liquid is at rest, since this is approximately the state after the package has been filled.

1.3 Motivation

The main motivation for our work is that faster movement results in higher production capacity, and hence decreases the production cost of each package. It is also of interest to understand the fundamental limitations. This may influence the design of future packaging systems.

If the amount of slosh in the package can be decreased, the empty space above the liquid in the package can also be decreased, and hence the amount of packaging material is reduced. This results in lower material cost and also environmental advantages, since a package with less material consumes less natural resources and produces less waste.

A systematic method for calculating acceleration references also simplifies the development process and reduces the development time and the time to adapt to new products. This results in lower development costs for the manufacturer since the tuning of the acceleration references today are performed by expensive development engineers. A systematic method for calculation of acceleration references together with the use of modern servo systems make it possible to optimize the packaging machine for different products in a simple manner.

1.4 Outline of the thesis

The outline of the thesis is as follows:

Chapter 2 presents the experimental setup and the measurement equipment. The mechanical construction of the setup and the servo system is described. The slosh measurement problem is also discussed and several measurement methods are described. A description of the external control system is also given.

Chapter 3 presents the slosh modeling problem. A review of the slosh modeling problem is given and the governing equations and common approximations are given. A linear model is also derived using the

Laplace and Bernoulli equations. Experiments are presented that show some of the phenomena encountered in the slosh. A simple linear model of the slosh is presented that can be used for synthesis of acceleration references.

Chapter 4 presents several different methods for calculation of acceleration references for horizontal motion. All methods are based on optimal control and the simple linear model presented in Chapter 3. The performance of the different acceleration references are also evaluated using experiments in the experimental setup presented in Chapter 2.

Some of the results in this chapter have or will be published in:

Grundelius, M. (1998): *Motion Control of Open Containers with Slosh Constraints*. Lic Tech thesis ISRN LUTFD2/TFRT--3222--SE, Department of Automatic Control, Lund Institute of Technology, Lund, Sweden.

Grundelius, M. and B. Bernhardsson (1999): "Motion control of open containers with slosh constraints." In *Proceedings of the 14th IFAC World Congress*. Beijing, P.R. China.

Grundelius, M. and B. Bernhardsson (1999): "Control of liquid slosh in an industrial packaging machine." In *Proceedings of the 1999 IEEE International Conference on Control Applications and IEEE International Symposium on Computer Aided Control System Design*. Kohala Coast, Hawaii.

Grundelius, M. and B. Bernhardsson "Motion control of open containers with slosh constraints." Accepted for publication in Control Engineering Practice.

Chapter 5 presents two methods that apply Iterative Learning Control to the movement problem. The methods uses the simple linear model of the slosh presented in Chapter 3 and data from one experiment to predict the surface elevation in the next iteration. Optimization is used to find the change in the acceleration reference that gives the desired performance. The methods are evaluated in simulations using a linear and a nonlinear process model as well as in experiments in the experimental setup.

Some of the results in this chapter have been published in:

Grundelius, M. and B. Bernhardsson (2000): "Constrained iterative learning control of liquid slosh in an industrial packaging machine." In *Proceedings of the 39th IEEE Conference on Decision and Control*. Sydney, Australia.

Grundelius, M. (2000): "Iterative optimal control of liquid slosh in an industrial packaging machine." In *Proceedings of the 39th IEEE Conference on Decision and Control*. Sydney, Australia.

Chapter 6 presents how rotation of the container can be utilized to decrease the surface elevation relative to the container wall when the container is accelerated horizontally. The simultaneous horizontal and rotational acceleration references are derived using optimal control and the simple linear model presented in Chapter 3. The derived acceleration references are evaluated in experiments.

Chapter 7 presents the conclusions, the use of the results in industry and some suggestions on possible future work.

2

Experimental setup

This chapter describes the equipment used in the experiments. The experimental setup has been constructed by Tetra Pak Research & Development AB. The slosh measurement devices have been developed and tested in collaboration with Tetra Pak Research & Development AB. The tilting device in the experimental setup was constructed at the department of Automatic Control.

The chapter is organized as follows: In Section 2.1 the mechanical construction of the experimental setup is described. Section 2.2 describes the servo systems used to control the position and angle of the package. The slosh measurement problem is discussed in Section 2.3 and several different measurement methods are presented. Finally in Section 2.4 the external motion control system implemented in the Matlab/Simulink environment on a PC running the Linux operating system is presented.

2.1 The mechanical construction

The experimental setup consists of a carriage mounted on a rubber belt driven by a standard servo system. See Figure 2.1 for a schematic picture and Figure 2.2 for photographs of the setup. The coupling between the motor and the belt determines the gear ratio; one revolution of the motor axis moves the carriage 0.05 m. A carton holder for one-liter packages from a packaging machine and the slosh sensor are mounted on the carriage. At each end of the belt a mechanical safety switch is positioned that cuts the power to the motor if the carriage should move past it. This ensures that the mechanical construction does not take any damage if the carriage goes out of control.

To enable tilting of the container a servo motor with gear box is mounted on the carriage. An aluminum beam is mounted on the gear box axle and the package holder is mounted on the beam. The vertical

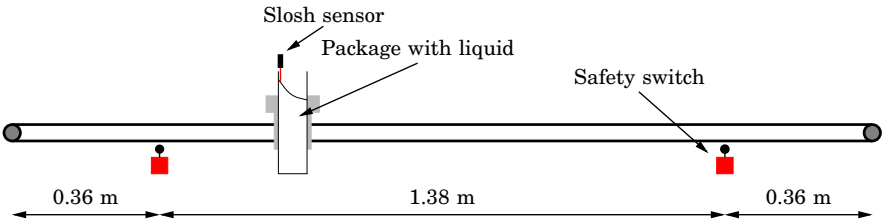

Figure 2.1 Schematic picture of experimental setup.

position of the package can easily be changed to obtain a different position of the rotational axis relative to the liquid. See Figure 2.3 for some photographs of the tilting mechanism.

2.2 The servo systems

Horizontal motion

The motor is controlled by an Atlas DMC (Digital Motion Controller) model DMC50720P manufactured by Atlas Copco, see Figure 2.2 for a photograph of the controller.

The controller is of PID type with feedforward to improve the trajectory following performance. The control loop is sampled with a period time of one millisecond. The acceleration reference is stored in the memory and is specified as a list of acceleration–duration pairs, where the acceleration is given in resolver increments per square second and the duration in milliseconds. The DMC program including the acceleration reference is downloaded using the serial port of a PC with the transfer rate 9600 bps. The time needed to download the program is about one minute.

The system can also be operated in open loop. A torque reference is read from one of the analog-in ports with a sampling period of one millisecond. The position can be measured using an encoder fitted to the motor axle with a resolution of 5000 increments per revolution. This is used when the position is controlled using the external control system described in Section 2.4

The servo motor is a four pole synchronous permanent magnetized AC motor manufactured by ELMO. The control system feeds the servo motor via a frequency converter with a switching frequency of 4 kHz.

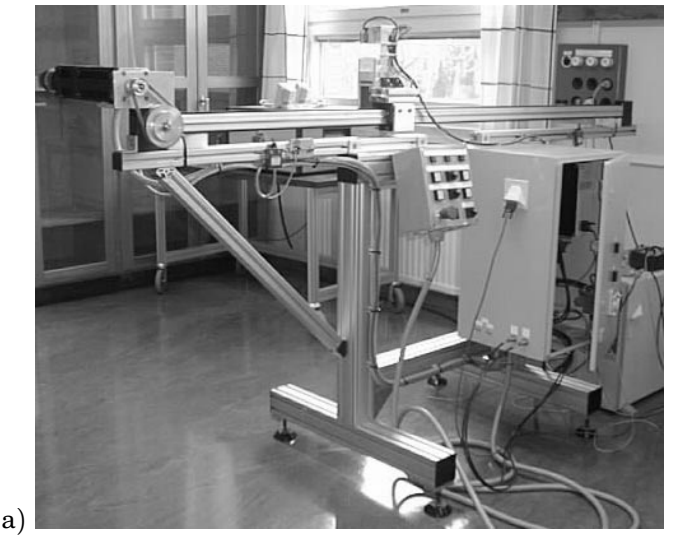

a)

b)

c)

Figure 2.2 Photographs of the experimental setup. (a) Overview of the experimental setup, (b) close-up on the cabinet with the Digital Motion Controller (DMC) and power supply and (c) close-up on the container and the laser displacement sensor.

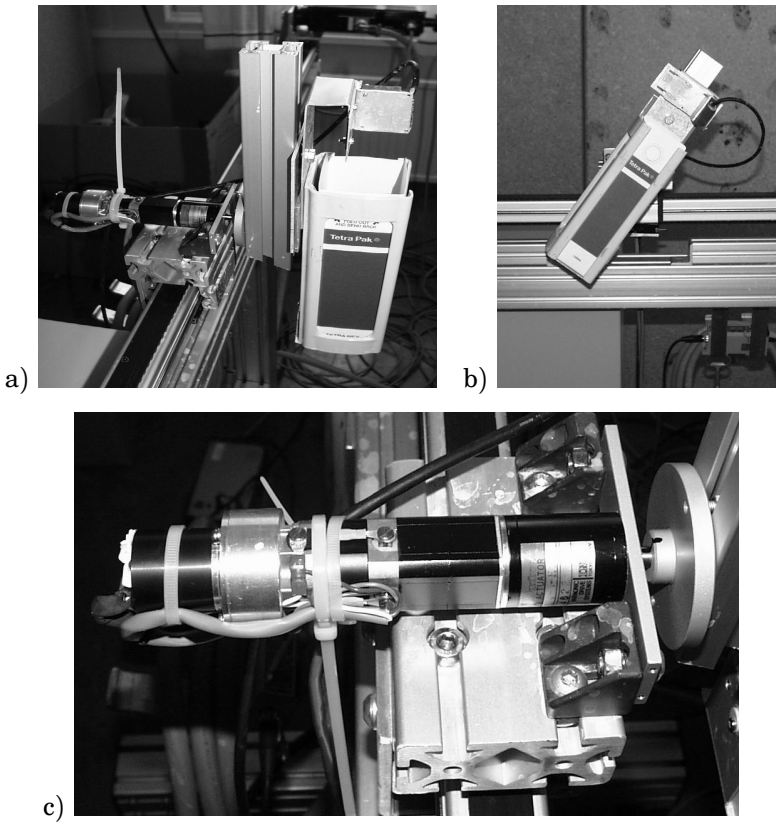

Figure 2.3 Photographs of the tilting mechanism on the experimental setup. (a) Overview of the carriage with the motor and the package holder, (b) side view of the tilted package and (c) close up of the servo system with, from left to right, encoder, tachometer, motor and gear box.

Rotational motion

The servo motor and gear box is a Hi.T Drive from Harmonic Drive Systems of model HT-6006-T-E. The system consist of a DC motor, a gear box with ratio 50:1, a tachometer and an encoder with a resolution of 800 increments per revolution of the motor axle. This gives 40000 increments per revolution of the gear box axle where the package is mounted.

The motor is fed from a standard voltage controlled amplifier which can deliver up to 2 A current.

The tilt angle is controlled using the external control system described in Section 2.4.

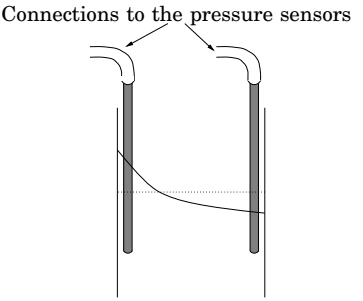

Figure 2.4 Illustration of the pressure based measurement setup.

2.3 Slosh measurements

When this work started there were no of-the-shelf system for measuring fast moving liquid surfaces and there were little to be found in the literature.

The slosh measurement is crucial for modeling of the slosh phenomenon and for performance evaluation of the designed acceleration references. Ultimately, one would like a measurement of the surface shape and the flow velocity within the fluid. This is, however, not possible today.

The most important measure in this application is the surface elevation at the walls of the container. The largest oscillations appear there and one of the control constraints is that the surface does not reach a certain level on the wall.

The measurement problem turned out to be nontrivial. A number of sensors were evaluated during a period of one year.

Pressure based measurement

The first attempt to get a measure of the surface elevation was to measure the pressure below the surface. A setup with two aluminum pipes with a diameter of 6 mm where put at each side of the container as shown in Figure 2.4. The pipes where connected to pressure sensors by plastic tubes.

This worked well when the surface was at rest, but when the surface was moving the measurement did not reflect the actual surface elevation. This was due to the fact that when the fluid is moving the pressure does not only depend on the depth but also on the flow velocity. This is a well known fact from hydrodynamics and now also known by us.

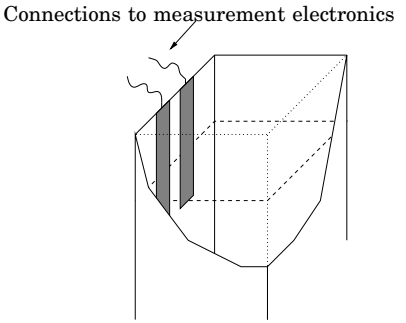

Figure 2.5 Illustration of the capacitance based measurement setup.

Capacitance based measurement

This method uses the difference in permittivity between water and air to measure the surface elevation. The capacitance between two conductors depends on the permittivity of the medium surrounding them, i.e. the height of water near the wall. The sensor is built up by two strips of 12 mm wide copper tape attached parallel to each other 5 mm apart on the outside of the paper carton package as illustrated in Figure 2.5.

This gives a good measure of the surface elevation when the surface is at rest. But when the surface is oscillating a thin layer of liquid is formed on the package wall. This thin layer of liquid moves down much slower than the surface of the liquid. This results in a very slow decay in the measured surface elevation. The measurement device works well as a sensor for the maximum slosh.

Ultrasonic based measurement

A standard ultrasonic distance sensor was also tried. It gave a good measure of the distance to the surface when the liquid was at rest or moving slowly. But when the surface was moving to wildly the sensor was not able to measure the distance.

Electrical contact based measurements

In this method the electrical conductivity of water is used to measure the surface elevation. The sensor is built up by 14 pins mounted 5 mm apart through the package wall and one ground plate as illustrated in Figure 2.6.

The measurement of the surface elevation is generated as a sum of all pins in electrical contact with the ground plate. This gives an output that can take 15 different values.

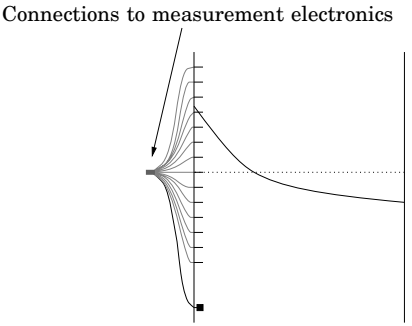

Figure 2.6 Illustration of the electrical contact based measurement setup.

The main drawback with this method is the low accuracy when measuring small oscillations. There were also some minor problems with water drops attached to the pins and the thin layer of water formed on the package wall.

Infrared laser based measurement

A laser displacement sensor manufactured by Keyence Corporation, sensor head model LB-11(W) with sensor controller LB-70(W), has been tested and used to measure the surface elevation with good results.

The sensor uses an infrared laser emitter and a Position Sensitive Detector (PSD) to determine the distance to the surface. An infrared laser ray is emitted from the sensor and scattered when it hits the surface. If the surface is highly reflective this sensor does not work. An infrared camera observes the surface at an angle of 11° relative the laser ray and the displacement is determined by the mean of the light distribution that hits the PSD, see Figure 2.7 for an illustration of the measurement system.

The measurement range of the sensor is between 60 mm and 140 mm. The response speed of the sensor can be set to 0.7 ms, 20 ms or 500 ms giving a resolution of 180 μm, 40 μm and 10 μm respectively. The fastest response speed, 0.7 ms, has been used in the experiments. The scattering of the laser ray is poor for water and therefore the water was dyed with white paint.

The sensor gives a good measure of the surface elevation and only occasionally loses track of the surface. These instants are easily identified since the output at these times saturates at the lower limit very rapidly.

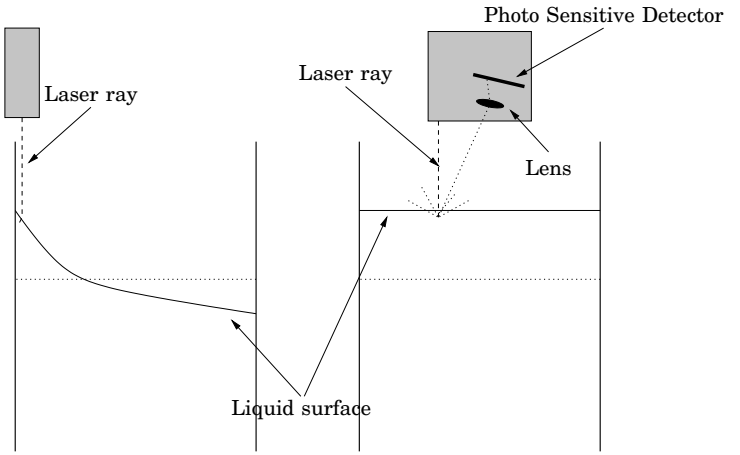

Figure 2.7 Illustration of the infrared laser measurement setup used in this thesis. The left illustration is the side view and the right illustration is the forward view.

Computer vision based measurement

The shape of the surface can be measured by a computer vision system. A small color video camera manufactured by ELMO, model QP49H, was mounted on the carriage. A rectangular window was cut in the top of the paper carton and covered with transparent plastic film. The water was dyed with red color to increase the contrast to the white carton. The camera was mounted parallel to the surface and perpendicular to the direction of movement, see Figure 2.8.

The signal from the video camera is recorded on a video tape. The video camera shoots 50 half frames per second which are recorded as 25 full images per second by the video recorder. Hence, each captured image contains two interlaced camera shots. A frame grabber is then used to get a digital representation of the images in the computer, see Figure 2.9 for an image from the video camera. The interlacing of the two frames can be seen in the figure as the gray area in the middle of the picture where there is liquid in one of the frames but not in the other.

The images are then processed in Matlab to extract the shape of the surface, see Figure 2.10. The figure shows the two surface shapes extracted from the image.

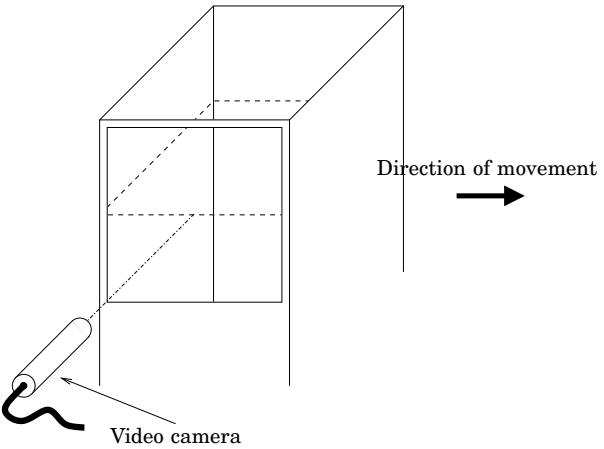

Figure 2.8 Illustration of the camera mounting in the computer vision system.

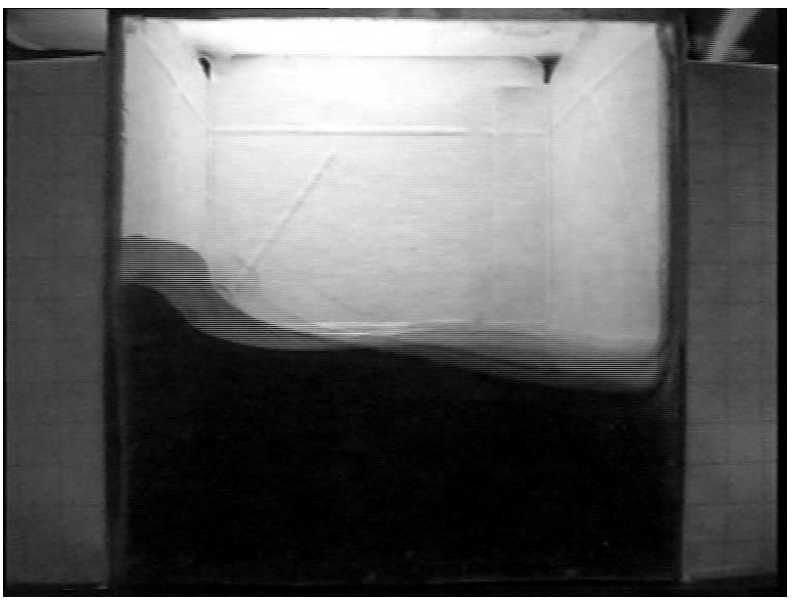

Figure 2.9 Image from the video camera. The interlacing of the two frames can be seen in the figure as the gray area in the middle of the picture where there is liquid in one of the frames and not in the other. The time between the frames is 20 ms.

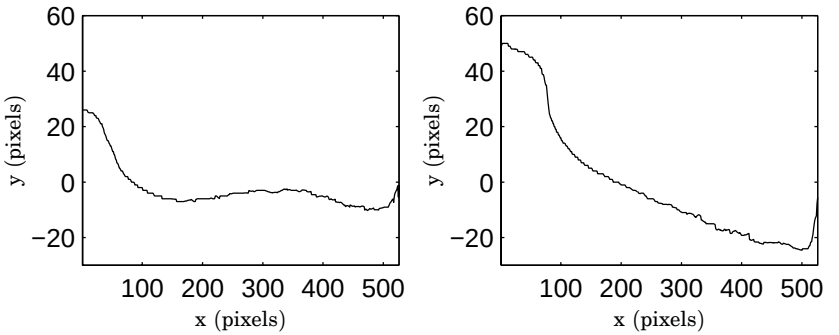

Figure 2.10 Extracted surface shapes from the image in Figure 2.9. The time between the two figures is 20 ms.

2.4 External motion control system

The Digital Motion Controller works well, but it is quite cumbersome to do experiments where you try different acceleration references since the reference is stored in the memory of the DMC. Each time the acceleration reference is changed the complete program needs to be recompiled and downloaded to the DMC.

Also the DMC only controls the horizontal movement. If a combined horizontal and rotational movement is desired the position and angle control need to be synchronized. Therefore, an external control system was implemented on a PC running the Linux operating system in the Matlab/Simulink environment. Simulink is made to run in real time using a block that halts the simulation and waits until the next sampling instant. There are blocks for analog-in/out and encoder-in signals that connect Simulink to the I/O-card. Information about Linux in Control is available at (`http://www.control.lth.se/~andersb/linux_in_control/`).

The DMC is set to run in open loop reading a torque reference from its analog-in port and the position is measured using the encoder, see Section 2.2.

The Simulink block diagram of the motion control system is shown in Figure 2.11. The system consists of five major functions each represented by a subsystem in the Simulink model. The functions are:

ReferenceGeneration Generates velocity and position references by integrating the horizontal and rotational acceleration references.

Controller Controls the position and the angle of the package using PID control with anti-windup and feedforward of the acceleration and ve-

locity reference. The position controller does not use any measurements or references used by the angle controller and vice versa.

System Contains the connections to the I/O-card and a safety net that limits the outputs and sets the output to zero if the package moves outside the allowed region or tilts too much. The block also contains a simulation model of the system used for testing of the other functions.

MotionObserver Kalman filter that estimates the position, velocity, angle and angular velocity of the container.

SloshObserver Kalman filter that estimates the surface elevation and rate of change in the surface elevation. The block also detects when sensor faults occur and the estimator is set to run in open loop while the fault occurs.

The system operates at two different sampling rates: the control runs with the sampling period 1 ms and the acceleration references are defined at a lower sampling rate typically 5 or 10 ms. The estimation of the surface elevation is at the same sampling rate as the acceleration references but the detection of sensor faults run at the fast sampling rate.

Both control loops are based on the following model of the servo motor and mechanics

$$J\ddot{y} + D\dot{y} + F \text{ sign } \dot{y} = u \tag{2.1}$$

where y is the position or angle, J is the inertia, D is the viscous friction, F is the static friction and u is the torque input. The parameters J, D and F are estimated using experiments, see [Lannegren, 1999].

The control law in both loops are

$$u = K_p e + K_i \int e\, dt + K_d \dot{e} + J\ddot{y}_r + D\dot{y}_r + F \text{ sign } \dot{y}_r \tag{2.2}$$

where $e = y_r - y$ and y_r is the position or angle reference. Note that since the position and angle reference is defined by the horizontal and rotational acceleration both the first and second derivative of y_r are available and no numerical differentiation is necessary. The controller gains K_* are calculated using LQ-control with the model in (2.1) augmented with a state for the integrated error.

If the true system is described by (2.1) and the control law in (2.2) is used then there would be no control error and no feedback would be necessary, hence $y = y_r$. However, feedback is needed since there are disturbances, modeling errors, a discrete-time controller implementation etc.

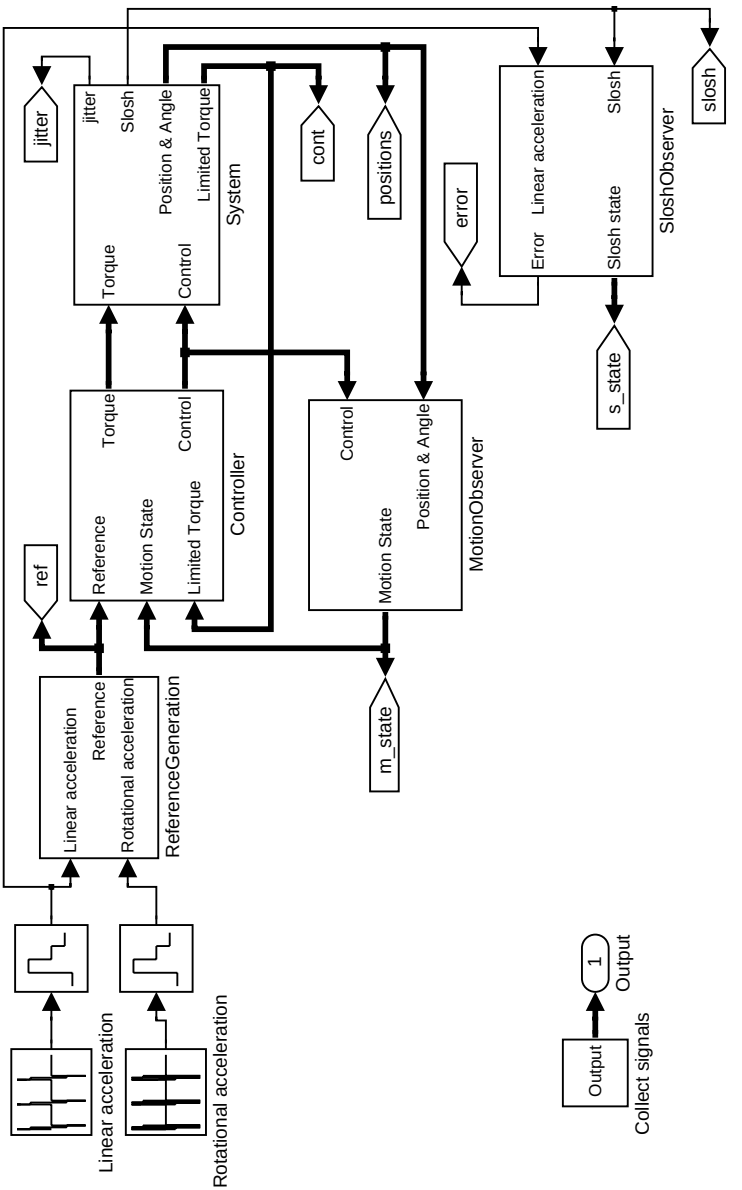

Figure 2.11 Simulink block diagram of the external motion control system used to control the package position and angle.

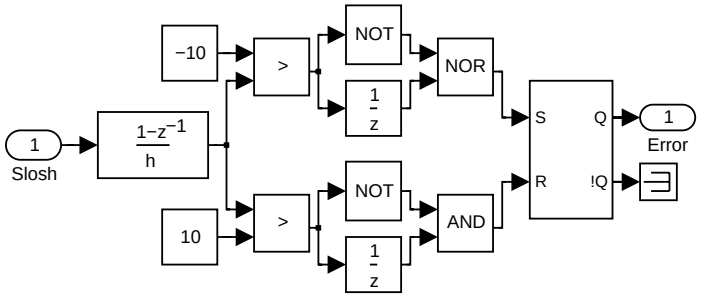

Figure 2.12 Simulink block diagram of the measurement error detector.

The Kalman filters are on the form

$$\hat{x}(k+1|k) = \Theta\hat{x}(k|k-1) + \Gamma u(k) + K\big(y(k) - C\hat{x}(k|k-1)\big)$$
$$\hat{x}(k|k) = \hat{x}(k|k-1) + K_f\big(y(k) - C\hat{x}(k|k-1)\big)$$

where Θ, Γ and C are obtained from zero-order-hold sampling of the models in (2.1) and (3.39). Since the position and angle are measured using encoders there is essentially no noise in the measurement only quantization errors, which are small, and when calculating the observer gains K and K_f the process noise is set much larger than the measurement noise in the motion observer to obtain a fast observer. The surface elevation observer is implemented only for horizontal acceleration.

When the sensor fails to measure the surface elevation the measurement rapidly saturates at the lower level, typically in less than 5 ms. The sensor faults are detected by differentiation of the surface elevation. When the sensor fault occurs there will be a large negative peak in the derivative. During the fault the derivative is zero and when the fault ends there is a large positive peak in the derivative. The detection is built using one differentiator, two comparators, one positive and one negative flank detector and one SR-latch, see Figure 2.12 for the Simulink block diagram.

The system is operated from the Matlab command line through functions that set the parameters in the Simulink model using the `set_param` command. The motion is executed by starting a simulation of the model with the `sim` command and the resulting data are obtained from the output variables of the function.

3

Modeling of slosh

This chapter covers different aspects of the slosh modeling problem. The purpose of the model is controller synthesis using optimal control. There is a tradeoff between model accuracy and model complexity since the optimal control problems become harder to solve for a more complex model. Therefore, the aim is to find a simple, preferable linear, model that describes the fluid motion within the container.

In different packaging machines there is a large variety of movements of the packages containing liquid. Typical examples are horizontal movement along a straight or curved path, vertical movement, rotations or combinations of these. Here, only horizontal motion along a straight path combined with rotation in the vertical plane aligned with the movement direction is studied.

Models are obtained both from the equations governing the fluid motion and from system identification on data obtained from experiments. The theoretical models are derived with the assumption that the oscillation is small.

In Section 3.1 the equations governing the flow in a fluid is described. A model of the liquid in a horizontally accelerated container is also derived. Section 3.2 presents some numerical and analytical solutions to the flow problem found in the literature. An experimental investigation of the slosh phenomenon is presented in Section 3.3 when the container is both accelerated horizontally and tilted. In Section 3.4 measurements of the surface profile using the vision system described in Section 2.3 is used to analyze the slosh phenomenon. The chapter is concluded in Section 3.5 where two simple models are presented: one for horizontal acceleration only and one for simultaneous horizontal and rotational acceleration.

3.1 Fluid dynamics

This section gives a brief description of different mathematical descriptions of fluid flow, for further details see [Shen, 1993], [Baldock and Bridgeman, 1981], [Coulson, 1955] and [Lamb, 1945].

Within the fluid

Fluid motion within the fluid is described by the Navier-Stokes equations. This is a set of nonlinear three dimensional partial differential equations. The first equation describes the conservation of mass

$$\frac{\partial \rho}{\partial t} + \nabla \cdot (\rho \mathbf{v}) = 0 \tag{3.1}$$

where ρ is the density of the fluid and $\mathbf{v} = (v_x,\ v_y,\ v_z)$ is the flow velocity vector field in the fluid and $(x,\ y,\ z)$ is the spatial coordinates. Equation (3.1) is referred to as the continuity equation in continuum mechanics.

The conservation of mass gives only one equation, but has four unknowns. Therefore, additional conditions are needed, unless the density ρ is known and the problem is one dimensional. The conservation of momentum (i.e. Newton's second law of motion) gives three more equations. For a so called Newtonian viscous fluid the conservation of momentum gives the equation

$$\rho \left(\frac{\partial \mathbf{v}}{\partial t} + (\mathbf{v} \cdot \nabla)\mathbf{v} \right) = -\nabla p + (\lambda + \mu)\nabla(\nabla \cdot \mathbf{v}) + \lambda \nabla^2 \mathbf{v} + \rho \mathbf{f} \tag{3.2}$$

where p is the pressure, λ the factor of volume compression, μ the viscosity and $\mathbf{f} = (f_x,\ f_y,\ f_z)$ is the external force vector field. The equations (3.1) and (3.2) are called the Navier-Stokes equations.

If the fluid is incompressible ($\lambda = 0$) and inviscid ($\mu = 0$) the Navier-Stokes equations become the Euler equations.

$$\nabla \cdot \mathbf{v} = 0 \tag{3.3}$$

$$\frac{\partial \mathbf{v}}{\partial t} + (\mathbf{v} \cdot \nabla)\mathbf{v} = -\frac{1}{\rho}\nabla p + \mathbf{f} \tag{3.4}$$

Inserting the vector identity $(\mathbf{v} \cdot \nabla)\mathbf{v} = \frac{1}{2}\nabla|\mathbf{v}|^2 + (\nabla \times \mathbf{v}) \times \mathbf{v}$ in (3.4) and assuming that the external force field has a potential ($\mathbf{f} = -\nabla V$) gives

$$\frac{\partial \mathbf{v}}{\partial t} + \frac{1}{2}\nabla|\mathbf{v}|^2 + (\nabla \times \mathbf{v}) \times \mathbf{v} = -\frac{1}{\rho}\nabla p - \nabla V \tag{3.5}$$

The assumption that the force field has a potential excludes forces generated by rotational acceleration of the container.

The pressure and the external forces can be eliminated from the equations by taking the curl of both sides of (3.5), since the curl of a gradient is zero. This gives

$$\frac{\partial \omega}{\partial t} + \nabla \times (\omega \times \mathbf{v}) = 0 \tag{3.6}$$

where $\omega = \nabla \times \mathbf{v}$ is called the vorticity of the flow. Now the equations (3.3) and (3.6) describe the velocity field.

If $\omega = 0$ everywhere at any time then also $\frac{\partial \omega}{\partial t} = 0$ everywhere and ω will still be zero everywhere in the future. Hence, $\omega = 0$ is a solution to (3.6). A flow satisfying $\omega = 0$ is irrotational and is called a potential flow. For potential flows there exists a potential ϕ such that

$$\mathbf{v} = \nabla \phi \tag{3.7}$$

Insertion of (3.7) in (3.3) gives

$$\nabla \cdot \nabla \phi = \nabla^2 \phi = 0 \tag{3.8}$$

which is known as Laplace's equation. Insertion of (3.7) and $\nabla \times \mathbf{v} = 0$ in (3.5) and integrating with respect to space gives

$$\frac{\partial \phi}{\partial t} + \frac{1}{2}|\nabla \phi|^2 + \frac{p}{\rho} + V = C(t) \tag{3.9}$$

where $C(t)$ is an arbitrary function of time. This equation is known as Bernoulli's equation.

Further approximations can be made if the width of the container is much larger then the depth of the liquid. The horizontal flow velocity in a fluid element is then assumed to be independent of the vertical position of the fluid element. This gives the Shallow Water Equations.

On the fluid boundary

The fluid boundaries in the problem considered are the container walls, bottom and the free surface of the fluid. On the container walls and bottom the boundary condition is that the velocity of the flow at the wall is zero in the normal direction of the wall. This gives

$$\mathbf{n} \cdot \mathbf{v} = 0 \quad \Rightarrow \quad \mathbf{n} \cdot \nabla \phi = 0 \tag{3.10}$$

where $\mathbf{n}$ is the normal direction of the wall.

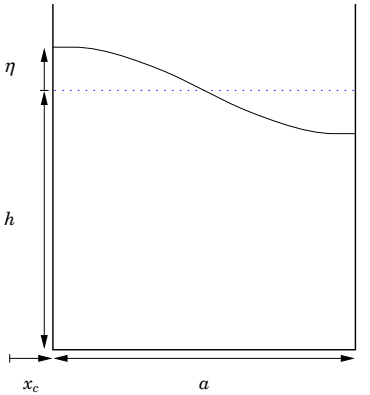

Figure 3.1 Illustration of the container.

On the fluid surface $z = \eta(t, x, y)$ there are two boundary conditions: one dynamic and one kinematic. The dynamical condition arises from the external forces acting on the surface. For a potential flow this can be expressed with Bernoulli's equation

$$\frac{\partial \phi(t,x,y,\eta)}{\partial t} + \frac{1}{2}|\nabla \phi(t,x,y,\eta)|^2 + \frac{p(t,x,y,\eta)}{\rho} + V(t,x,y,\eta) = C(t) \quad (3.11)$$

The kinematic condition states that a fluid particle originally on the free surface will remain on the free surface forever and is for a potential flow expressed by

$$\frac{\partial \eta}{\partial t} + \frac{\partial \phi}{\partial z}\frac{\partial \eta}{\partial x} + \frac{\partial \phi}{\partial y}\frac{\partial \eta}{\partial y} = \frac{\partial \phi}{\partial z} \quad (3.12)$$

Fluid flow in a horizontally accelerated open container

A container with rectangular cross section with length a, width b and liquid depth h is accelerated horizontally along a line parallel to two of the walls, see Figure 3.1.

Since the movement is parallel to two of the walls it is assumed that the flow velocity is zero in the direction perpendicular to the movement. The problem can then be reduced to two dimensions. Two coordinate systems are used: one fixed $(\bar{x},\ \bar{z})$ and one that moves along with the container $(x,\ z)$. The relation between the coordinates are

$$\begin{aligned} x &= \bar{x} - x_c\ , & e_x &= e_{\bar{x}} \\ z &= \bar{z}\ - h, & e_z &= e_{\bar{z}} \end{aligned}$$

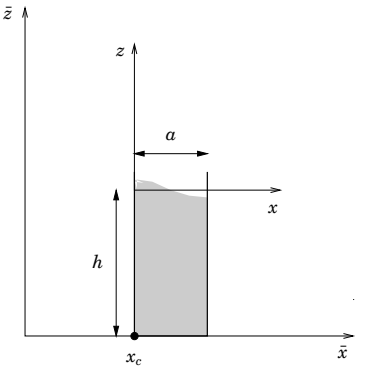

Figure 3.2 Illustration of the two coordinate systems.

where x_c is the position of the container and e_* are the corresponding base vectors. Figure 3.2 illustrates the relation between the two coordinate systems.

The fluid in the container is further assumed to be incompressible and inviscid and the flow is assumed to be irrotational. The surface elevation above the point $(x, 0)$ is given by $\eta(t, x)$. The forces that act on the fluid is gravity and the horizontal acceleration. Gravity gives the force field $f_g(\bar{x}, \bar{z}) = -ge_{\bar{z}}$ and the horizontal acceleration gives the force field $f_a(\bar{x}, \bar{z}) = -\ddot{x}_c e_{\bar{x}}$. Transformation to the coordinate system of the container gives the following force field and potential

$$f(x, z) = -ge_z - \ddot{x}_c e_x \ , \qquad V = gz + \ddot{x}_c x \tag{3.13}$$

The equations (3.8), (3.10), (3.11), (3.12) and (3.13) give the following description of the fluid flow in the container

$$\nabla^2 \phi(t, x, z) = 0 \tag{3.14}$$

$$\frac{\partial \phi(t, x, z)}{\partial t} + \frac{p(t, x, z)}{\rho} + \frac{1}{2}|\nabla \phi(t, x, z)|^2 + gz + u(t)x = C(t) \tag{3.15}$$

$$\frac{\partial \eta(t, x)}{\partial t} + \frac{\partial \phi(t, x, z)}{\partial x}\frac{\partial \eta(t, x)}{\partial x} = \frac{\partial \phi(t, x, z)}{\partial z} \tag{3.16}$$

$$\frac{\partial \phi(t, 0, z)}{\partial x} = 0 \ , \quad \frac{\partial \phi(t, a, z)}{\partial x} = 0 \ , \quad \frac{\partial \phi(t, x, -h)}{\partial z} = 0 \tag{3.17}$$

where (3.15) and (3.16) are evaluated on the free surface (i.e. $z = \eta(t, x)$) and $u(t) = \ddot{x}_c$ is the horizontal acceleration of the container.

The flow problem is solved using separation of variables. Insertion of $\phi(t,x,z) = T(t)X(x)Z(z)$ in (3.14) gives the equation

$$T(t)X''(x)Z(z) + T(t)X(x)Z''(z) = 0$$

this gives

$$\frac{X''(x)}{X(x)} = -\frac{Z''(z)}{Z(z)} = -\lambda \tag{3.18}$$

The following equations is obtained from (3.17) and (3.18)

$$\begin{cases} X'' + \lambda X = 0 \\ X'(0) = 0 \\ X'(a) = 0 \end{cases} \tag{3.19}$$

$$\begin{cases} Z'' - \lambda Z = 0 \\ Z'(-h) = 0 \end{cases} \tag{3.20}$$

Nontrivial solutions to (3.19) and (3.20) are only obtained for $\lambda \geq 0$.

$$\lambda = 0 \;\Rightarrow\; \begin{cases} X(x) = a_1 x + a_2 \\ Z(z) = b_1 z + b_2 \end{cases}$$

Insertion of the boundary conditions gives

$$\begin{cases} X'(0) = a_1 = 0 \\ X'(a) = a_1 = 0 \\ Z'(-h) = -b_1 = 0 \end{cases} \quad \Rightarrow \quad \begin{cases} a_1 = 0 \\ b_1 = 0 \end{cases}$$

This gives the mode shapes

$$X_0(x) = a_0(t)\,, \qquad Z_0(z) = b_0(t) \tag{3.21}$$

Solving (3.19) and (3.20) for $\lambda > 0$ gives

$$\lambda > 0 \;\Rightarrow\; \begin{cases} X(x) = a_1 \cos\sqrt{\lambda}x + a_2 \sin\sqrt{\lambda}x \\ Z(z) = b_1 \cosh\sqrt{\lambda}z + b_2 \sinh\sqrt{\lambda}z \end{cases}$$

Insertion of the boundary conditions gives

$$\begin{cases} X'(0) = a_2\sqrt{\lambda} = 0 \\ X'(a) = a_1\sqrt{\lambda}\sin\sqrt{\lambda}a + a_2\sqrt{\lambda}\cos\sqrt{\lambda}a = 0 \\ Z'(-h) = -b_1\sqrt{\lambda}\sinh\sqrt{\lambda}h + b_2\sqrt{\lambda}\cosh\sqrt{\lambda}h = 0 \end{cases}$$

which has the solutions

$$\begin{cases} a_2 = 0 \\ \lambda_n = \dfrac{n^2\pi^2}{a^2},\ n = 1, 2, \dots \\ b_1 = b_2 \dfrac{\cosh\sqrt{\lambda_n}h}{\sinh\sqrt{\lambda_n}h} \end{cases}$$

This gives the following mode shapes

$$X_n(x) = a_n(t)\cos\frac{n\pi}{a}x\ , \quad Z_n(y) = b_n(t)\frac{\cosh\frac{n\pi}{a}h}{\sinh\frac{n\pi}{a}h}\cosh\frac{n\pi}{a}(z+h) \quad (3.22)$$

The potential is now given by (3.21) and (3.22) which gives

$$\phi(t,x,z) = T_0(t) + \sum_{n=1}^{\infty} T_n(t)\cos\frac{n\pi}{a}x\cosh\frac{n\pi}{a}(z+h) \quad (3.23)$$

where all constants are lumped togheter in $T_n(t)$.

The functions $T_n(t)$ can now be found from (3.15). It is assumed that the flow velocity is small and that the quadratic term in (3.15) is small. It is also assumed the the pressure is equal everywhere on the surface, setting $C(t) = p(t,x,\eta(t,x))/\rho$ gives

$$\frac{\partial\phi(t,x,\eta(t,x))}{\partial t} + g\eta(t,x) + u(t)x = 0 \quad (3.24)$$

Differentiation of (3.24) with respect to time gives

$$\frac{\partial^2\phi(t,x,\eta(t,x))}{\partial t^2} + \frac{\partial^2\phi(t,x,\eta(t,x))}{\partial t\partial z}\dot{\eta}(t,x) + g\dot{\eta}(t,x) + \dot{u}(t)x = 0$$

Insertion of (3.16) and neglecting all nonlinear terms and assuming that the surface elevation is small ($\eta(t,x) \approx 0$) gives

$$\frac{\partial^2\phi(t,x,0)}{\partial t^2} + g\frac{\partial\phi(t,x,0)}{\partial z} = -\dot{u}(t)x$$

Insertion of the potential in (3.23) gives

$$T_0''(t) + \sum_{n=1}^{\infty}\left(T_n''(t)\cosh\frac{n\pi h}{a} + T_n(t)\frac{n\pi g}{a}\sinh\frac{n\pi h}{a}\right)\cos\frac{n\pi}{a}x = -\dot{u}(t)x$$

Expansion of the right hand side with the base functions $\cos \frac{n\pi}{a} x$ gives

$$-\dot{u}(t)x = -\dot{u}(t)a \left(\frac{1}{2} + 2 \sum_{n=1}^{\infty} \frac{(-1)^n - 1}{n^2 \pi^2} \cos \frac{n\pi}{a} x \right)$$

The uniqueness of the cosine expansion gives the following differential equations for $T_n(t)$

$$T_n''(t) + \omega_n^2 T_n(t) = \begin{cases} -\frac{a}{2}\dot{u}(t), & n = 0 \\ b_n \dot{u}(t), & n \text{ odd} \\ 0, & n \text{ even} \end{cases}$$

with

$$\omega_n = \sqrt{\frac{n\pi g}{a} \tanh \frac{n\pi h}{a}}, \qquad b_n = \frac{4a}{n^2 \pi^2 \cosh \frac{n\pi h}{a}} \tag{3.25}$$

Note that the applied horizontal acceleration only excites the odd numbered modes.

The surface elevation in the point x_m can now be calculated from (3.24), this gives

$$\eta(t, x_m) = -\frac{1}{g} \left(\frac{\partial \phi(t, x_m, 0)}{\partial t} + u(t) x_m \right)$$

where it is assumed that the surface elevation is small ($\eta(t,x) \approx 0$). Insertion of the potential $\phi(t, x_m, 0)$ gives

$$\eta(t, x_m) = -\frac{1}{g} \left(T_0'(t) + \sum_{n=1}^{\infty} c_n(x_m) T_n'(t) + u(t) x_m \right)$$

with

$$c_n(x_m) = \cos \frac{n\pi x_m}{a} \cosh \frac{n\pi h}{a}$$

Combining the input and output equations gives the model

$$\eta(t, x_m) = \frac{1}{g} \left(\frac{a}{2} - x_m - \sum_{n=1,\ n \text{ odd}}^{\infty} \frac{b_n c_n(x_m) p^2}{p^2 + \omega_n^2} \right) u(t)$$

where p is the differential operator $\frac{d}{dt}$. Insertion of b_n and $c_n(x_m)$ gives

$$\eta(t, x_m) = \frac{1}{g} \left(\frac{a}{2} - x_m - \sum_{n=1,\ n \text{ odd}}^{\infty} \frac{4a}{n^2 \pi^2} \cos \frac{n\pi x_m}{a} \left(1 - \frac{\omega_n^2}{p^2 + \omega_n^2} \right) \right) u(t)$$

The first term of the sum is the cosine series of $a/2 - x_m$ and hence the surface elevation above the point x_m for a rectangular container is given by

$$\eta(t, x_m) = \frac{4a}{g\pi^2} \left(\sum_{n=1,\ n \text{ odd}}^{\infty} \frac{1}{n^2} \cos \frac{n\pi x_m}{a} \frac{\omega_n^2}{p^2 + \omega_n^2} \right) u(t) \tag{3.26}$$

Validity of assumptions

The assumption that the fluid is incompressible is valid for liquids but not for gases. The approximation that the viscosity is negligible is however more questionable. For water it is valid but not for yoghurt. Irrotational flow is a solution to the Euler equations and therefore possible in a mathematical sense. However, any flow has a non zero viscosity and a nonuniform density, which always causes rotation of fluid elements. However, in many cases the vorticity is so weak that the flow can be considered irrotational. The surface tension has also been neglected in the modeling.

The approximations used when deriving the response to horizontal acceleration are all based on the fact that the surface elevation is small and that the rate of change of the surface elevation is small. The validity of these approximations depends on what the model is used for. Hence, if the model is used for synthesis of acceleration references the resulting surface elevation and rate of change must be small to obtain the expected behavior.

3.2 Related work

This section describes some previous work on modeling and simulation of motion induced liquid slosh.

Numerical approaches

In [Armenio and La Rocca, 1996] the fluid is modeled in two dimensions by both the Reynolds Averaged Navier-Stokes Equations (RANSE) for a incompressible flow and the Shallow Water Equations (SWE). Both problems are solved numerically with different finite element methods (FEM). The numerical solutions are compared with experiments which show that the RANSE model is closer to the real measurements than the SWE model.

The free surface flow problem with moving boundaries is described in [Kelkar and Patankar, 1997]. A numerical method is proposed which handles two fluid flows where both fluids are incompressible or where one of the fluids is compressible and the other one is incompressible. Moving

grids are used to accommodate the motion of the domain boundaries. The volume-of-fluid (VOF) technique is used to track the free boundary between the two fluids.

In [Romero and Ingber, 1995] the flow is described as a potential flow using the Laplace equation. The dynamic boundary condition on the free surface is the so called damping modified Bernoulli equation. The damping in the Bernoulli equation is a simple way to include viscosity in the model. The problem is solved using a boundary element method (BEM). The boundary on the free surface is updated to track the motion of the free surface.

Analytical approaches

The flow problem is solved analytically in [Venugopal and Bernstein, 1996]. The flow is described by the Laplace equation and the dynamic boundary condition on the free surface is described by the Bernoulli equation. The problem is solved in the same way as in Section 3.1 and the result is a linear state space model.

In [Miles, 1976] the flow problem is solved using an approach based on Lagrange mechanics. The fluid is modeled as a potential flow by the Laplace equation. The solution for a rectangular container with width a and liquid depth h is that the surface elevation above the point x_m is described by

$$\eta(t, x_m) = \sum_{n=1}^{\infty} q_n(t)\psi_n(x_m) \ , \quad \psi_n(x) = \sqrt{2}\cos\frac{n\pi}{a}x \tag{3.27}$$

The functions $q_k(t)$ are given by the following nonlinear differential algebraic equations (DAE)

$$\sum_{m=1}^{\infty}\left(a_{mn}\ddot{q}_m + \sum_{l=1}^{\infty} b_{lmn}\dot{q}_l\dot{q}_m\right) + gq_n = c_n u \ , \quad n = 1, 2, \ldots \tag{3.28}$$

where a_{mn} and b_{lmn} are functions of $\mathbf{q} = (q_1, \ldots, q_\infty)$ and u is the applied horizontal acceleration. The coefficients are given by

$$\begin{aligned} a_{mn} &= \delta_{mn}a_n + \sum_{l=1}^{\infty}\left(a_{lmn}q_l + \frac{1}{2}\sum_{j=1}^{\infty} a_{jlmn}q_j q_l + \ldots\right) \\ b_{lmn} &= \frac{1}{2}\left(\frac{\partial a_{mn}}{\partial q_l} + \frac{\partial a_{nl}}{\partial q_m} - \frac{\partial a_{lm}}{\partial q_n}\right) \\ c_n &= -\frac{1}{a}\int_0^a x\psi_n \, dx = a\sqrt{2}\frac{1-(-1)^n}{n^2\pi^2} \end{aligned}$$

with

$$\delta_{mn} = \begin{cases} 1, & m = n \\ 0, & m \neq n \end{cases}$$

$$a_n = \frac{g}{\omega_n^2}, \qquad \omega_n = \sqrt{\frac{n\pi g}{a} \tanh \frac{n\pi h}{a}}$$

$$a_{lmn} = C_{lmn} - D_{lmn} a_m a_n$$

$$a_{jlmn} = -D_{jlmn}(a_m + a_n) + 2 \sum_{i=1}^{\infty} D_{jmi} D_{lni} a_i a_m a_n$$

The coefficients C_* and D_* are given by

$$C_{lmn} = \frac{1}{a} \int_0^a \psi_l \psi_m \psi_n \, dx$$

$$D_{lmn} = \frac{1}{a} \int_0^a \psi_l \frac{\partial \psi_m}{\partial x} \frac{\partial \psi_n}{\partial x} \, dx \qquad D_{jlmn} = \frac{1}{a} \int_0^a \psi_j \psi_l \frac{\partial \psi_m}{\partial x} \frac{\partial \psi_n}{\partial x} \, dx$$

Note that $c_n = 0$ for even n which means that the horizontal acceleration does not directly excite the even numbered modes. However, they are excited by the nonlinear coupling with the other modes. Linearization of this model around the equilibrium point $\mathbf{q} = 0$ results in the same model as derived previously given in (3.26).

3.3 The slosh phenomenon

This section presents a number of experiments that illustrate some of the behavior encountered in the slosh phenomenon. In all experiments presented in this section a container with width $a = 0.07$ m and liquid depth $h = 0.2$ m was used.

Repeatability

The repeatability of the slosh phenomenon was investigated by running the same experiment several times. The acceleration reference given below was run five times, with $u_{max} = 3$ m/s^2.

$$u(t) = \begin{cases} u_{max} & 0 \leq t < 0.15 \\ -u_{max} & 0.15 \leq t < 0.30 \\ 0 & 0.30 \leq t \end{cases} \tag{3.29}$$

Figure 3.3 shows the results of the experiments. When the measurements from four of the five different experiments are plotted on top of each other

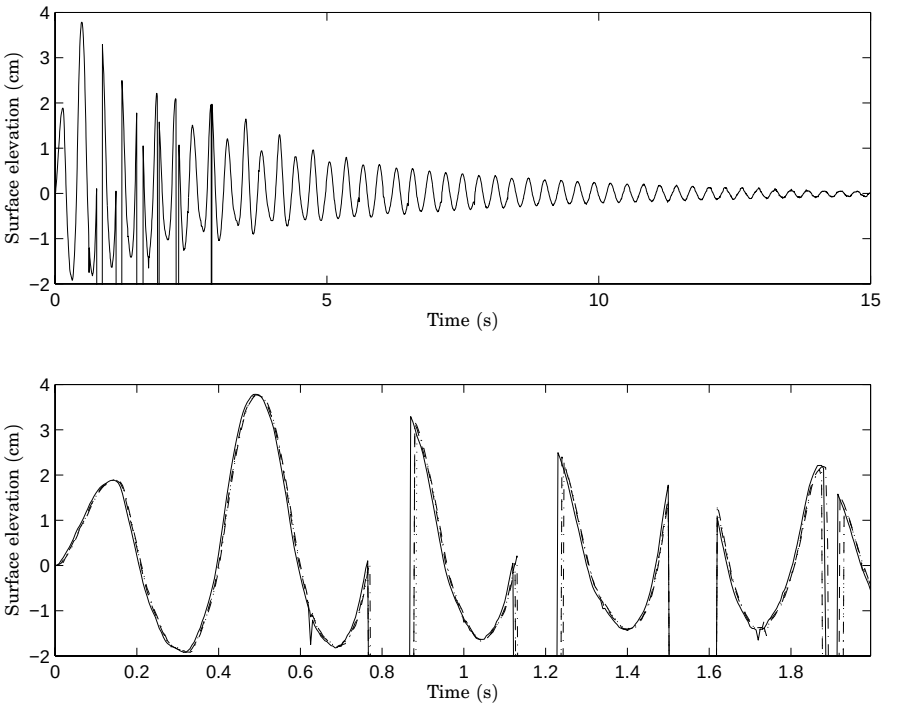

Figure 3.3 Results from experiments with the acceleration profile in (3.29) with $u_{max} = 3$ m/s^2. The upper plot shows measurements from one experiment, and the lower plot shows the measurements from four different experiments plotted on top of each other. The discontinuities at time 0.77 etc. are due to measurement faults.

it is seen that the measurements are very close. The figure shows that even the measurement faults occur at almost the same time instants.

To get a measure of how close the experiments are, the standard deviation is calculated for each time instant. The calculation of the standard deviation $\sigma(t)$ is given by

$$\sigma(t) = \sqrt{\frac{1}{4}\sum_{i=1}^{5}(s_i(t) - m(t))^2}\ , \qquad m(t) = \frac{1}{5}\sum_{i=1}^{5} s_i(t)$$

where $s_i(t)$ is the measured surface elevation of experiment $i = 1, \ldots, 5$ and $m(t)$ is the average of all experiments. The standard deviation $\sigma(t)$ is shown in Figure 3.4.

The figure shows that there are some very large peaks for $t < 0.5$. These are due to the measurement faults which do not occur at exactly the

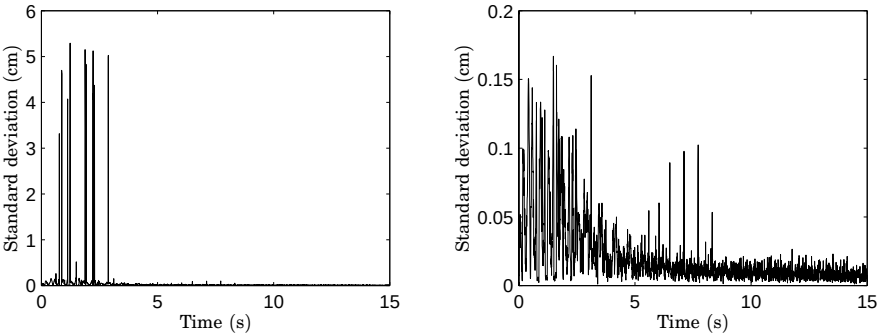

Figure 3.4 The standard deviation from the five experiments. The left plot shows the standard deviation for all values of t and in the right plot those instants when the standard deviation is greater than 0.2 are removed.

same time instants. In the right plot the time instants when the standard deviation is larger than 0.2 was removed (27 points were removed). This shows that the standard deviation is about 0.1 cm in the beginning (i.e. for large oscillation amplitudes) and about 0.01 cm in the end (i.e. for small oscillation amplitudes). The standard deviation is small compared to the measured value shown in Figure 3.3 and the conclusion is that the repeatability of the slosh is very high.

Linearity

To investigate the linearity of the slosh phenomenon the following acceleration reference was used for different values of u_{max}.

$$u(t) = \begin{cases} u_{max} & 0 \leq t < 0.4 \\ -u_{max} & 0.4 \leq t < 0.8 \\ 0 & 0.8 \leq t < 1.8 \\ -u_{max} & 1.8 \leq t < 2.2 \\ u_{max} & 2.2 \leq t < 2.6 \\ 0 & 2.6 \leq t < 3.6 \end{cases} \tag{3.30}$$

Figure 3.5 shows experiments with the acceleration reference in (3.30) for nine different values of u_{max}. If the slosh phenomenon was linear, then the response normalized with u_{max} should be independent of u_{max}. Figure 3.6 shows the normalized surface elevation for some values of u_{max}, where the normalized surface elevation is defined as

$$s_N = \frac{\text{Surface elevation}}{u_{max}}$$

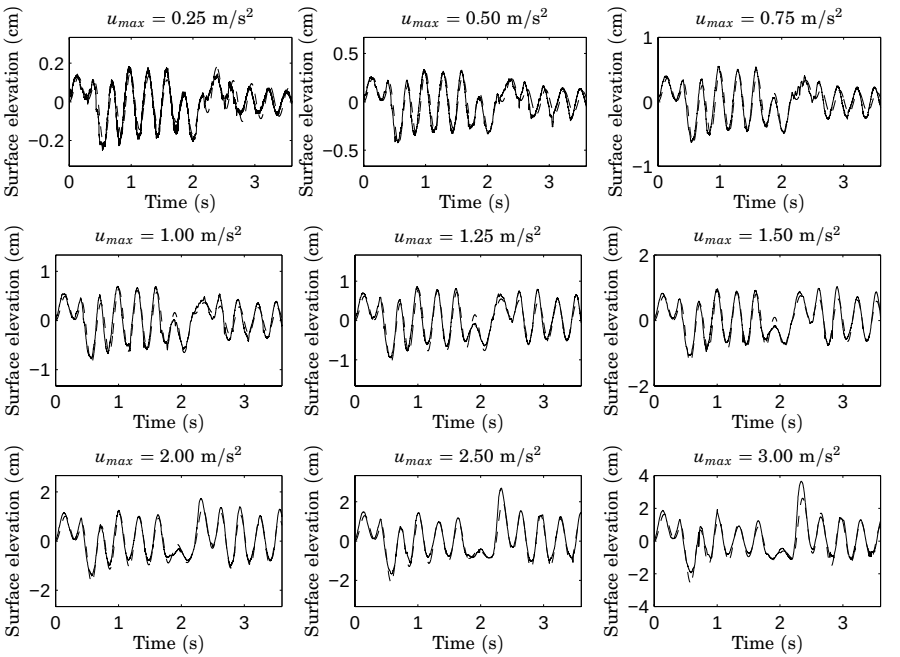

Figure 3.5 Results from experiments with the acceleration profile given in (3.30) for different values of u_{max}. The measured surface elevation (solid) and the simulated surface elevation (dashed). The simulation is done using the model in (3.31) with the parameters in Table 3.1.

The normalized slosh is the same for $u_{max} < 1$ m/s^2, but for larger values the responses are very different. Thus the slosh phenomenon is nonlinear.

The slosh is an oscillation phenomenon, therefore a simple model would be a poorly damped second order linear system. The parameterization of the transfer function is given below

$$G(s) = \frac{K\omega^2}{s^2 + 2\zeta\omega s + \omega^2} \tag{3.31}$$

The parameters of the transfer function in (3.31) was fitted using numerical optimization to the data from the experiments with different values of u_{max}. Simulations of the estimated models are shown in Figure 3.5 for different values of u_{max}. The estimated parameters are shown in Table 3.1. The figure shows that the simulated surface elevation is very close to the measured surface elevation. In the table it can be observed

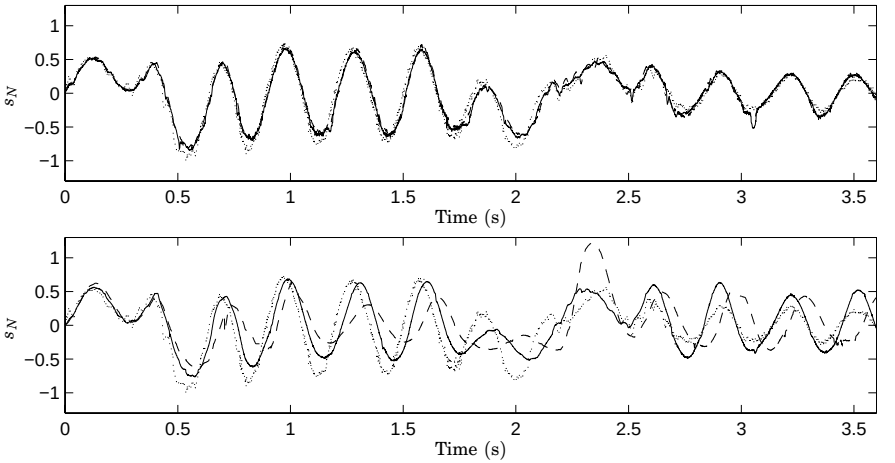

Figure 3.6 The normalized surface elevation; the upper plot shows $u_{max} = 0.25$ m/s^2 (dotted), $u_{max} = 0.50$ m/s^2 (solid) and $u_{max} = 0.75$ m/s^2 (dashed); the lower plot shows $u_{max} = 0.25$ m/s^2 (dotted), $u_{max} = 1.25$ m/s^2 (solid) and $u_{max} = 3.00$ m/s^2 (dashed).

u_{max} (m/s^2)	K	ω (rad/s)	ζ
0.25	0.263	21.2	0.024
0.50	0.252	20.9	0.014
0.75	0.251	20.8	0.012
1.00	0.251	20.7	0.008
1.25	0.252	20.6	0.007
1.50	0.251	20.5	0.008
2.00	0.258	20.3	0.013
2.50	0.267	20.0	0.021
3.00	0.286	19.8	0.031

Table 3.1 Estimated parameters of the transfer function (3.31) for different values of u_{max}. The experiments indicates that ω is amplitude dependent.

that the estimated value of ω decreases with increased amplitude of the input u_{max}. This indicates that the oscillation frequency of the slosh is amplitude dependent.

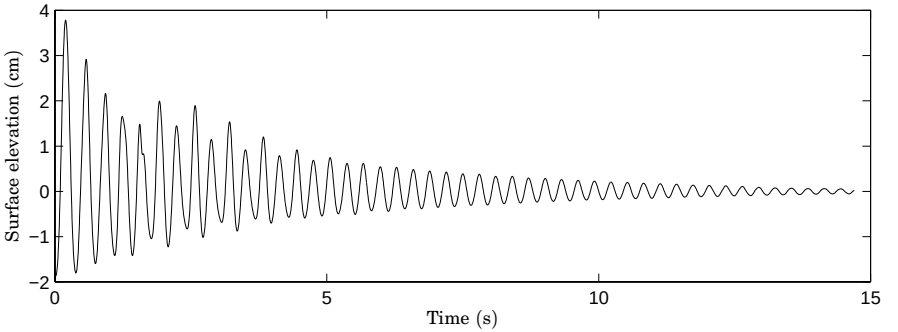

Figure 3.7 The free oscillation when the acceleration profile in (3.29) is used with $u_{max} = 3$. The measurement faults are removed and the measurement is low-pass filtered.

Nonlinearities

An easy way to identify the oscillation frequency is to study the free oscillation. The oscillation is started by applying the acceleration reference in (3.29), with $u_{max} = 3$ m/s^2. Figure 3.7 shows the free oscillation from the same experiment as the data in the upper plot of Figure 3.3, the measurement faults are removed and the measurement is low-pass filtered, with a bandwidth of 100 rad/s.

The oscillation frequency can be calculated from the time between the zero crossings of the surface elevation. If T_k is the time of the kth zero crossing then the oscillation frequency of the kth half period is given by

$$\omega_k = \frac{4\pi}{T_{k+1} - T_k}$$

The amplitude of the kth half period is calculated as

$$A_k = \max_{T_k < t < T_{k+1}} |s(t)|$$

where $s(t)$ is the surface elevation. Figure 3.8 shows A_k as a function of T_k for the same experiment as shown in Figure 3.7. In the figure the amplitude of the positive and negative half periods are drawn as two separate lines, this shows that the amplitude of the positive half periods is larger than the amplitude of the negative half periods. This illustrates another nonlinear phenomenon of the slosh, the asymmetric oscillation.

The amplitude dependent oscillation frequency indicated in Table 3.1 can also be seen from the free oscillation. First the amplitude A_k and the

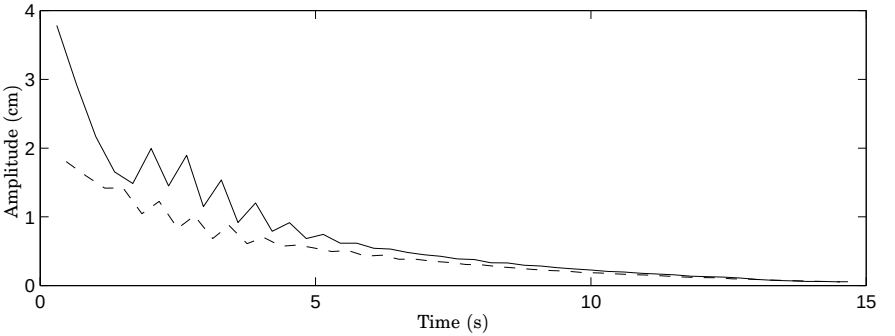

Figure 3.8 The oscillation amplitude as a function of time, positive half periods (solid) and negative half periods (dashed). The oscillation is asymmetric for large amplitudes.

oscillation frequency ω_k are made smoother by taking the mean over four half periods to form $\bar{A}_k$ and $\bar{\omega}_k$.

$$\bar{A}_k = \frac{1}{4}\sum_{i=0}^{3} A_{k+i} \ , \qquad \bar{\omega}_k = \frac{1}{4}\sum_{i=0}^{3} \omega_{k+i}$$

Figure 3.9 shows $\bar{\omega}_k$ as a function $\bar{A}_k$. The figure clearly shows that the oscillation frequency decreases with increased oscillation amplitude. A solution of the free oscillation problem in [Miles, 1976] gives the following dependence between the amplitude and oscillation frequency

$$\omega = \omega_1\sqrt{1 + \frac{\pi^2 A^2}{32a^2}(9T^{-4} - 12T^{-2} - 3 - 2T^2)}, \ T = \tanh\frac{\pi h}{a} \qquad (3.32)$$

For the container used here this becomes

$$\omega = 20.98\sqrt{1 - 503.6A^2}$$

The theoretical dependence between the amplitude and oscillation frequency is also shown in Figure 3.9. The figure shows that the experimental result is reasonably close to the theoretical. One reason for the difference is that the theoretical dependency is calculated for a stationary oscillation but the experiment is for a decaying oscillation.

Rotational acceleration

When the container is tilted it is obvious that the stationary surface elevation relative to the container wall is changed. The relation between

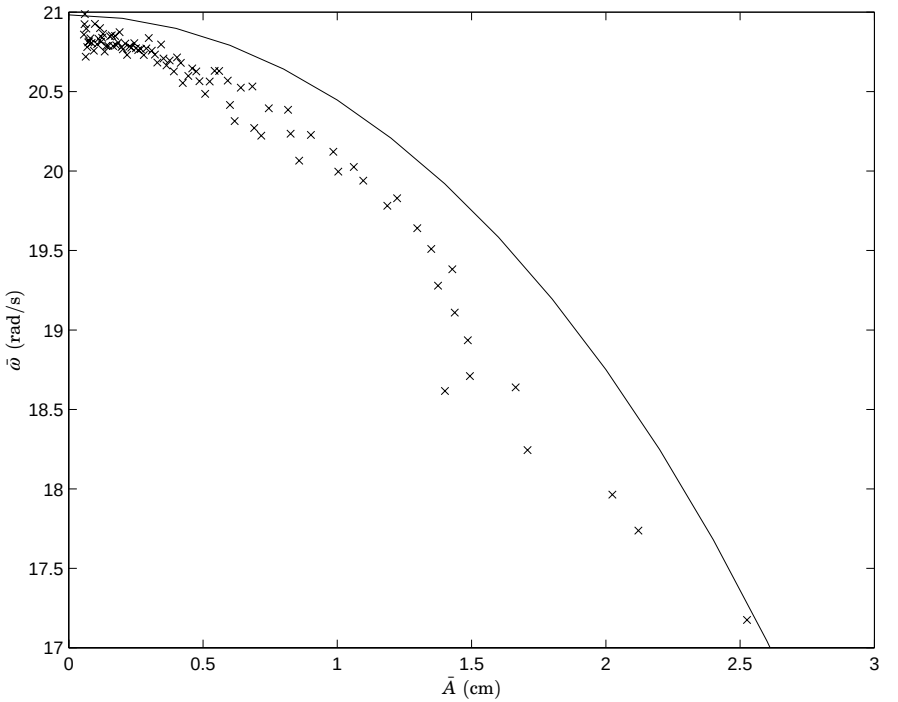

Figure 3.9 The oscillation frequency as a function of the oscillation amplitude. The solid line shows the theoretical dependence from (3.32) and the crosses shows the experimental values.

the angle of the container, θ, and the stationary surface elevation on the backward side of the container, s_0, at the wall is

$$s_0 = -\frac{a}{2}\tan\theta$$

where a is the container width. The stationary surface elevation on the forward side is the same but with opposite sign.

The response to rotational acceleration is examined for different positions of the rotational axis. The rotational axis is positioned in the center of the container horizontally and the distance y_r from the liquid surface vertically.

The following rotational acceleration u_r is applied for different values

of u_{max} and y_r

$$u_r(t) = \begin{cases} u_{max} & 0 \leq t < 0.1 \\ -u_{max} & 0.1 \leq t < 0.2 \\ 0 & 0.2 \leq t < 1.0 \\ -u_{max} & 1.0 \leq t < 1.1 \\ u_{max} & 1.1 \leq t < 1.2 \\ 0 & 1.2 \leq t < 2.0 \\ -u_{max} & 2.0 \leq t < 2.1 \\ u_{max} & 2.1 \leq t < 2.2 \\ 0 & 2.2 \leq t < 3.0 \\ u_{max} & 3.0 \leq t < 3.1 \\ -u_{max} & 3.1 \leq t < 3.2 \\ 0 & 3.2 \leq t < 4.0 \end{cases} \tag{3.33}$$

Figure 3.10 shows the results of the experiments for $u_{max} = [10, 20, 40]$ rad/s^2 and $y_r = [0, -1, \ldots, -6]$ cm, where 0 is on the surface and a negative value is below the surface. The figure shows that the smallest oscillation is obtained for $y_r = -3$ cm and that the response is relatively independent of u_{max}. For $y_r = -3$ cm only a small oscillation is visible and the change in surface elevation is mostly due to the tilting of the container. Note that the surface elevation is measured relative to the container.

To simplify the modeling it is desirable to have a decoupling between the rotational acceleration and surface oscillation. This can be obtained if the position of the rotational axis is chosen such that rotational acceleration gives the least excitation of the oscillation. Hence, the position of the rotational axis is chosen to be 3 cm below the liquid surface.

To explore if the response to simultaneous horizontal and rotational acceleration is linear, experiments were performed when the container was moved and tilted simultaneously. The horizontal acceleration $u_h(t)$ in (3.34) and the rotational acceleration $u_r(t)$ in (3.35) were applied for $a_{max} = [0, 0.5, 1]$ m/s^2 and $r_{max} = [0, 5, 10]$ rad/s^2. The rotational axis was positioned 3 cm below the surface during the experiments.

$$u_h(t) = \begin{cases} a_{max} & 0 \leq t < 0.4 \\ -a_{max} & 0.4 \leq t < 0.8 \\ 0 & 0.8 \leq t < 1.8 \\ -a_{max} & 1.8 \leq t < 2.2 \\ a_{max} & 2.2 \leq t < 2.6 \\ 0 & 2.6 \leq t < 3.6 \end{cases} \tag{3.34}$$

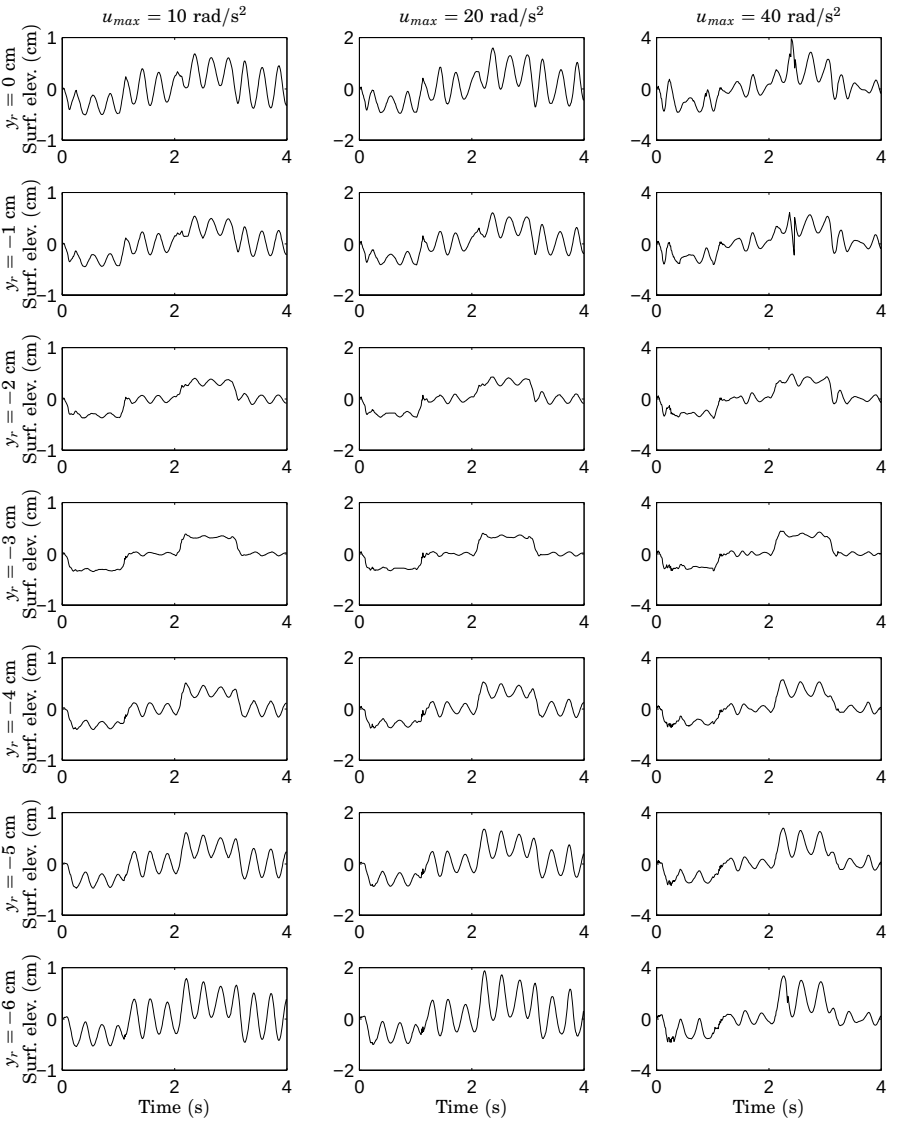

Figure 3.10 The surface elevation when the container is rotated using the rotational acceleration in (3.33) for different values of u_{max} and different vertical positions for the rotational axis y_r. The surface oscillation is very different for different rotational centers. The smallest oscillation is obtained when the rotational axis is 3 cm below the liquid surface at rest.

$$u_r(t) = \begin{cases} r_{max} & 0 \leq t < 0.1 \\ -r_{max} & 0.1 \leq t < 0.3 \\ r_{max} & 0.3 \leq t < 0.4 \\ -r_{max} & 0.4 \leq t < 0.5 \\ r_{max} & 0.5 \leq t < 0.7 \\ -r_{max} & 0.7 \leq t < 0.8 \\ 0 & 1.2 \leq t < 1.8 \\ -r_{max} & 1.8 \leq t < 1.9 \\ r_{max} & 1.9 \leq t < 2.1 \\ -r_{max} & 2.1 \leq t < 2.2 \\ r_{max} & 2.2 \leq t < 2.3 \\ -r_{max} & 2.3 \leq t < 2.5 \\ r_{max} & 2.5 \leq t < 2.6 \\ 0 & 2.6 \leq t < 3.6 \end{cases} \tag{3.35}$$

The previous investigation with only horizontal acceleration showed that the system behaves linearly only for small values of the excitation and of the oscillation amplitude. Therefore, only relatively small values of a_{max} and r_{max} were used.

The results of the experiments are shown in the figures 3.11 and 3.12. Figure 3.11 shows the surface elevation when the container is either moved or tilted and Figure 3.12 shows the surface elevation when the container is both moved and tilted simultaneously. Figure 3.12 also shows the superposition of the responses to only horizontal and rotational acceleration for comparison with the response when the corresponding references are used simultaneously. Figure 3.12 shows that the measured surface elevation when the references are used simultaneously is very close to the superposition of the responses when either a_{max} or r_{max} are zero. Hence, the response to horizontal and rotational acceleration can be considered to be independent if $u_h(t)$, $u_r(t)$ and the oscillation amplitude are small.

A simple way to model the surface elevation oscillation is using a second order poorly damped linear oscillator. The excitation of the oscillator is chosen as the horizontal and rotational acceleration. The surface elevation is then given as a sum of the oscillator output and the stationary surface elevation depending on the container angle. This gives the follow-

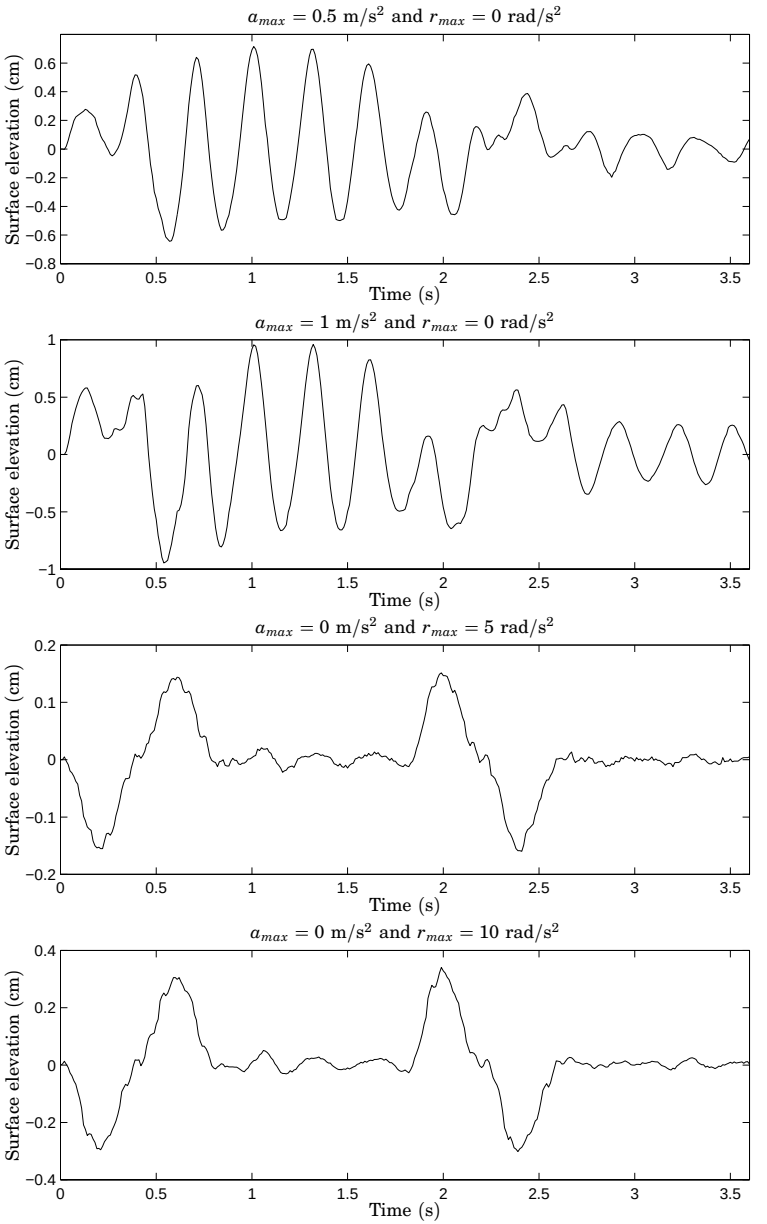

Figure 3.11 Surface elevation when the horizontal and rotational acceleration references in (3.34) and (3.35) are used for different values of a_{max} and r_{max}. The position of the rotational axis is $y_r = -3$ cm.

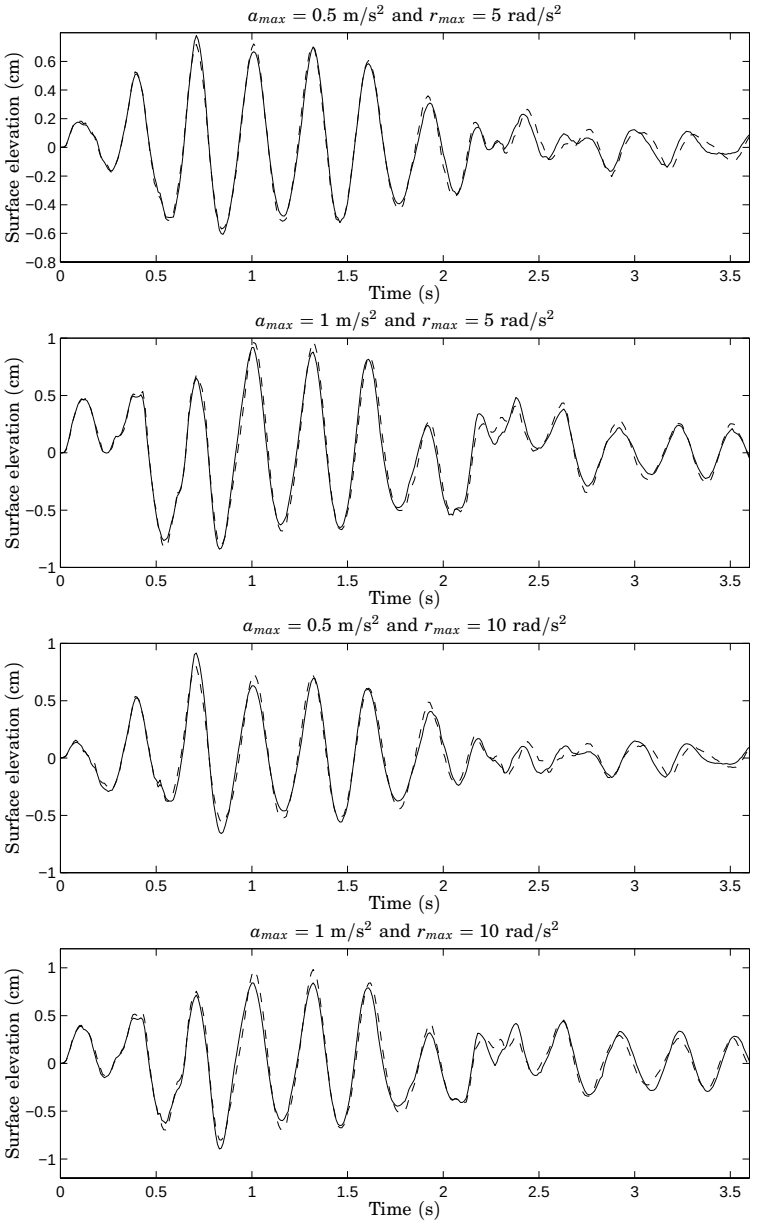

Figure 3.12 Surface elevation when the horizontal and rotational acceleration references in (3.34) and (3.35) are used for different values of a_{max} and r_{max}. The dashed line is the superposition of responses when the container is either moved or tilted with the corresponding acceleration reference. The simultaneous response is very close to the superposition of the responses with either a_{max} or r_{max} equal to 0. Hence, the response to horizontal and rotational acceleration is independent.

r_{max}	a_{max} (m/s^2)		
(rad/s^2)	0	0.5	1
0		$\omega = 20.9$ $\zeta = 0.409$E-3 $K_t = 3.49$E-3 $K_r = -$	$\omega = 20.7$ $\zeta = 6.75$E-3 $K_t = 2.89$E-3 $K_r = -$
5	$\omega = 20.3$ $\zeta = 25.6$E-3 $K_t = -$ $K_r = 2.51$E-6	$\omega = 20.9$ $\zeta = 5.47$E-3 $K_t = 2.85$E-3 $K_r = 39.2$E-6	$\omega = 20.8$ $\zeta = 8.26$E-3 $K_t = 2.77$E-3 $K_r = 10.2$E-6
10	$\omega = 20.1$ $\zeta = 22.3$E-3 $K_t = -$ $K_r = 2.35$E-6	$\omega = 20.9$ $\zeta = 5.68$E-3 $K_t = 2.89$E-3 $K_r = 19.9$E-6	$\omega = 20.7$ $\zeta = 12.2$E-3 $K_t = 2.82$E-3 $K_r = 8.71$E-6

Table 3.2 Estimated parameters for the model in (3.36) for the experiments shown in the figures 3.11 and 3.12. The control inputs used are given in (3.34) and (3.35) for a_{max} and r_{max} given in the table.

ing system description

$$\begin{bmatrix} \ddot{x} \\ \dot{x} \\ \ddot{\theta} \\ \dot{\theta} \end{bmatrix} = \begin{bmatrix} -2\zeta\omega & -\omega^2 & 0 & 0 \\ 1 & 0 & 0 & 0 \\ 0 & 0 & 0 & 0 \\ 0 & 0 & 1 & 0 \end{bmatrix} \begin{bmatrix} \dot{x} \\ x \\ \dot{\theta} \\ \theta \end{bmatrix} + \begin{bmatrix} K_t\omega^2 & K_r\omega^2 \\ 0 & 0 \\ 0 & 1 \\ 0 & 0 \end{bmatrix} \begin{bmatrix} u_h(t) \\ u_r(t) \end{bmatrix} \tag{3.36}$$
$$s(t) = x(t) - \frac{a}{2}\tan\theta(t)$$

The parameters ω, ζ, K_t and K_r in (3.36) were estimated using the System Identification Toolbox in Matlab for the different experiments. The estimated parameters are presented in Table 3.2.

The table shows that the estimates of ω, ζ and K_t are relatively consistent for all experiments and K_r is consistent for the experiments with only rotational movement. When the container is simultaneously moved and tilted the estimates of K_r are very inconsistent. This is probably because the oscillation caused by the horizontal acceleration is much larger than caused by the rotational acceleration.

To explore if the response is independent for other vertical positions of the rotational axis, experiments were made for the vertical positions $y_r = [-2, -3, -4]$ cm with $r_{max} = 10$ rad/s^2 and $a_{max} = [0, 1]$ m/s^2. The surface elevation response is shown in Figure 3.13 which also shows the

a_{max}	y_r (cm)		
(m/s^2)	-2	-3	-4
0	$\omega = 21.2$ $\zeta = 16.0$E-3 $K_t = -$ $K_r = -22.3$E-6	$\omega = 20.1$ $\zeta = 22.4$E-3 $K_t = -$ $K_r = 2.35$E-6	$\omega = 20.9$ $\zeta = 16.0$E-3 $K_t = -$ $K_r = 26.6$E-6
1	$\omega = 21.0$ $\zeta = 11.2$E-3 $K_t = 2.85$E-3 $K_r = -20.7$E-6	$\omega = 20.7$ $\zeta = 12.2$E-3 $K_t = 2.82$E-3 $K_r = 8.71$E-6	$\omega = 20.6$ $\zeta = 10.2$E-3 $K_t = 2.94$E-3 $K_r = 29.4$E-6

Table 3.3 Estimated parameters for the model in (3.36) for the experiments shown in Figure 3.13. The control inputs used are given in (3.34) and (3.35) for $r_{max} = 10$ rad/s^2 and a_{max} as given in the table. The experiments are performed for three vertical positions of the rotational axis as given in the table.

superposition of the responses to only horizontal and rotational acceleration. The figure shows that there is a large difference in the response to only rotational acceleration for the different positions of the rotational axis which was concluded previously in this section. The response to simultaneous translation and rotation is close to the superposition of the responses to only translation and rotation except when $y_r = -2$ cm where a small difference can be seen. However, the difference is not significant and the response to $u_h(t)$ and $u_r(t)$ seems to be quite independent.

Estimation of the parameters in (3.36) was made similarly as for the previous experiments and the results are presented in Table 3.3. The estimated parameters are very consistent except for K_r when $y_r = -3$ cm which were also seen in the previous experiments. When $y_r = -2$ cm or -4 cm the estimates of K_r are more consistent since there is more excitation of the oscillation through the rotation.

3.4 Analysis of vision data

Using the vision system presented in Section 2.3 a measurement of the surface shape can be made.

The data obtained from the vision system is the function $S(t, x)$ sampled both in time and in space, where $S(t, x)$ is the surface elevation at time t in the horizontal position x relative to the container. The sampling interval is $h_t = 20$ ms in time and $h_s = 0.133$ mm in space for this particular experiment. The container is 0.07 m wide which gives 526 data points

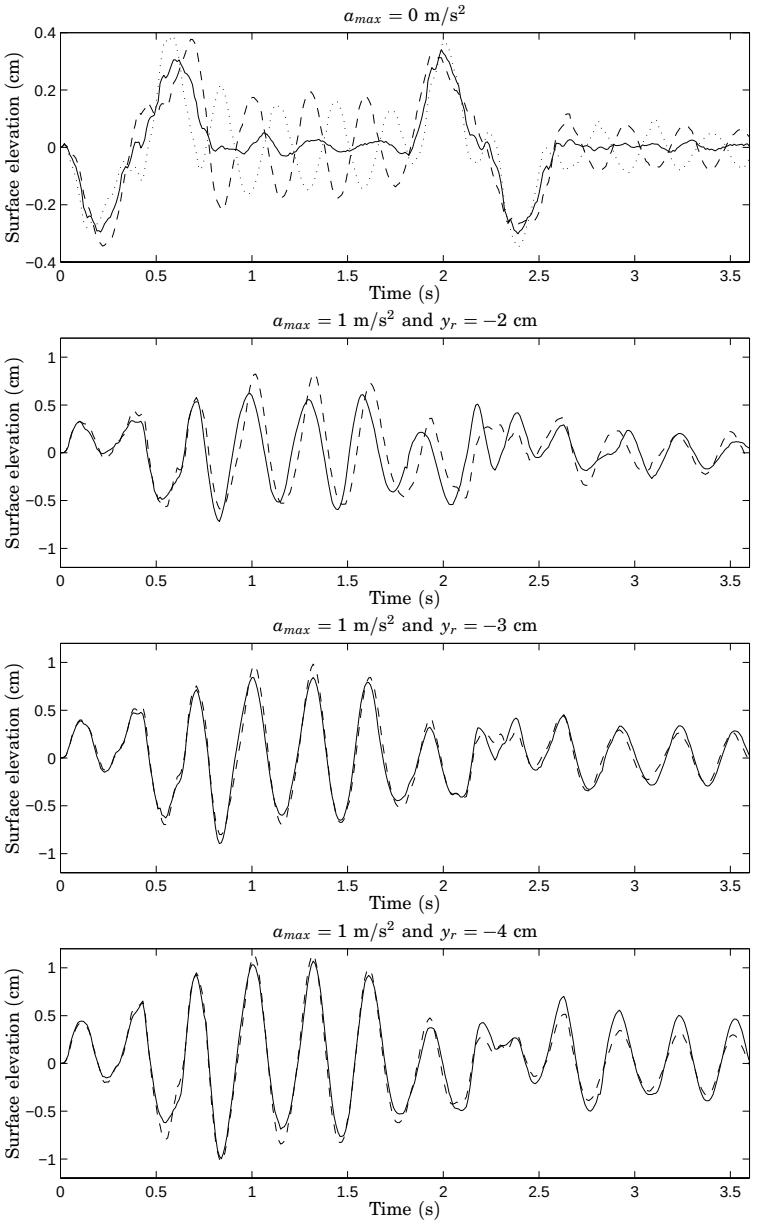

Figure 3.13 Surface elevation when the horizontal and rotational acceleration references in (3.34) and (3.35) are used for different values of a_{max} and y_r with $r_{max} = 10$ rad/s^2. The upper plot shows the response when $a_{max} = 0$ rad/s^2 and $y_r = -2$ cm (dotted), -3 cm (solid) and -4 cm (dashed) the three lower plots show the response when $a_{max} = 1$ rad/s^2 where the dashed line is the superposition of response to only horizontal and rotational acceleration.

and the duration of the experiment is 4 s which gives 200 data points. This gives the sampled surface elevation $S(kh_t, lh_s)$ with $k = 0, 1, \ldots, 199$ and $l = 0, 1, \ldots, 525$.

Figure 3.14 and Figure 3.15 show the surface elevation shape sampled in time with the sampling period 40 ms, hence twice the period time of the vision system. The acceleration reference used is given in (3.30) with $u_{max} = 2.0$ m/s^2. The figures show that the surface shape is quite irregular and far from a tilting plane or the first order mode $\cos \frac{\pi}{a} x$.

The models given in (3.26), (3.27) and (3.28) are based on separation of variables and describes the surface shape by

$$S(t, x) = \sum_{n=1}^{\infty} c_n(t) \cos \frac{n\pi}{a} x$$

where a is the width of the container. The behavior is then given by a system of differential equations in c_n.

Using the vision system a measurement of the surface shape is obtained and the coefficients $c_n(t)$ can be calculated for the actual surface shape. The coefficients are calculated using the following discrete approximation of the integral $c_n(t) = \frac{2}{a} \int_0^a s(t, x) \cos \frac{n\pi x}{a} \, dx$

$$c_n(kh_t) = \frac{2}{526} \sum_{l=0}^{525} S(kh_t, lh_s) \cos \frac{n\pi l}{525} \tag{3.37}$$

Figure 3.16 shows the amplitude of the six first modes as a function of time for this experiment. The figure shows that the first mode has the largest amplitude and that the amplitude decreases for the higher modes. For the linear model in (3.26) only the odd numbered modes are excited. However, the figure shows that all modes are excited. In Table 3.4 the maximum amplitude of the eight first modes normalized with the maximum of the first mode is given. The maximum amplitude decreases quite fast, approximately in the order of $1/n^2$, which is the same as for the linear model in (3.26).

In Figure 3.16 the oscillation of the first mode is not asymmetric which means that the asymmetric oscillation is caused by the excitation of the even numbered modes. Particularly the second mode which is the largest and mostly positive will raise the surface elevation on both sides of the container.

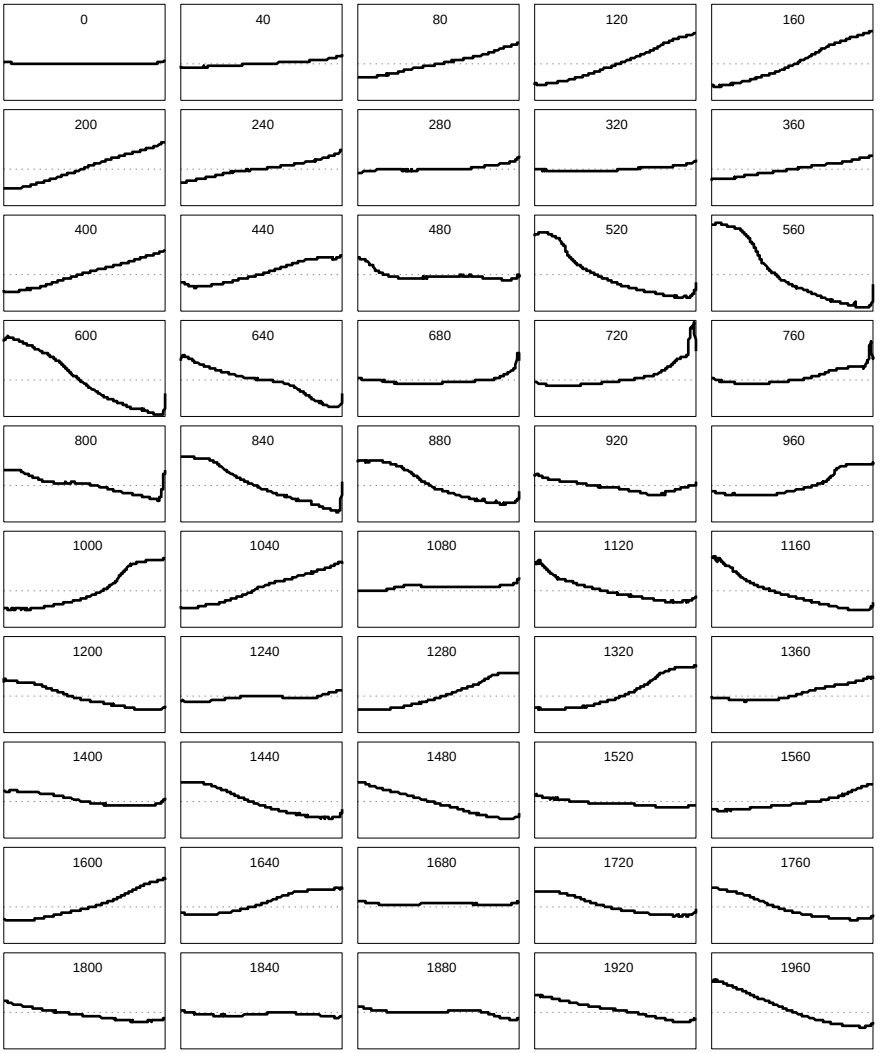

Figure 3.14 The surface profile when the acceleration reference in (3.30) is used with $u_{max} = 2$ m/s^2. Each frame shows the surface viewed from a direction perpendicular to the direction of movement, see Section 2.3. The number in the frame shows the time in milliseconds from the beginning of the movement. The scaling is equal in the x- and y-axis. The frame rate is 25 frames per second and the movement continues in Figure 3.15.

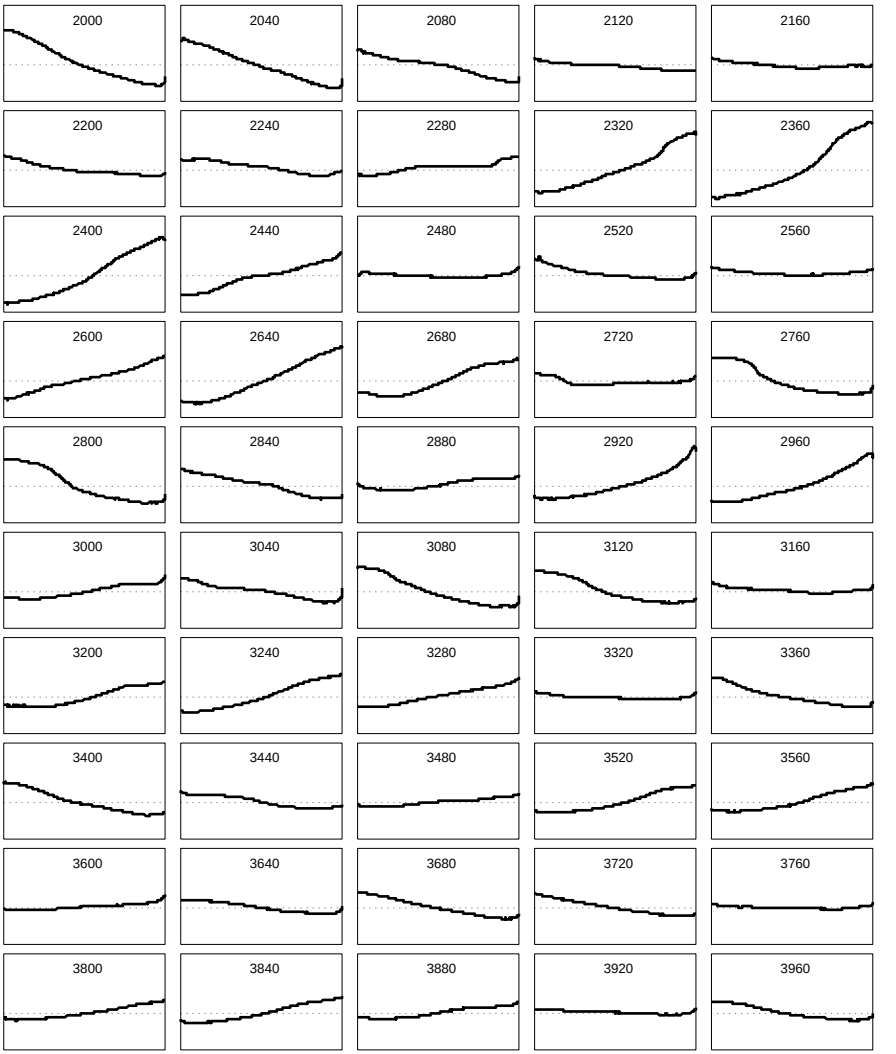

Figure 3.15 See Figure 3.14 for description.

n	1	2	3	4	5	6	7	8
$\frac{\max\|c_n(t)\|}{\max\|c_1(t)\|}$	1.00	0.28	0.12	0.10	0.06	0.06	0.04	0.04

Table 3.4 The maximum of the amplitude for the eight first modes calculated using (3.37). The maximum amplitude decreases fast as n is increased.

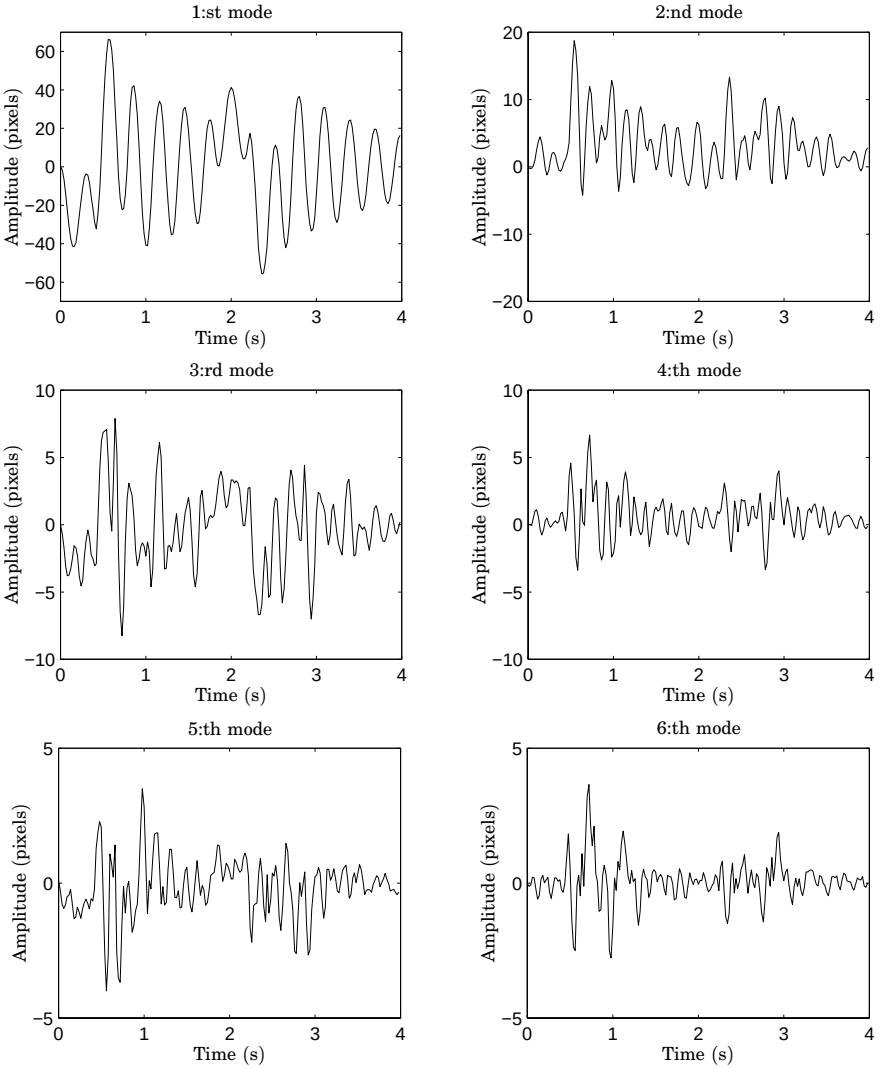

Figure 3.16 The amplitude of the six first modes given by (3.37). The amplitude is largest for the first mode and decreases for the higher modes. Note the different scales on the y-axes.

3.5 A simple usable model

Previously in this chapter models have been derived using fluid dynamics and using system identification. In this section the results are summarized and condensed into a simple model that can be used for controller synthesis.

The theoretical model in (3.26) is an infinite sum of oscillators with decaying gains and the analysis of the surface profile using the vision system shows that the amplitude of the higher order modes are decaying relatively fast. In the theoretical model in (3.26) only the odd numbered modes are excited. In the model derived by Miles in (3.28) the even numbered modes are excited through the nonlinear coupling with the other modes.

The examination of the surface profile using the vision system showed that the first mode has the largest amplitude and that the second mode is about one fourth and the third about one eight of the first mode, see Table 3.16.

The system identification performed in this chapter has shown that it is possible to get a good fit using a second order linear model for both horizontal and rotational acceleration.

Horizontal acceleration

The slosh response to horizontal acceleration is modeled by a second order poorly damped linear system with the states chosen as: x_2 – the surface elevation at the backward wall of the container and x_1 – the rate of change in the surface elevation divided by the oscillation frequency. This gives the following state space representation of the slosh model

$$\begin{bmatrix} \dot{x}_1 \\ \dot{x}_2 \end{bmatrix} = \begin{bmatrix} -2\zeta\omega & -\omega \\ \omega & 0 \end{bmatrix} \begin{bmatrix} x_1 \\ x_2 \end{bmatrix} + \begin{bmatrix} b_1 \\ 0 \end{bmatrix} u_h(t) \tag{3.38}$$

where ω is the oscillation frequency in radians per second, ζ the relative damping and $u_h(t)$ is the applied horizontal acceleration. The parameter b_1 can be determined by studying the stationary gain of the system. If the applied horizontal acceleration is equal to g the force field affecting the liquid is rotated 45° relative to the horizon. In stationarity the surface is flat and orthogonal to the force field. The stationary value of the surface elevation is then $a/2$ where a is the width of the container. Insertion of the stationary values in (3.38) gives

$$\begin{bmatrix} 0 \\ 0 \end{bmatrix} = \begin{bmatrix} -2\zeta\omega & -\omega \\ \omega & 0 \end{bmatrix} \begin{bmatrix} 0 \\ \frac{a}{2} \end{bmatrix} + \begin{bmatrix} b_1 \\ 0 \end{bmatrix} g \quad \Longrightarrow \quad b_1 = \frac{a\omega}{2g}$$

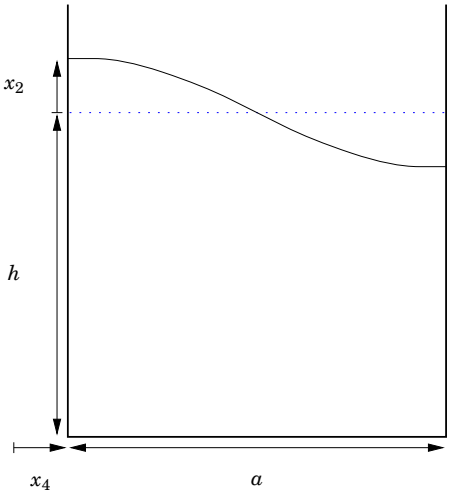

Figure 3.17 Illustration of the container corresponding to the model in (3.39).

The motion of the container is modeled by a double integrator. It is assumed that the motion control system follows the acceleration reference exactly. This gives the complete container model for horizontal acceleration

$$\begin{bmatrix} \dot{x}_1 \\ \dot{x}_2 \\ \dot{x}_3 \\ \dot{x}_4 \end{bmatrix} = \underbrace{\begin{bmatrix} -2\zeta\omega & -\omega & 0 & 0 \\ \omega & 0 & 0 & 0 \\ 0 & 0 & 0 & 0 \\ 0 & 0 & 1 & 0 \end{bmatrix}}_{A} \begin{bmatrix} x_1 \\ x_2 \\ x_3 \\ x_4 \end{bmatrix} + \underbrace{\begin{bmatrix} \frac{a\omega}{2g} \\ 0 \\ 1 \\ 0 \end{bmatrix}}_{B} u_h(t) \tag{3.39}$$

$$\begin{bmatrix} s \\ p \end{bmatrix} = \begin{bmatrix} 0 & 1 & 0 & 0 \\ 0 & 0 & 0 & 1 \end{bmatrix} x$$

where x_4 is the container position and x_3 the container velocity. The outputs of the model are the surface elevation relative to the container wall, s, and the container position, p. See Figure 3.17 for an illustration of the container.

For a rectangular container with liquid depth h and width a the oscillation frequency is given by (3.25)

$$\omega = \omega_1 = \sqrt{\frac{g\pi}{a} \tanh \frac{h\pi}{a}}$$

The container used in the experiments has $h = 0.2$ m and $a = 0.07$ m which gives the theoretical value $\omega = 21.0$ rad/s. This is approximately the same value as the experiments showed for small oscillation amplitudes, see Table 3.1 and Figure 3.9. The theoretical value of the damping is $\zeta = 0$ but the experiments showed that the damping is about 0.015.

Horizontal and rotational acceleration

The previous examinations of the response to rotational acceleration showed that the response depends on the position of the rotational axis and that the coupling to the response from horizontal acceleration is small.

The slosh is modeled in the same way as for only horizontal acceleration with a second order linear system. With the inputs horizontal and rotational acceleration and the states are chosen as: x_2 – the surface elevation relative to the horizon at the backward wall of the container, x_1 – that rate of change in surface elevation divided by the oscillation frequency, x_4 – the container position, x_3 – the container velocity, x_6 the container angle and x_5 – the angular velocity. The container angle, x_6, changes the stationary surface elevation relative to the container wall as

$$s_0 = -\frac{a}{2}\tan x_6$$

This gives the complete container model for horizontal and rotational acceleration

$$\begin{bmatrix} \dot{x}_1 \\ \dot{x}_2 \\ \dot{x}_3 \\ \dot{x}_4 \\ \dot{x}_5 \\ \dot{x}_6 \end{bmatrix} = \underbrace{\begin{bmatrix} -2\zeta\omega & -\omega & 0 & 0 & 0 & 0 \\ \omega & 0 & 0 & 0 & 0 & 0 \\ 0 & 0 & 0 & 0 & 0 & 0 \\ 0 & 0 & 1 & 0 & 0 & 0 \\ 0 & 0 & 0 & 0 & 0 & 0 \\ 0 & 0 & 0 & 0 & 1 & 0 \end{bmatrix}}_{A} \begin{bmatrix} x_1 \\ x_2 \\ x_3 \\ x_4 \\ x_5 \\ x_6 \end{bmatrix} + \underbrace{\begin{bmatrix} \frac{a\omega}{2g} & b_2 \\ 0 & 0 \\ 1 & 0 \\ 0 & 0 \\ 0 & 1 \\ 0 & 0 \end{bmatrix}}_{B} \begin{bmatrix} u_h(t) \\ u_r(t) \end{bmatrix}$$

$$\begin{bmatrix} s \\ p \\ \theta \end{bmatrix} = \begin{bmatrix} 0 & 1 & 0 & 0 & 0 & 0 \\ 0 & 0 & 0 & 1 & 0 & 0 \\ 0 & 0 & 0 & 0 & 0 & 1 \end{bmatrix} x + \begin{bmatrix} -\frac{a}{2}\tan x_6 \\ 0 \\ 0 \end{bmatrix} \tag{3.40}$$

where the same values of ω and ζ as for the model for horizontal acceleration applies, $u_h(t)$ is the applied horizontal acceleration and $u_r(t)$ is the applied rotational acceleration. The parameter b_2 depends on the position of the rotational axis and can take both positive and negative values, see Table 3.3. The outputs of the model are the surface elevation relative to the container wall, s, the container position, p, and the container angle, θ. See Figure 3.18 for an illustration of the container.

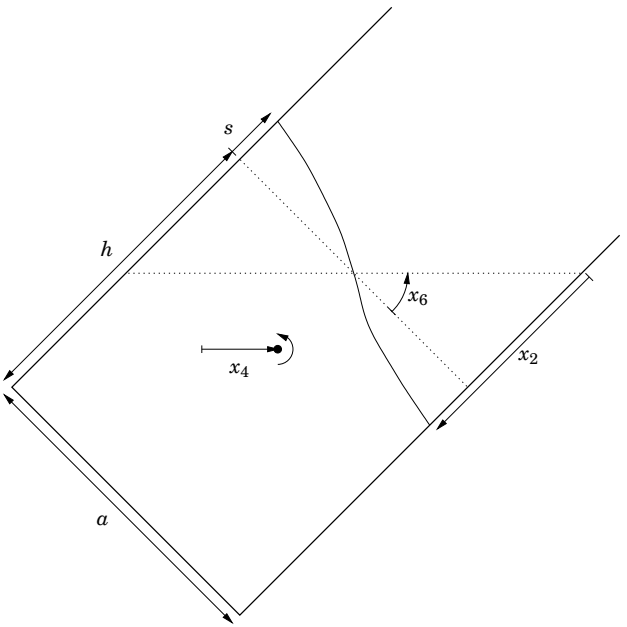

Figure 3.18 Illustration of the container corresponding to the model in (3.40).

4

Horizontal motion

This chapter describes different methods of calculating an acceleration reference that meets the specifications using optimal control and the simple linear model in (3.39) presented in Section 3.5.

Section 4.1 describes how the problem has been approached in industry. Related work is presented in Section 4.2. The problem is formulated as an optimal control problem in Section 4.3. Minimum time solutions are given in the sections 4.4 and 4.5. However, these acceleration references prove to work for small slosh amplitudes only. Therefore, as an alternative approach, a minimum energy solution is given in Section 4.6. In Section 4.7 an analytical solution is given to a modified version of the minimum energy problem. Each of the previous mentioned sections contains experimental evaluations of the described acceleration strategy. In Section 4.8 some implementation issues are discussed and in Section 4.9 the minimum energy problem is solved for the discrete time case. The chapter is summarized with the conclusions in Section 4.10

4.1 Industrial practice

The acceleration references have traditionally been implemented using mechanical devices such as gear boxes and cam discs. This has resulted in very inflexible systems where the acceleration reference cannot easily be altered. Therefore, the acceleration references have been designed such that they fulfill the specifications for a whole range of products and production rates. Since the fluid dynamics are very different for different products (compare for example skim milk with yoghurt) this has lead to conservative and non-optimal acceleration references, i.e. slow movement and reduced production capacity.

The introduction of servo systems to control the movement offers an increased amount of flexibility. It is now possible to use different accel-

eration references for different products and production rates. This has given rise to an increased interest in systematic methods for calculation of acceleration references for the movement.

The solution, up till now, has been to use a predetermined structure of the acceleration reference with a few parameters that have proven to work and is easy to implement using the mechanical devices. The parameters are tuned using experiments and the experience of the development engineers. This procedure is very time consuming and expensive and often leads to a conservative design, since the easiest way to decrease the slosh if it is too large is to slow down the movement.

4.2 Related work

In this section some related work is presented. The major difference between previous work and the work presented in this thesis is that here a large amount of slosh is allowed and the goal is to move as fast as possible.

In [Yano *et al.*, 1996] the problem is approached using optimal control and H^∞ control theory. The slosh is modeled as a pendulum with damping. A reference trajectory for the position and the surface elevation is calculated by solving a nonlinear optimal control problem. An H^∞ feedback controller designed for the linearized model is used which measures both the position and the surface elevation in the container. The H^∞ controller is used because there are large differences in the behavior for different liquid depths and the H^∞ controller is believed to also be able to deal with other model uncertainties.

The method is evaluated in experiments with good results. The oscillation frequency of the liquid in the container is between 11.3 rad/s and 15.1 rad/s depending of the liquid depth. The maximum acceleration for the experiments are 2 m/s^2, the movement time is 3 s, the movement distance is 1 m and the ratio between maximum surface elevation and the container width is 0.1.

A notch-filter solution to the slosh-free movement problem is suggested in [Feddema *et al.*, 1997]. The approach is based on a second order linear slosh model, similar to the one described in Section 3.5. The acceleration reference is obtained by filtering an acceleration reference which is determined to move the container as fast as possible without any constraints on the slosh. This acceleration reference is given by the bang-bang signal

$$u(t) = \begin{cases} u_{max} & 0 \leq t < t_s \\ -u_{max} & t_s \leq t < 2t_s \\ 0 & 2t_s \leq t \end{cases} \tag{4.1}$$

where $t_s = \sqrt{L/u_{max}}$. The acceleration reference in (4.1) is then filtered through the following notch-filter

$$G_f(s) = \frac{\sigma^3}{\omega^2} \frac{s^2 + 2\zeta\omega s + \omega^2}{(s+\sigma)^3}$$

where ω and ζ have the same values as in the slosh model given in (3.39). The idea is to avoid excitation of the oscillatory mode of the liquid.

The acceleration strategy is evaluated in experiments with good results. The oscillation frequency of the container is 10.6 rad/s, the maximum acceleration is 0.75 m/s^2, the movement time is 2.3 s, the movement distance is 0.5 m and the ratio between the maximum surface elevation and the container width is 0.04.

Figure 4.1 shows simulations with this acceleration strategy applied to our system for some different response speeds of the filter, with $\omega =$ 21.0 rad/s, $\zeta = 0$, movement distance 0.2 m. The figure shows that the movement time is considerably increased for $\sigma = 30$ rad/s and $\sigma =$ 54 rad/s gives a very large maximum acceleration.

The primal objective in the two approaches presented in [Yano *et al.*, 1996] and [Feddema *et al.*, 1997] is to have as little slosh as possible and ultimately no slosh at all. Therefore, the strategies are only evaluated at slosh levels much smaller than considered in this thesis. Compared to our case the ratio between the maximum surface elevation and container width is small, 0.1 and 0.04 respectively compared to 0.5 in the case considered here. In order to suppress the slosh even more, movement strategies where the container is tilted are examined in [Feddema *et al.*, 1997], [Yano *et al.*, 1999] and in Chapter 6.

In [Dietze and Schmidt, 1997] the problem is solved using optimal control techniques and the same slosh model as presented in Section 3.5. In the optimization the control signal is discretized and the cost function

$$\frac{\alpha^2}{2}[s^2(T) + \dot{s}^2(T)] + \frac{\beta^2}{2}\int_0^T u^2(t)\, dt$$

where s is the surface elevation and u is the acceleration, is numerically minimized for different values of α and β with constraints on $|u(t)|$ and trajectory constraints on $s(t)$. This approach is very similar to the one presented in Section 4.6. No experimental results are presented in the report.

In [Dubois *et al.*, 1999] the slosh is modeled by the linearized Shallow Water Equations. It is shown that the surface can be parameterized by the horizontal coordinate of a particular point in the system, the fully flat output, and a periodic function. It is also shown that the system is

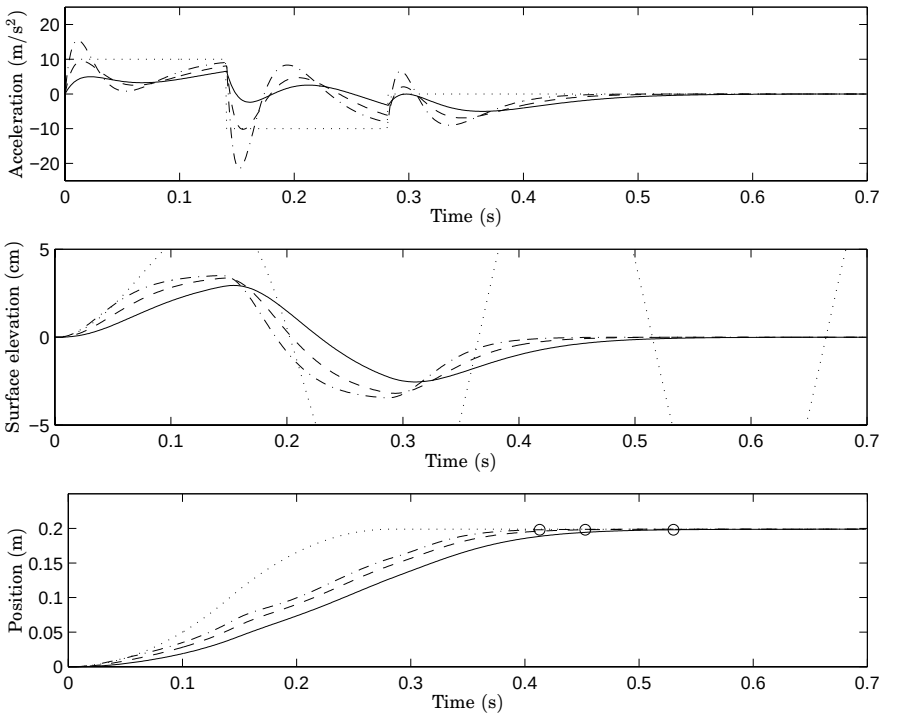

Figure 4.1 Simulations with the notch-filter acceleration reference. Response of the bang-bang acceleration (dotted), $\sigma = 54$ rad/s (dash-dotted), $\sigma = 42$ rad/s (dashed) and $\sigma = 30$ rad/s (solid). The circles in the position diagram show when the position is 0.198 m for the different values of σ. The movement time is increased for small values of σ and the peaks in the acceleration reference is increased for large values of σ.

not controllable but it is possible to control the system from one steady state to another steady state. The acceleration reference is obtained by finding a control that connects two steady states. The calculated acceleration reference is simulated using the nonlinear model, which works for small slosh amplitudes but the performance degrades as movement time is decreased and the slosh amplitude increases. The use of the shallow water equations limits this solution to containers where the liquid depth is much smaller than the container width and the method is therefore of limited practical use.

Another field that is closely related is anti-swing control of overhead and rotary cranes, see [Mårtensson, 1972], [Gustafsson, 1995] and [Lee

et al., 1997]. The swinging load is typically modeled as a pendulum. Linearization of the pendulum gives the same model as the one presented in Section 3.5. The main difference is that the angle of the pendulum is often measured and used for feedback.

4.3 Optimal control

Several different methods for calculation of acceleration references are presented in this and the following sections. All methods are based on optimal control of the simple linear slosh model presented in Section 3.5. The proposed optimal control problems are solved either numerically or analytically. The calculated acceleration references are evaluated using experiments.

The control problem

The problem is to move the container from the filling station to the sealing station of the packaging machine. This movement is performed repeatedly where the same acceleration reference is applied in every step. The number of movement steps is typically between 3 and 5. Between each movement step the package must be standing still while the package is filled. During the movement the surface elevation at the walls of the package must be below a certain level.

This problem can be solved using optimal control techniques although it is not straight forward since the control input is repeated several times. Also the acceleration reference will depend on the number of steps and the time between the movement steps. Hence, if the filling time is decreased the acceleration reference needs to be recalculated.

By introducing additional constraints the acceleration reference can be made independent of the number of steps and the time between the steps. By ensuring that the slosh is at rest in the beginning of each movement step the slosh response will be the same in all steps. If the slosh is at rest at the end of each step it will also be at rest at the beginning of the next step. This will result in a standard optimal control problem.

The constraints

The constraints used when solving the optimal control problems are

C1. Acceleration: $|u(t)| \leq u_{max}$

C2. Surface elevation: $|x_2(t)| \leq s_{max}$

C3. Initial state: $x(0) = [\,0 \quad 0 \quad 0 \quad 0\,]^T$

C4. Terminal state: $x(T) = [\,0 \quad 0 \quad 0 \quad L\,]^T$

where T is the movement time for one step and L is the length of one step.

The movement distance $L = 0.2$ m is used in all simulations and experiments. The maximum surface elevation $s_{max} = 0.035$ m is used where nothing else is mentioned. This corresponds to a 45 degree surface elevation angle relative to the horizon.

Stored internal slosh

A measure of the energy stored within the oscillation is introduced and denoted the stored internal slosh.

DEFINITION 4.1
If $s(t)$ denotes the surface elevation and $\dot{s}(t)$ its time derivative the stored internal slosh $s_i(t)$ is defined as

$$s_i(t) = \sqrt{s(t)^2 + \left(\frac{\dot{s}(t)}{\omega}\right)^2} = \sqrt{x_1(t)^2 + x_2(t)^2}$$

The stored internal slosh represents the amplitude of the oscillation at time t when $u = 0$ and $\zeta = 0$ for the model in (3.39).

Proof: When $u = 0$ and $\zeta = 0$ the the surface oscillation can be written as $s(t) = A \sin \omega t$ where A is the oscillation amplitude. Differentiation gives $\dot{s}(t) = \omega A \cos \omega t$. This gives the stored internal slosh

$$s_i(t) = \sqrt{A^2 \sin^2 \omega t + A^2 \cos^2 \omega t} = A$$

hence the surface oscillation amplitude. □

4.4 Minimum time solution

The natural approach is to solve a minimum time problem since the goal is to move a fast as possible. The minimum time acceleration reference is found by minimizing the following cost function J with respect to T subject to the constraints C1–C4 and the slosh model in (3.39), where

$$J = \int_0^T 1 \, dt$$

Numerical solution

A numerical solution to the optimal control problem is obtained using the Matlab toolbox RIOTS (Recursive Integration Optimal Trajectory Solver), see [Schwartz and Polak, 1996].

RIOTS can only solve fixed time optimal control problems. Therefore, the variable-time minimum time problem has to be transformed to a fixed time problem. This can be done by augmenting the system with a constant state that scale the dynamics and represents the terminal time. The system now becomes

$$\begin{aligned} \dot{x}(t) &= (Ax(t) + Bu(t))z(t) \\ \dot{z}(t) &= 0 \end{aligned}$$

and the cost function becomes

$$J = z(T)$$

If this problem is solved with $T = 1$ the minimum time will be $T_{opt} = z(T)$.

The numerical minimum time solution is shown in Figure 4.2 for three values of u_{max} and the movement times are given in Table 4.1. The solution is of bang-bang type where the acceleration switches either between four different values $\pm u_{max}$ and $\pm u_{con}$ when u_{max} is greater than u_{con} or otherwise between $\pm u_{max}$, where $u_{con} = 2s_{max}g/a$ is the acceleration needed to keep the surface elevation on the boundary of the constraint C2.

Calculation of switching times

Experience shows that if $u_{max} \geq 2s_{max}g/a$ then the time optimal acceleration profile can be divided into five independent operations:

1. Bring the surface up to the level s_{max} as fast as possible with $\dot{s} = 0$ at the end.
2. Keep the surface at level s_{max}.

u_{max} (m/s^2)	T_{opt} (ms)
4.90	433
9.81	383
19.62	353
∞	286

Table 4.1 The minimum movement times from the solution of the minimum-time problem, $L = 0.2$ m, $s_{max} = 3.5$ cm and $\omega = 21.0$ rad/s. Simulations of the solutions are shown in Figure 4.2.

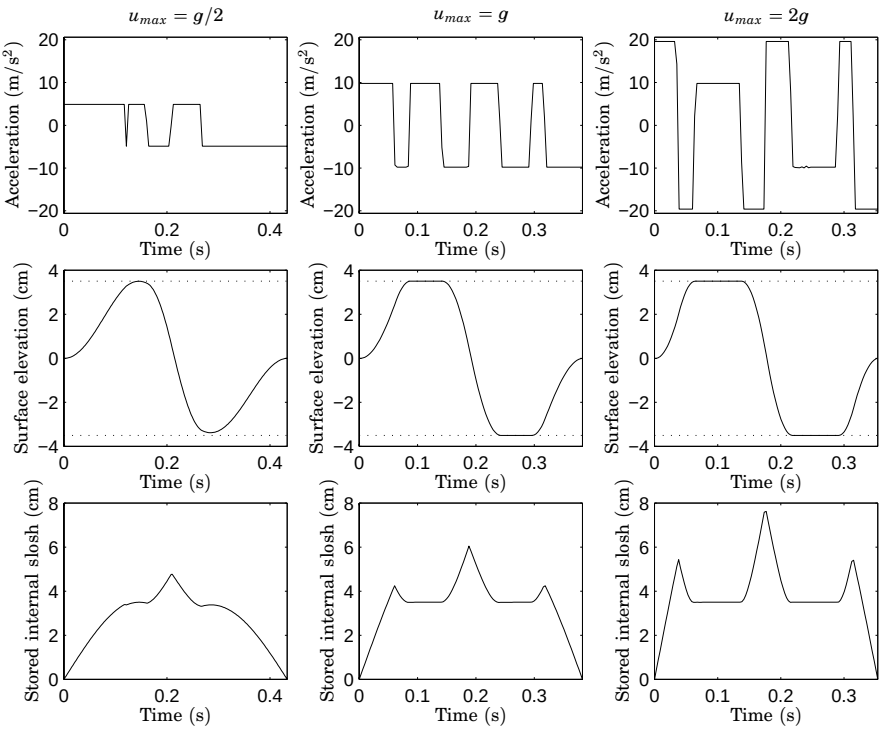

Figure 4.2 Numerical solution of the minimum time problem, with $u_{max} = g/2$ (left), $u_{max} = g$ (center) and $u_{max} = 2g$ (right). The movement distance is $L = 0.2$ m and the maximum allowed surface elevation is $s_{max} = 3.5$ cm. The resulting movement times are $T = 433$ ms, $T = 383$ ms and $T = 353$ ms respectively.

3. Move the surface from s_{max} to $-s_{max}$ as fast as possible with $\dot{s} = 0$ at the end.
4. Keep the surface at level $-s_{max}$.
5. Bring the surface to 0 as fast as possible with $\dot{s} = 0$ at the end.

The acceleration profile can be parameterized as

$$u(t) = \begin{cases} u_{max} & 0 \le t < t_1 \\ -u_{max} & t_1 \le t < t_2 \\ u_{con} & t_2 \le t < t_3 \\ -u_{max} & t_3 \le t < t_4 \\ u_{max} & t_4 \le t < t_5 \\ -u_{con} & t_5 \le t < t_6 \\ u_{max} & t_6 \le t < t_7 \\ -u_{max} & t_7 \le t < T \end{cases}$$

where $u_{con} = 2s_{max}g/a$ is the acceleration needed to keep the surface at the constant level s_{max}. The switching times can be parameterized as $t_1 = d_1$, $t_2 = t_1 + d_2$, $t_3 = t_2 + d_3$, $t_4 = t_3 + d_4$, $t_5 = t_4 + d_4$, $t_6 = t_5 + d_3$, $t_7 = t_6 + d_2$ and $T = t_7 + d_1$. Now the durations d_1, d_2 and d_4 can be obtained from the solutions of the differential equation

$$\dot{x} = \begin{bmatrix} 0 & -\omega \\ \omega & 0 \end{bmatrix} x + \begin{bmatrix} a\omega/2g \\ 0 \end{bmatrix} u \tag{4.2}$$

where the damping is neglected ($\zeta = 0$).

Solving (4.2) with the boundary values $x(0) = [\,0 \quad 0\,]^T$ and $x(t_2) = [\,0 \quad s_{max}\,]^T$ gives

$$d_1 = \frac{1}{\omega} \arccos\left(2\cos(2d_2) - \frac{u_{max} + u_{con}}{u_{max}}\right) - d_2$$
$$d_2 = \frac{1}{\omega} \arccos\left(\frac{4u_{max}^2 + 2u_{max}u_{con} + u_{con}^2}{4u_{max}^2 + 4u_{max}u_{con}}\right)$$

Solving (4.2) with the boundary values $x(t_3) = [\,0 \quad s_{max}\,]^T$ and $x(t_5) = [\,0 \quad -s_{max}\,]^T$ gives

$$d_4 = \frac{1}{\omega} \arccos\left(\frac{u_{max}}{u_{max} + u_{con}}\right)$$

The duration d_3 is obtained by solving $\ddot{y} = u$ with the boundary values $\dot{y}(0) = 0$, $y(0) = 0$ and $\dot{y}(T) = 0$, $y(T) = L$, which gives

$$d_3 = \frac{1}{u_{con}}\Big(u_{max}(d_2 - d_1) - u_{con}d_4 + [u_{max}^2(d_2 - d_1)^2 + u_{max}u_{con}(d_2^2 - 2d_1d_2 - d_1^2 + d_4^2) + u_{con}^2 d_4^2 + u_{con}L]^{\frac{1}{2}}\Big)$$

The calculated switching times correspond well with the numerical solutions of the problem.

Now the theoretical minimum movement time if there is no constraint of the control signal can be calculated. The limit of d_1, d_2, d_3 and d_4 can be calculated as u_{max} tends to infinity. This gives $d_1 = 0$, $d_2 = 0$, $d_3 = \sqrt{L/u_{con}}$ and $d_4 = 0$.

Figure 4.3 shows the movement time for different values of u_{max}. The minimum movement time for movement disregarding the slosh is also shown. The figure shows that when u_{max} is greater than 5 m/s^2 only a small decrease in movement time is achieved if u_{max} is increased.

Experimental evaluation of the minimum time strategy

Practical evaluations of the minimum-time strategy in the experimental setup have shown that the strategy only works well for small values of s_{max} and u_{max}. For larger values the surface is not a rest at the end of the movement and the maximum slosh is much larger than s_{max}. Since we want to evaluate the strategy when the slosh constraint is active, s_{max} is chosen such that $u_{con} = u_{max}$ this gives $s_{max} = \frac{a}{2g}u_{max}$. The movement times for the different acceleration references are shown in Table 4.2.

Typical results of the experiments are shown in Figure 4.4. The figure shows that for small values of u_{max} the slosh roughly corresponds to the calculated slosh shown in Figure 4.2 except for a high frequency oscillation. However, as u_{max} is increased the performance is drastically degraded.

One reason for this could be the amplitude dependent oscillation frequency, see Section 3.3. To explore this, experiments were done with acceleration profiles calculated for different values of ω. However, this lead to no improvements.

Insight into why the performance degrades can be obtained by studying the stored internal slosh s_i shown in Figure 4.2. The figure shows that in the middle of the movement, s_i is first increased and then decreased. This pumping of energy in and out of the system requires a very accurate model to be successful. From Figure 4.4 we also see that the largest deviations appear in the middle of the movement.

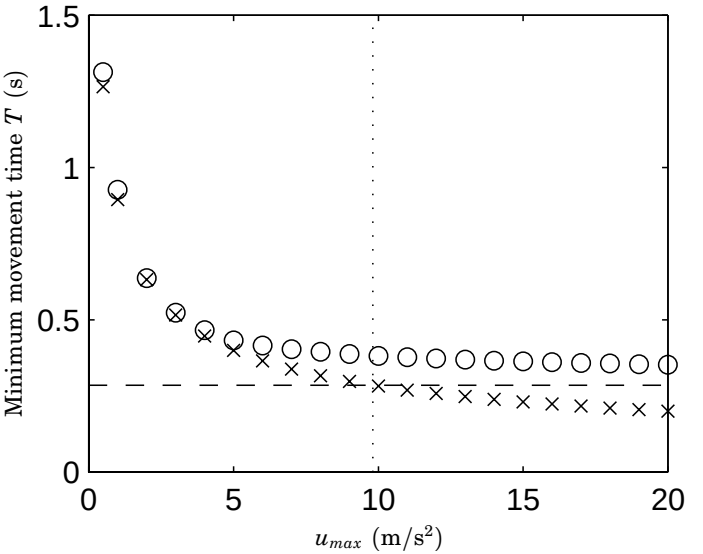

Figure 4.3 The minimum movement time for different values of u_{max} with $L = 0.2$ m, $s_{max} = 3.5$ cm and $\omega = 21.0$ rad/s; taking the slosh into account ($\circ$) and disregarding the slosh ($\times$). The dotted line shows the value of u_{con} and the dashed line shows the value of the theoretical minimum movement time $T = 2\sqrt{L/u_{con}} = 286$ ms when $u_{max} = \infty$ taking the slosh into account. See also Table 4.1.

u_{max} (m/s^2)	0.5	1	1.5	2	2.5	3	3.5	4
T (ms)	1361	991	827	729	662	613	575	544

Table 4.2 The minimum movement times for the different values of u_{max}, with $L = 0.2$ m, $s_{max} = au_{max}/(2g)$ and $\omega = 21.0$ rad/s.

4.5 Modified minimum time solution

To avoid the problems experienced in Section 4.4 an additional constraint is added. The excessive peaking of the stored internal slosh can be limited by adding the constraint

C5. Stored internal slosh: $s_i(t) = \sqrt{x_1^2(t) + x_2^2(t)} \leq i_{max}$

The same cost function as in the original minimum time problem is now minimized subject to the constraints C1–C5 and the slosh model in (3.39).

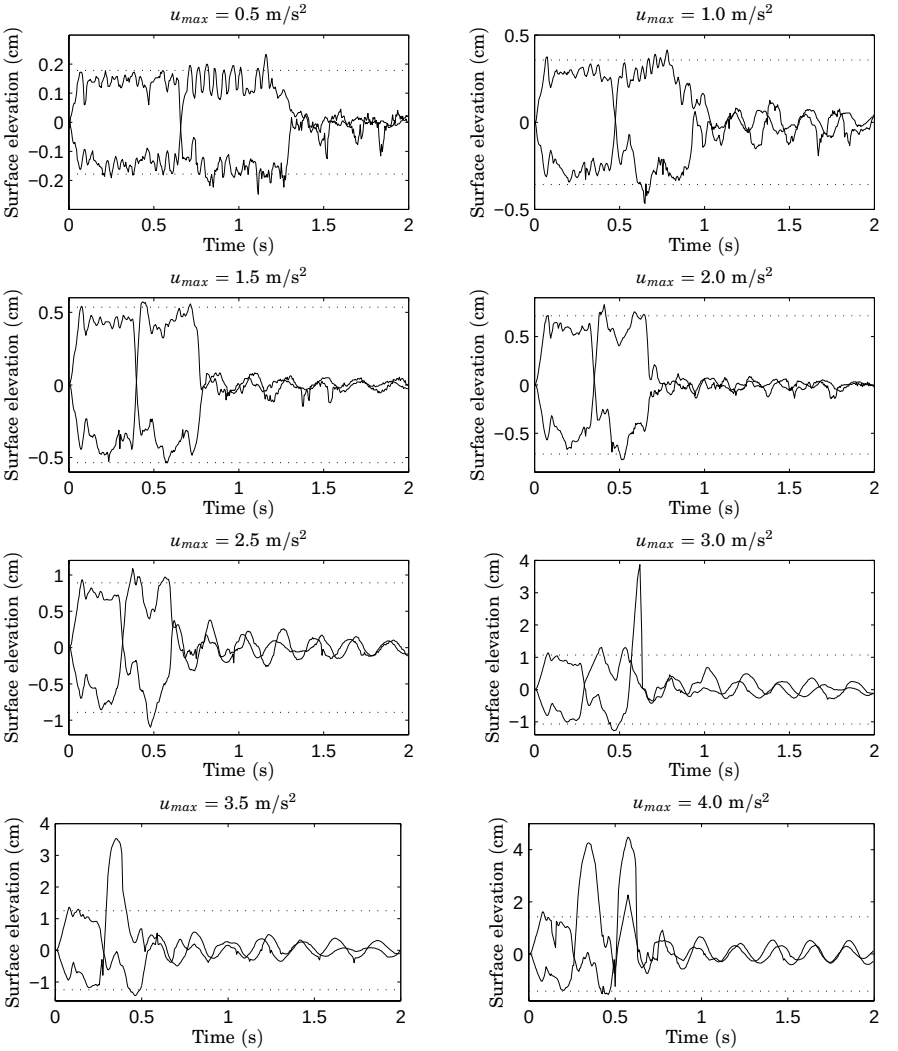

Figure 4.4 Data from experiments with the minimum-time acceleration profile for movement in several steps for varying values of the maximum acceleration. The dotted lines show $\pm s_{max} = \pm \frac{a}{2g} u_{max}$. Each plot shows two experiments, one with the sensor in the front and one with the sensor in the back of the container. The results are good for small values of u_{max} but for larger values of u_{max} the performance degrades. See Table 4.2 for the movement times.

u_{max} (m/s^2)	i_{max} (cm)	T (ms)
4.90	3.5	436
	3.75	435
	5.5	434
9.81	3.5	390
	3.75	387
	5.5	383
19.62	3.5	368
	3.75	364
	5.5	354

Table 4.3 The minimum movement times from the numerical solution of the modified minimum time problem, $L = 0.2$ m, $s_{max} = 3.5$ cm and $\omega = 21.0$ rad/s. Compare with the movement times from the original minimum time problem in Table 4.1. The constraint on the stored internal slosh leads to a slight increase in the movement time.

Numerical solution

The modified minimum time problem is solved in the same way as the original minimum time problem. The numerical solutions are shown in the figures 4.5, 4.6 and 4.7 for three different values of i_{max}. The movement times are shown in Table 4.3.

Compared to the original minimum time problem the movement times are only slightly increased. When $i_{max} = 3.5$ cm the peaks in the stored internal slosh are eliminated and the movement times are the longest. The movement times are increased with 0.5 %, 1.8 % and 4.2 % respectively with $u_{max} = g/2$, g and $2g$.

Calculation of switching times

The modified minimum time acceleration profile is built up by the same five independent operations as the original minimum time acceleration reference when $u_{max} \geq 2s_{max}g/a$ and $i_{max} \geq s_{max}$, experience shows that each operation is divided into sub operations to deal with the extra constraint:

1. Bring the surface up to the level s_{max} as fast as possible with $\dot{s} = 0$ at the end.

   i Bring the stored internal slosh up to i_{max}.

   ii Keep the stored internal slosh at i_{max}.

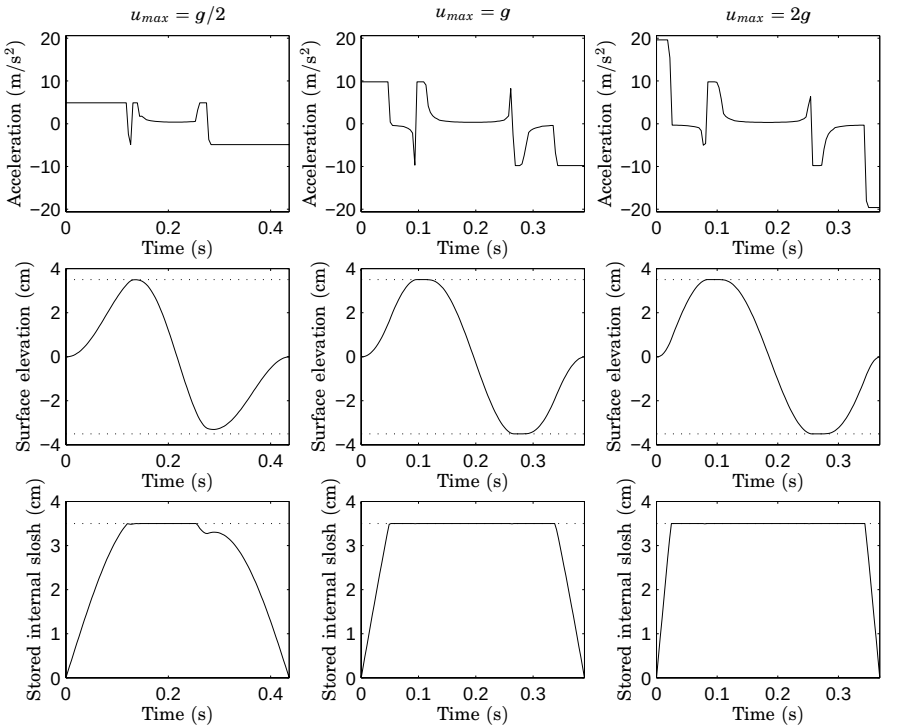

Figure 4.5 Numerical solution of the modified minimum time problem, with $u_{max} = g/2$ (left), $u_{max} = g$ (center) and $u_{max} = 2g$ (right). The movement distance is $L = 0.2$ m, the maximum allowed surface elevation is $s_{max} = 3.5$ cm and the maximum allowed stored internal slosh is $i_{max} = 3.5$ cm. The resulting movement times are $T = 436$ ms, $T = 390$ ms and $T = 368$ ms.

iii Bring the surface up to s_{max} and the stored internal slosh down to s_{max}.

2. Keep the surface at level s_{max}.
3. Move the surface from s_{max} to $-s_{max}$ as fast as possible with $\dot{s} = 0$ at the end.
   i Bring the stored internal slosh up to i_{max}.
   ii Keep the stored internal slosh at i_{max}.
   iii Bring the surface down to $-s_{max}$ and the stored internal slosh down to s_{max}.
4. Keep the surface at level $-s_{max}$.

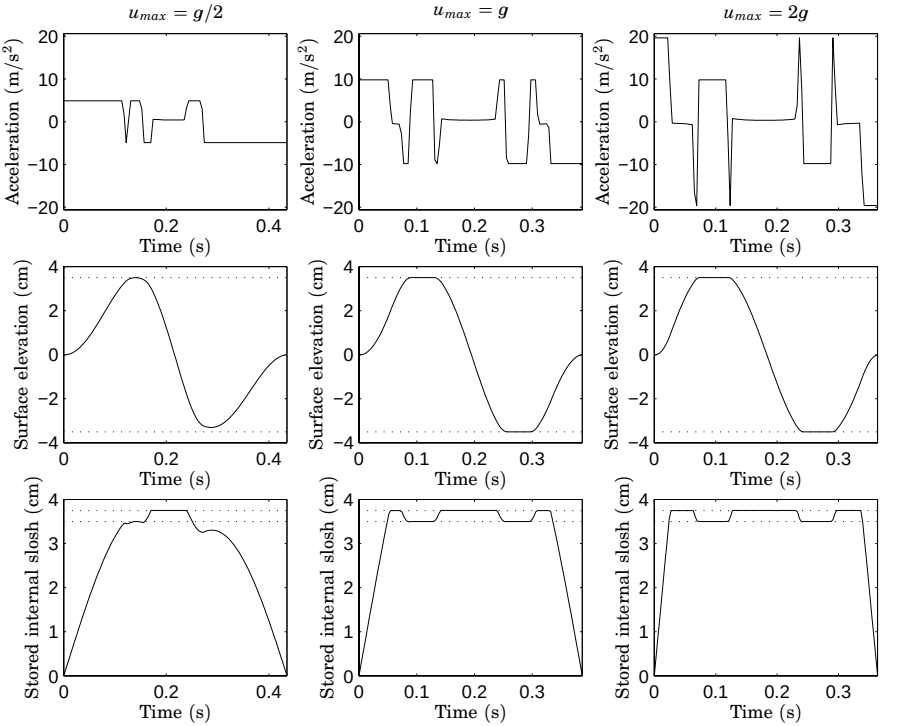

Figure 4.6 Same as Figure 4.5 with $i_{max} = 3.75$ cm.

5. Bring the surface to 0 as fast as possible with $\dot{s} = 0$ at the end.

   i Bring the stored internal slosh up to i_{max}.

   ii Keep the stored internal slosh at i_{max}.

   iii Bring the surface up to zero and the stored internal slosh down to zero.

The modified minimum time acceleration reference can be parameter-

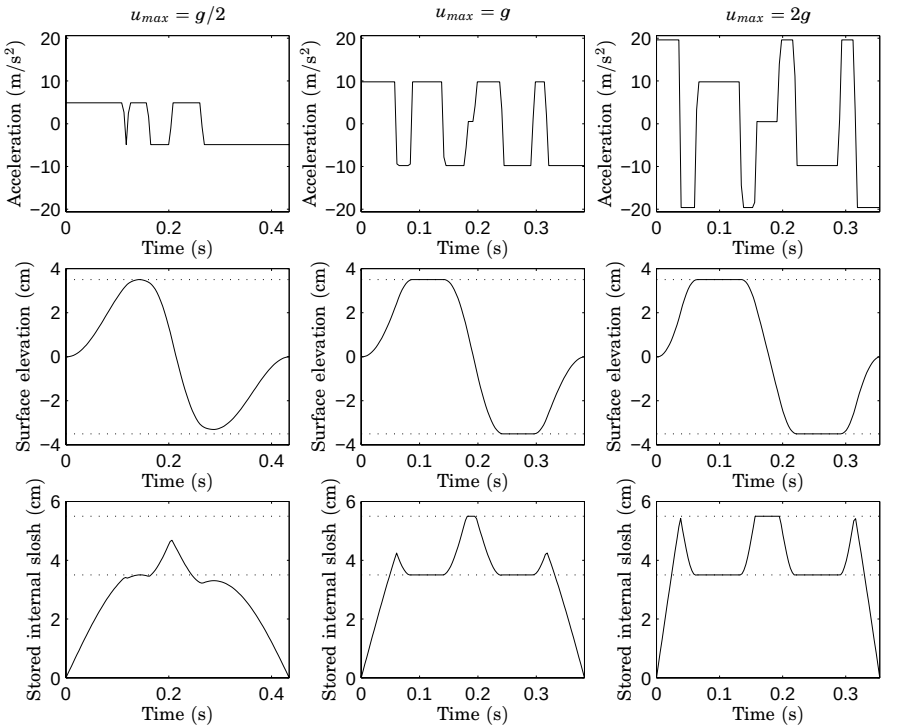

Figure 4.7 Same as Figure 4.5 with $i_{max} = 5.5$ cm.

ized as

$$u(t) = \begin{cases} u_{max} & 0 \le t < t_1 \\ u_i(t) & t_1 \le t < t_2 \\ -u_{max} & t_2 \le t < t_3 \\ u_{con} & t_3 \le t < t_4 \\ -u_{max} & t_4 \le t < t_5 \\ u_i(t) & t_5 \le t < t_6 \\ u_{max} & t_6 \le t < t_7 \\ -u_{con} & t_7 \le t < t_8 \\ u_{max} & t_8 \le t < t_9 \\ u_i(t) & t_9 \le t < t_{10} \\ -u_{max} & t_{10} \le t < T \end{cases}$$

where $u_{con} = 2s_{max}g/a$ is the acceleration needed to keep the surface

at a constant level and $u_i(t)$ is the control signal needed to keep the stored internal slosh s_i at a constant level when the surface is moving. An expression for $u_i(t)$ is obtained from the time derivative of the stored internal slosh.

$$\dot{s}_i(t) = \frac{1}{s_i(t)} \left(s(t)\dot{s}(t) + \frac{\dot{s}(t)\ddot{s}(t)}{w^2} \right)$$

Since we are interested in the case when $s_i(t)$ is a non-zero constant and hence $\dot{s}_i(t) = 0$ we get

$$s(t)\dot{s}(t) + \frac{\dot{s}(t)\ddot{s}(t)}{w^2} = 0$$

Insertion of $\ddot{s} = -2\zeta\omega\dot{s} - \omega^2 s - a\omega^2 u/(2g)$ gives

$$-\frac{1}{g\omega}\dot{s}(t)(4\zeta g\dot{s}(t) + a\omega u(t)) = 0 \quad \Rightarrow \quad u_i(t) = \frac{4\zeta g\dot{s}(t)}{a\omega}$$

since $\dot{s}(t) \neq 0$. This shows that the control signal necessary to keep the stored internal slosh at a constant level depends on the surface elevation velocity and the relative damping.

The movement switching times are symmetric and can be parameterized as $t_1 = d_1$, $t_2 = t_1 + d_2$, $t_3 = t_2 + d_3$, $t_4 = t_3 + d_4$, $t_5 = t_4 + d_5$, $t_6 = t_5 + d_6$, $t_7 = t_6 + d_5$, $t_8 = t_7 + d_4$, $t_9 = t_8 + d_3$, $t_{10} = t_9 + d_2$ and $T = t_{10} + d_1$. It might happen that $t_{i+1} = t_i$. For the case when $i_{max} = s_{max}$ and $\zeta = 0$ the switching times can be calculated in the same way as for the original minimum time problem and are then given by

$$\begin{aligned}
d_1 &= \frac{2}{\omega} \arctan\left(\frac{u_{con}}{\sqrt{4u_{max}^2 - u_{con}^2}} \right) \\
d_2 &= \frac{1}{\omega} \arccos\left(\frac{u_{con}}{2u_{max}} \right) \\
d_3 &= 0 \\
d_4 &= \frac{1}{2u_{con}}(-2u_{max}d_1 - u_{con}d_6 + \\
&\qquad [4u_{max}^2 d_1^2 - 4u_{max}u_{con}(d_1^2 + 2d_1d_2) + u_{con}^2 d_4^2 + 4u_{con}L]^{\frac{1}{2}}) \\
d_5 &= 0 \\
d_6 &= \frac{\pi}{\omega}
\end{aligned}$$

The switching times when $i_{max} > s_{max}$ and when $\zeta \neq 0$ are harder to calculate analytically.

u_{max} (m/s^2)	1	2	3	4	5	6	7	7.5
T (ms)	995	734	618	550	503	468	441	430

Table 4.4 The minimum movement times for the different values of u_{max} for the modified minimum-time acceleration profiles, with $L = 0.2$ m, $i_{max} = s_{max} = au_{max}/(2g)$ cm and $\omega = 21.0$ rad/s. The movement time is only slightly increased compared to the movement times for the original minimum-time problem in Table 4.2.

Experimental evaluation of the modified minimum time strategy

The evaluation of the modified minimum time acceleration references was done in the same way as for the original minimum time acceleration references, with $s_{max} = i_{max} = \frac{a}{2g}u_{max}$ to ensure that the constraints are active. The minimum movement times are shown in Table 4.4 and typical results from the experiments are shown in Figure 4.8.

A comparison with the experimental results with the profiles obtained from the original minimum-time problem, shown in Figure 4.4, reveals that larger values of u_{max} and s_{max} can be used before the performance degrades.

In an attempt to improve the performance, acceleration profiles calculated for different values of ω were tested. However, this lead to no improvements.

A conclusion that can be drawn is that limiting the stored internal slosh has a positive effect and the minimum movement times are only slightly increased compared to the original minimum-time problem. The acceleration profiles are however still useless for fast movements.

4.6 Minimum energy solution

One way of making the acceleration reference smoother is to solve an minimum energy problem instead. The cost function

$$J = \int_0^{T_{opt}+\Delta} u^2(t)\, dt$$

is minimized subject to the constraints C1–C4 and the slosh model in (3.39). Here T_{opt} is the movement time from the solution of the minimum time problem and Δ is the extra time allowed for the movement.

Numerical solution

The problem was solved numerically with RIOTS and the result is shown in Figure 4.9 for different values of Δ and u_{max}. The figure shows that

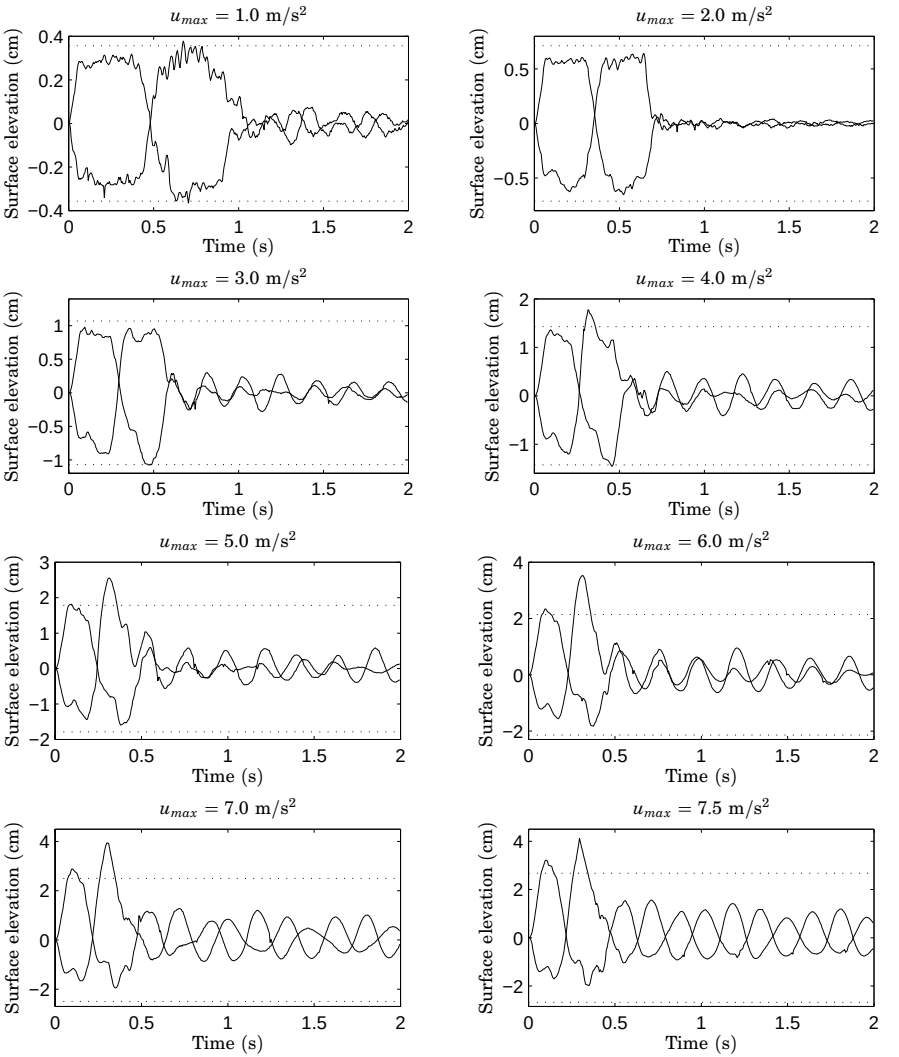

Figure 4.8 Data from experiments with the modified minimum-time acceleration profile for movement in several steps for varying values of u_{max}. The dotted lines shows $\pm s_{max} = \pm i_{max} = \pm \frac{a}{2g} u_{max}$. Each plot shows two experiments, one with the sensor in the front and one with the sensor in the back of the container. Compared with Figure 4.4 larger values of u_{max} can be used before the performance degrades.

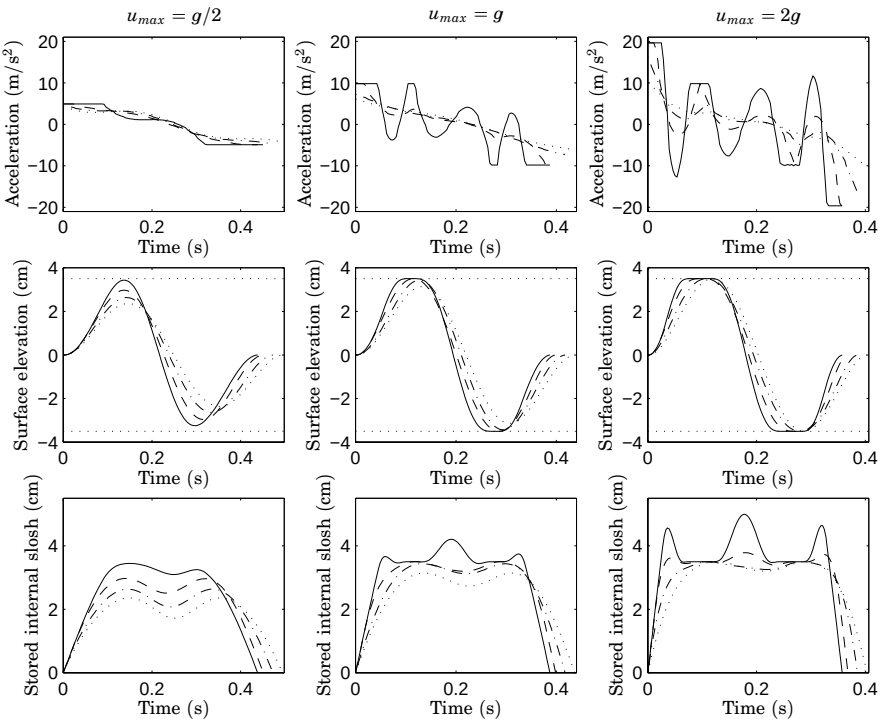

Figure 4.9 Numerical solution of the minimum-energy problem with $u_{max} = g/2$ (left), $u_{max} = g$ (center) and $u_{max} = 2g$ (right) for different values of Δ; $\Delta = 0.02T_{opt}$ (solid), $\Delta = 0.05T_{opt}$ (dashed), $\Delta = 0.10T_{opt}$ (dash dotted) and $\Delta = 0.15T_{opt}$ (dotted).

by increasing the movement time slightly we can make the acceleration reference much smoother. Notice that when Δ is sufficiently large neither the slosh nor the control constraint is active.

Experimental evaluation of the minimum energy strategy

The minimum energy acceleration references are evaluated for different values of Δ and ω with $u_{max} = 9.81$ m/s^2 and $s_{max} = 3.5$ cm. Table 4.5 shows the movement times and the relative increase in movement time for different values of ω. The acceleration profiles are calculated for five movement times T and three values of ω.

Since the minimum movement time T_{opt} depends on ω, the relative increase in movement time is different for different values of ω. The results of the experiments are shown in Figure 4.10. In the two plots for $\omega = 21.0$ rad/s with $T = 417$ ms and $T = 444$ ms, the sensor was not

	T (ms)	417	444	478	520	570
$\omega = 21.0$ rad/s	Δ/T_{opt} (%)	9	16	25	36	49
$T_{opt} = 383$ ms	$\max u$ (m/s^2)	7.35	5.73	4.58	4.03	3.97
	$\max s$ (cm)	3.47	3.05	2.58	2.06	1.63
$\omega = 19.5$ rad/s	Δ/T_{opt} (%)	7	14	23	33	46
$T_{opt} = 390$ ms	$\max u$ (m/s^2)	8.81	6.65	4.95	3.86	3.44
	$\max s$ (cm)	3.43	3.05	2.63	2.17	1.69
$\omega = 18.0$ rad/s	Δ/T_{opt} (%)	5	11	20	30	43
$T_{opt} = 399$ ms	$\max u$ (m/s^2)	9.81	8.14	5.82	4.15	3.21
	$\max s$ (cm)	3.42	3.02	2.63	2.22	1.79

Table 4.5 The relative increase in movement time, the maximum of the applied acceleration and the simulated maximum slosh are shown for different values of the movement time T and different ω from the numerical solution of the problem.

able to measure the surface elevation between $t \approx 0.5$ s and $t \approx 0.7$ s, which resulted in the straight lines in the plots.

Figure 4.10 shows that the performance can be increased by adjusting the value of ω. When $T = 570$ ms the best performance is achieved with $\omega = 21.0$ rad/s, for $T = 478$ ms $\omega = 19.5$ rad/s gives the best performance and $\omega = 18.0$ rad/s gives the best performance when $T = 417$ ms. If performance is defined as the amplitude of the surface elevation oscillations after the movement is performed, the smaller amplitude the better performance.

4.7 Modified minimum energy solution

Analytical solutions to the minimum energy problem can actually easily be obtained with the following modifications to the constraints:

- The constraint on the control signal (C1) is removed
- The slosh inequality constraint (C2) is replaced with a quadratic penalty on the slosh

A motivation for the modifications can be found in the numerical solutions of the original minimum energy problem shown in Figure 4.9. There it can be seen that for the case when $u_{max} = g$ neither the control nor the slosh constraint is active when $\Delta \geq 0.1T_{opt}$.

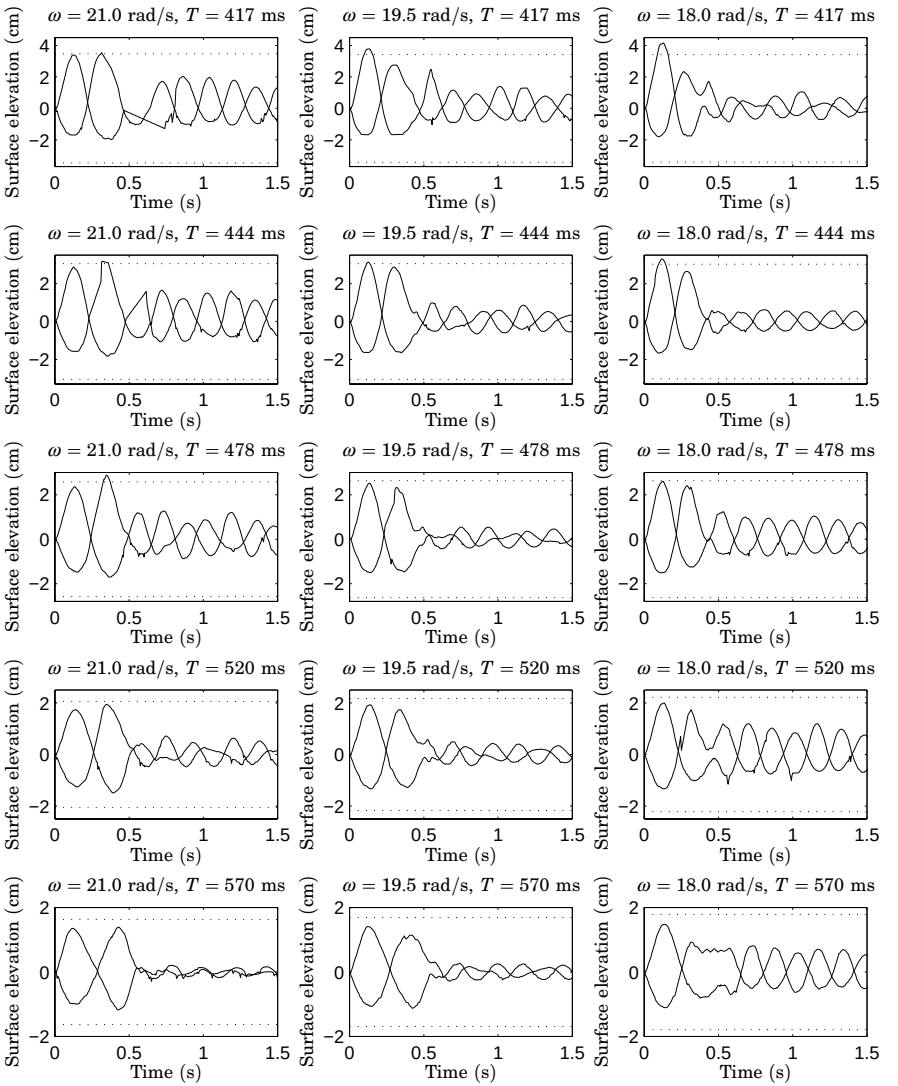

Figure 4.10 Data from experiments with the minimum energy acceleration reference for varying values of the movement time T and the oscillation frequency ω in the slosh model used for optimization. The dotted lines show the simulated maximum and minimum slosh, see Table 4.5. Each plots show two experiments, one with the sensor in the front and one with the sensor in the back of the container. The figure shows that the best performance is obtained for different values of ω for the different movement times and that the surface elevation corresponds relatively well with the simulated surface elevation.

This gives the following cost function and constraints

$$\begin{aligned} J =& \frac{1}{2}\int_0^T x^T(t)Qx(t) + Ru^2(t)\ dt \\ x(0) =& \begin{bmatrix} 0 & 0 & 0 & 0 \end{bmatrix}^T \\ x(T) =& \begin{bmatrix} 0 & 0 & 0 & L \end{bmatrix}^T \end{aligned} \tag{4.3}$$

The control $u(t)$ that minimizes J is obtained by simultaneously solving the system equation (3.39) and the adjoint Euler-Lagrange equations, see [Bryson and Ho, 1975]

$$\dot{\lambda}^T = -\frac{\partial H}{\partial x} \tag{4.4}$$

$$\frac{\partial H}{\partial u} = 0 \tag{4.5}$$

where the Hamiltonian is

$$H = \frac{1}{2}(x^T Qx + Ru^2) + \lambda^T(Ax + Bu)$$

Equations (3.39), (4.4) and (4.5) give

$$\begin{bmatrix} \dot{x} \\ \dot{\lambda} \end{bmatrix} = \underbrace{\begin{bmatrix} A & -\frac{1}{R}BB^T \\ -Q & -A^T \end{bmatrix}}_{M} \begin{bmatrix} x \\ \lambda \end{bmatrix} \tag{4.6}$$

and

$$u = -\frac{1}{R}B^T\lambda \tag{4.7}$$

The solutions to (4.6) can be written as

$$\begin{bmatrix} x(t) \\ \lambda(t) \end{bmatrix} = \Phi(t) \begin{bmatrix} x(0) \\ \lambda(0) \end{bmatrix} \tag{4.8}$$

where $\Phi(t) = e^{Mt}$. The boundary values are given in (4.3), while $\lambda(0)$ and $\lambda(T)$ are free. Insertion of $x(0)$ in (4.8) then gives

$$x(t) = \Phi_{1:4,5:8}(t)\lambda(0) \tag{4.9}$$

$$\lambda(t) = \Phi_{5:8,5:8}(t)\lambda(0) \tag{4.10}$$

where $\Phi_{1:4,5:8}(t)$ means the sub matrix with rows 1 to 4 and columns 5 to 8 of $\Phi(t)$. Evaluation of (4.9) at time T gives

$$\lambda(0) = [\Phi_{1:4,5:8}(T)]^{-1}x(T) \tag{4.11}$$

The optimal control $u(t)$ is hence

$$u(t) = -\frac{1}{R} B^T \Phi_{5:8,5:8}(t) [\Phi_{1:4,5:8}(T)]^{-1} x(T) \tag{4.12}$$

A special case

In the original minimum energy problem there is no penalty on the state trajectory, and if the movement time is sufficiently large neither the control nor the slosh constraint is active. This motivates an investigation of the special case when there is no penalty on the state trajectory (i.e. $Q = 0$). When $Q = 0$ and $R = 1$ we get

$$\Phi(t) = \begin{bmatrix} e^{At} & \Phi_{1:4,5:8}(t) \\ 0 & e^{-A^T t} \end{bmatrix}$$

Model with no damping If the damping is neglected in the model (i.e. $\zeta = 0$) we get

$$B^T \Phi_{5:8,5:8}(t) = \begin{bmatrix} \frac{a\omega}{2g} \cos \omega t & -\frac{a\omega}{2g} \sin \omega t & 1 & -t \end{bmatrix}$$

hence we get

$$u(t) = -\frac{a\omega}{2g} (\lambda_1(0) \cos \omega t - \lambda_2(0) \sin \omega t) - \lambda_3(0) + \lambda_4(0) t \tag{4.13}$$

where $\lambda(0)$ is given by (4.11).

Model with damping With the damping in the model (i.e. $\zeta \neq 0$) we get

$$B^T \Phi_{5:8,5:8}(t) = \begin{bmatrix} \frac{a\omega e^{\omega\zeta t}}{2g\sqrt{1-\zeta^2}} (\sqrt{1-\zeta^2} \cos \omega_m t + \zeta \sin \omega_m t) \\ -\frac{a\omega e^{\omega\zeta t}}{2g\sqrt{1-\zeta^2}} \sin \omega_m t \\ 1 \\ -t \end{bmatrix}^T$$

where $\omega_m = \omega\sqrt{1-\zeta^2}$. This gives

$$u(t) = -\frac{a\omega e^{\omega\zeta t}}{2g\sqrt{1-\zeta^2}} [\lambda_1(0)\sqrt{1-\zeta^2} \cos \omega_m t + (\lambda_1(0)\zeta - \lambda_2(0)) \sin \omega_m t] - \lambda_3(0) + \lambda_4(0) t \tag{4.14}$$

where $\lambda(0)$ is given by (4.11).

Experimental evaluation of the modified minimum energy strategy

The control strategies in (4.13) and (4.14) are evaluated for the movement in several steps. The container is moved 0.2 m five times and the movement time is 460 ms and the filling time between the movements is 440 ms.

If we use the nominal value of $\omega = 21.0$ rad/s given by (3.25) when calculating the acceleration reference the expected performance is not achieved in experiments. This is due to the amplitude dependent oscillation frequency. A way of quantifying the performance is to study the remaining oscillation after the movement has been performed.

DEFINITION 4.2
Define the residual slosh $r(t)$ as

$$r(t) = s(t + T) \ , \ \text{for } t \geq 0$$

where $s(t)$ is the surface elevation and T is the movement time. The performance measure R is then defined as

$$R = \sqrt{\int_0^\infty r^2(t) \, dt}$$

□

To increase the performance, the model parameters ω and ζ were tuned using experiments. First experiments were done with acceleration references calculated for different values of ω, with $\zeta = 0$. The performance measure R from these experiments are shown in Figure 4.11. This gave $\omega = 19.1$ rad/s as a minimizer of R. This value of ω was then used in the experiments with acceleration references calculated for different values of ζ. Figure 4.11 shows R for different values of ζ. The performance measure R is minimized for $\zeta = 0.013$.

The surface elevation when five consecutive movements are performed is shown in Figure 4.12. In Figure 4.13 the surface elevation from each movement cycle is plotted upon each other. The figure shows that there is only a small difference between each movement cycle, and the acceleration reference fulfills the specifications. Since the residual slosh is small the performance is independent of the time between the movements (i.e. the filling time), and therefore the same acceleration reference can be used even if the filling time is changed which is an advantage.

Figure 4.14 shows the surface shape obtained using the vision measurement system described in Section 2.3 when the container is moved one step. The acceleration reference is calculated using the modified minimum energy approach with the model parameters $\omega = 19.0$ rad/s and

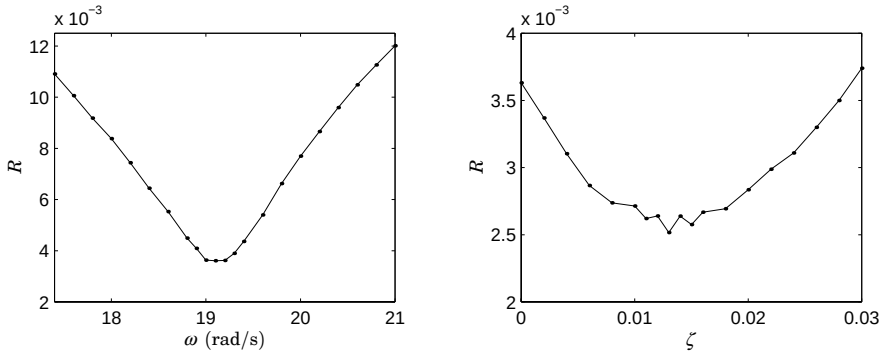

Figure 4.11 The left plot shows the performance measure R for different values of ω with $\zeta = 0$, where $\omega = 19.1$ minimizes R. In the right plot R is shown for different values of ζ with $\omega = 19.1$, where $\zeta = 0.013$ minimizes R.

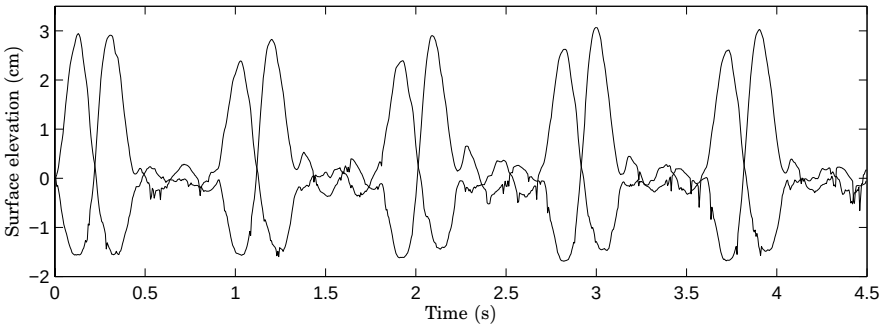

Figure 4.12 Experiment when the container is moved five times showing the surface elevation in the back and in the front. The movement length of each step is $L = 0.2$ m, the movement time is $T = 460$ ms and the time between each step is 440 ms. The performance is satisfactory and the maximum slosh constraint is not violated.

$\zeta = 0$. The movement time is 0.46 s and the movement distance is 0.2 m. The figure shows that the surface shape is far from the shape of the first order mode assumed in the model.

In Figure 4.15 the amplitude of the six first oscillation modes are shown. The amplitudes are obtained in the same way as described in Section 3.4. The figure shows that the first mode is dominant but the higher order modes are not negligible.

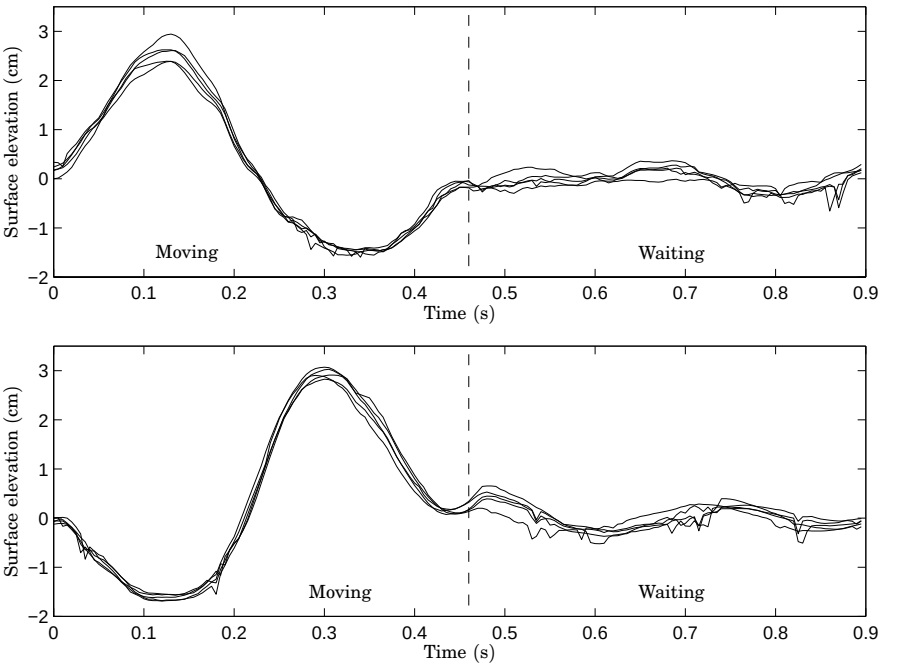

Figure 4.13 Experiment when the container is moved five times showing the surface elevation. The movement cycles are plotted upon each other. To the left of the dashed line the container is moving and to the right of the dashed line it is standing still. The upper plot shows the surface elevation in the back and the lower plot shows the surface elevation in the front.

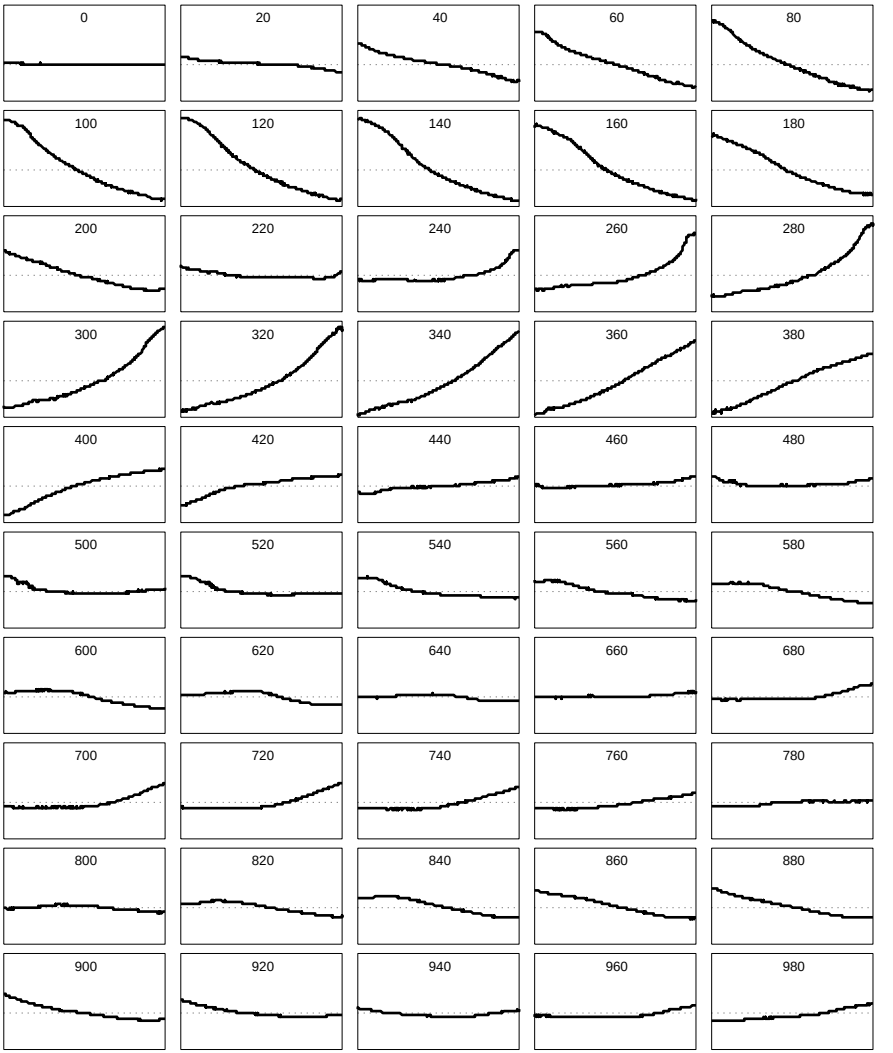

Figure 4.14 The surface shape when the container is moved using the modified minimum energy approach. The number in each frame is the time in milliseconds from the beginning of the movement. The movement distance is 0.2 m and the movement time is 0.46 s. The parameters used in the slosh model are $\omega = 19.0$ rad/s and $\zeta = 0$.

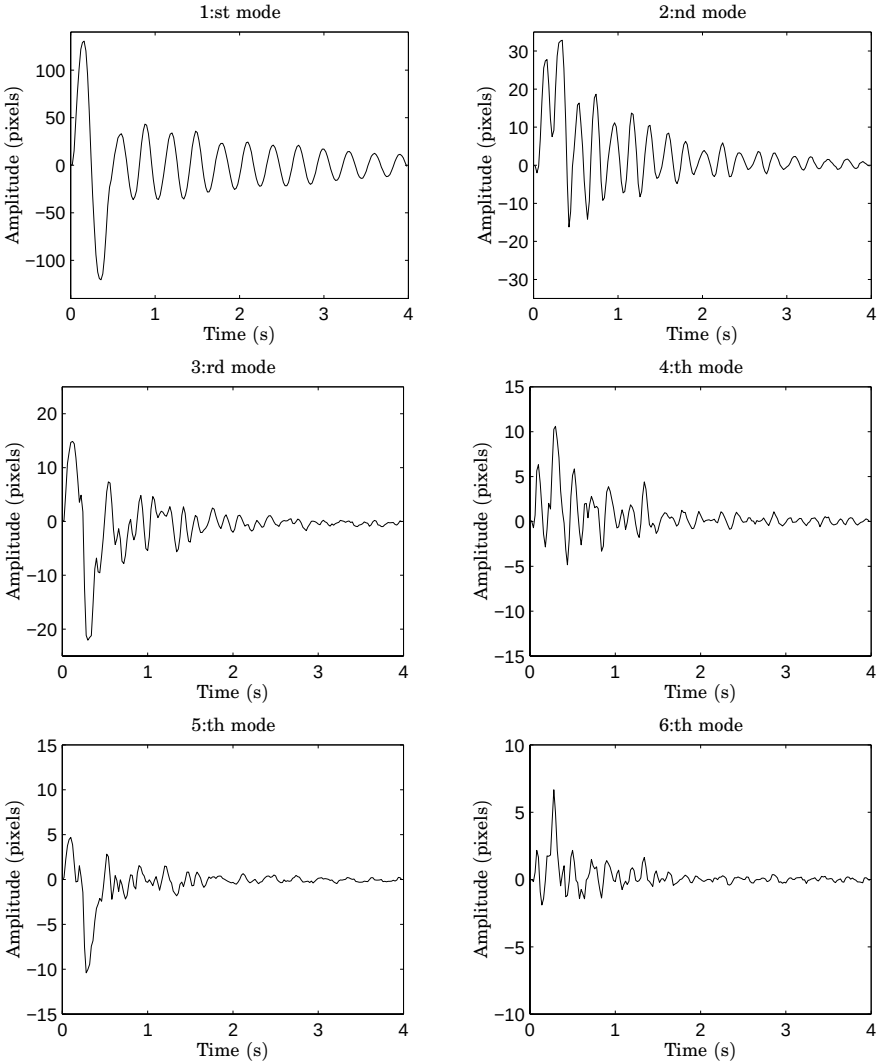

Figure 4.15 The amplitude of the six first oscillation modes obtained from the surface shapes in Figure 4.14. The figure shows that the first mode is dominant but the higher order modes are not negligible, especially not the second mode.

4.8 Implementation issues

All acceleration references calculated so far are continuous functions. However, the control systems is implemented in a computer which works in discrete time. Therefore, the acceleration references need to be discretized.

The implementation of the motion control system can be done in many ways. The trajectory can be represented by the acceleration reference or by a position reference. If a position reference is used then the discretization is simple. One can simply choose points from the continuous position trajectory as position reference. The continuous position trajectory is easy to obtain from the solutions of the optimal control problems.

When an acceleration reference is used it is important that the final velocity is zero and that the final position is the desired. This is not fulfilled if the continuous acceleration reference is sampled. Therefore the discretization must be made such that the velocity and position constraints are satisfied. Since the acceleration reference is integrated in the control system to generate position and velocity references the integration algorithms in the control system need to be known.

Now follows a description of a simple algorithm to discretize the continuous acceleration reference $a_c(t)$. The result should be a piecewise constant discrete reference $a_d(kh)$ where h is the sampling period. The sampling period is chosen such that the movement time is Nh. This gives that $a_d(kh)$ is zero for $k < 0$ and $k > N-1$.

If the acceleration reference is piecewise constant then the velocity will be piecewise linear and the position piecewise quadratic. It is further assumed that the following integration routines are used in the control system

$$v(kh) = h\sum_{i=0}^{k} a_d(ih) \qquad p(kh) = \frac{h}{2}\sum_{i=0}^{k} v((i-1)h) + v(ih) \tag{4.15}$$

where $v(t)$ is the velocity reference and $p(t)$ is the position reference. The constraints that $a_d(kh)$ need to satisfy are $v(Nh) = 0$ and $p(Nh) = L$ where L is the desired movement distance.

One way to find $a_d(kh)$ is to solve the following optimization problem

$$\begin{aligned} &\min_{a_d(kh)} \int_0^{Nh} \left(a_c(t) - a_d\left(\left\lfloor \frac{t}{h} \right\rfloor h \right) \right)^2 dt \\ &\text{subject to: } v(Nh) = 0 \\ &\qquad\qquad\quad p(Nh) = L \end{aligned}$$

where $\lfloor x \rfloor$ is the largest integer less than x and $v(Nh)$ and $p(Nh)$ are given by (4.15).

Here a simple scheme will be proposed. The method is based on the fact that if the discrete time acceleration reference $a_d(kh)$ does not fulfill the constraints then there exists constants b and c such that $c(a_d(kh)-b)$ fulfills the constraints. The constants b and c can easily be calculated; first b is found by calculating the resulting velocity if the reference is applied and dividing it by N. The resulting position is calculated for $a_t(kh) = a_d(kh)-b$, c is then given by the resulting position divided by the desired position L. This gives the following algorithm:

ALGORITHM 4.1
Construction of discrete acceleration reference $a_d(t)$ that fulfills the movement constraints from a continuous acceleration reference $a(t)$.

1. Sample N points from the continuous acceleration reference $a(t)$ with the sampling period h to get $a_s(kh)$.
2. Calculate the velocity $v(kh)$ for $a_s(kh)$ using (4.15). This gives the bias term
$$b = \frac{v(Nh)}{N}$$
3. Calculate the temporary reference
$$a_t(kh) = a_s(kh) - b$$
4. Calculate the position $p(kh)$ for $a_t(kh)$ using (4.15). This gives the gain
$$c = \frac{p(Nh)}{L}$$
5. The compensated acceleration reference is now given by
$$a_d(kh) = ca_t(kh)$$

□

The sampling of $a(t)$ can be done in several ways, here are some examples:

$$\begin{aligned} a_s(kh) &= a(kh) && \text{(I)} \\ a_s(kh) &= a(kh+h) && \text{(II)} \\ a_s(kh) &= a(kh+h/2) && \text{(III)} \end{aligned} \tag{4.16}$$

The different sampling methods in (4.16) are evaluated using simulation for several sampling intervals when the container is moved 0.2 m in

		Before			After
		$v(Nh)$ (m/s)	$L - p(Nh)$ (m)	$s_i(Nh)$ (m)	$s_i(Nh)$ (m)
$h = 0.02$ s	(I)	1.01E-1	-2.31E-2	8.88E-4	2.43E-3
	(II)	-1.01E-1	2.36E-2	8.88E-4	2.43E-3
	(III)	-8.74E-16	3.77E-4	3.70E-5	3.70E-5
$h = 0.005$ s	(I)	2.53E-2	-5.81E-3	2.23E-4	6.13E-4
	(II)	-2.53E-2	5.84E-3	2.23E-4	6.13E-4
	(III)	-4.13E-16	2.36E-5	2.27E-6	2.27E-6
$h = 0.001$ s	(I)	5.07E-3	-1.17E-3	4.46E-5	1.23E-4
	(II)	-5.07E-3	1.17E-3	4.46E-5	1.23E-4
	(III)	1.11E-16	9.44E-7	9.06E-8	9.06E-8

Table 4.6 Results from simulation with the different samplings methods in (4.16) for different sampling periods. The terminal velocity, the terminal position error and the terminal stored internal slosh is shown before the compensation is applied. The terminal stored internal slosh after compensation has been applied is also shown.

0.46 s. The acceleration reference is calculated using the modified minimum energy approach with $\omega = 21.0$ rad/s, $\zeta = 0$, $Q = 0$ and $R = 1$. Table 4.6 shows the results of the simulations. The table shows the terminal velocity, the terminal position error and the terminal stored internal slosh without compensation and the terminal stored internal slosh with compensation.

The simulations show that the velocity and the position errors decrease as the sampling period is decreased. The errors are also considerably smaller for method III than for method I and II, especially the velocity error.

The stored internal slosh represents the amount of surface elevation oscillation when the movement has been performed and should be as small as possible. The simulations show that the stored internal slosh decreases as the sampling period is decreased and that it is smaller for sampling method III. Notice that the stored internal slosh is increased after the compensation for method I and II but not for method III.

The simulations show that sampling method III gives the best performance and it has been used in the implementation of the acceleration references.

Another implementation issue is the quantization of the acceleration reference. Most motion control systems are implemented using fixed point arithmetics. Therefore, the quantized acceleration reference needs to ful-

fill the motion constraints. This is a hard problem and has not been considered during this work.

4.9 Discrete time calculations

One way to avoid the discretization problem is to directly solve a discrete time optimal control problem. First a description of the system is needed when the input is a piecewise constant signal with a constant sampling period h. This is obtained by standard zero order hold sampling of the continuous system description in (3.39), which gives

$$x(kh+h) = A_d x(kh) + B_d u(kh)$$

where the discrete time states directly correspond to the continuous time states.

Now the following discrete time minimum energy optimal control problem can be formulated when the container is moved the distance L in time $T = Nh$

$$\begin{aligned}
&\min_u \sum_{k=0}^{N-1} u^2(kh) \\
&\text{subject to: } x(kh+h) = A_d x(kh) + B_d u(kh) \\
&\qquad x(0) = [\,0 \quad 0 \quad 0 \quad 0\,]^T \\
&\qquad x(Nh) = [\,0 \quad 0 \quad 0 \quad L\,]^T \\
&\qquad |u(kh)| \le u_{max}, \quad k = 0,\ldots,N-1 \\
&\qquad |x_2(kh)| \le s_{max}, \quad k = 1,\ldots,N
\end{aligned}$$

By introducing the vectors

$$\begin{aligned}
U &= [\,u(0) \quad u(h) \quad \ldots \quad u((N-1)h)\,]^T \\
X_i &= [\,x_i(h) \quad x_i(2h) \quad \ldots \quad x_i(Nh)\,]^T,\ i = 1,\ldots,4
\end{aligned}$$

and the matrices

$$G_i = \begin{bmatrix} g_i(h) & 0 & \ldots & 0 \\ g_i(2h) & g_i(h) & \ldots & 0 \\ \vdots & \vdots & \ddots & \vdots \\ g_i(Nh) & g_i((N-1)h) & \ldots & g_i(h) \end{bmatrix},\ i = 1,\ldots,4$$

where $g_i(kh)$ is the pulse response from the input to state x_i the system can be described by

$$X_i = G_i U,\ i = 1, \ldots, 4$$

since the initial condition is zero. Now the optimal control problem can be written as

$$\begin{aligned} &\min_U\ U^T U \\ &\text{subject to:}\quad CU = [\,0 \quad 0 \quad 0 \quad L\,]^T \\ &\qquad\qquad |U| \leq U_{max} \\ &\qquad\qquad |G_2 U| \leq S_{max} \end{aligned}$$

where U_{max} and S_{max} are constant vectors of length N and

$$C = \begin{bmatrix} g_1(Nh) & g_1((N-1)h) & \ldots & g_1(h) \\ g_2(Nh) & g_2((N-1)h) & \ldots & g_2(h) \\ g_3(Nh) & g_3((N-1)h) & \ldots & g_3(h) \\ g_4(Nh) & g_4((N-1)h) & \ldots & g_4(h) \end{bmatrix}$$

This is a standard quadratic programming problem which is easily solved using any of the numerous numerical solvers available. If the inequality constraints are removed it is also easy to solve analytically.

Using quadratic programming it is also easy to solve the global problem considering all movement steps and not requiring the surface to be at rest between the movements.

The problem now is to find $u(kh)$ that moves the container the distance L on the time $T_m = Nh$. When the acceleration reference is repeated O times with a waiting time of $T_w = Mh$ between each movement the surface elevation must not exceed s_{max}.

First a description of the surface elevation on the form $G_{2eO}U$ when the acceleration reference is repeated is needed. This can be obtained in the same way as in the single movement case. The total time of the problem is now $(N+M)Oh$, which gives that the surface elevation response from the first movement is given by $G_{2e}U$ with

$$G_{2e} = \begin{bmatrix} g_2(h) & 0 & \ldots & 0 \\ g_2(2h) & g_2(h) & \ldots & 0 \\ \vdots & \vdots & \ddots & \vdots \\ g_2(Nh) & g_2((N-1)h) & \ldots & g_2(h) \\ \vdots & \vdots & & \vdots \\ g_2(Jh) & g_2((J-1)h) & \ldots & g_2((J-N+1)h) \end{bmatrix}$$

where $J = (N + M)O$ is the total number of samples. When the acceleration reference is repeated the surface elevation response is given by $G_{2eO}U$ with

$$G_{2eO} = \sum_{k=0}^{I-1} \begin{bmatrix} 0_{k(N+M)} \\ G_{2e_{(O-k)(N+M)}}) \end{bmatrix}$$

where 0_n is a zero matrix with N columns and n rows and G_{2e_n} is the n upper rows of G_{2e}. This gives the quadratic program

$$\begin{aligned} &\min_U \ U^T U \\ &\text{subject to:} \quad CU = [0 \quad L]^T \\ &\qquad\qquad\quad |U| \leq U_{max} \\ &\qquad\qquad\quad |G_{2eO}U| \leq S_{max} \end{aligned}$$

where S_{max} is a constant vector of length J and

$$C = \begin{bmatrix} g_3(Nh) & g_3((N-1)h) & \dots & g_3(h) \\ g_4(Nh) & g_4((N-1)h) & \dots & g_4(h) \end{bmatrix}$$

Investigation of behavior

The behavior of the method is studied by solving the problem for different movement and waiting times when the container is moved five times. The quadratic program is solved using the function `quadprog` in Matlab. The model parameters were $\omega = 21.0$ rad/s, $\zeta = 0$, $a = 0.07$ m and the movement distance was $L = 0.2$ m. The constraints were $u_{max} = g$ and $s_{max} = 0.035$ m and the sampling period was $h = 5$ ms.

The problem is solved for two waiting times 500 ms and 450 ms and four movement times 500 ms, 400 ms, 390 ms and the minimum movement time for the different waiting times which is 380 and 385 ms respectively. The solutions for $T_w = 500$ ms are shown in Figure 4.16 and for $T_w = 450$ ms in Figure 4.17.

The figures show that the solutions are very different. When the waiting time is 500 ms the resulting minimum movement time is 380 ms which is less than the minimum movement time when the surface is required to be at rest. The figure also shows that the surface elevation constraint is seldom active except in the first movement step. In the case when the movement time is 500 ms the surface elevation constraint is never active and the acceleration reference is simply a ramp which is the same as minimum energy acceleration reference if the slosh is not taken into account.

When the waiting time is 450 ms the resulting minimum movement time is 385 ms and the movement is such that the surface is at rest at

the end of the movement. The surface elevation constraint is active in almost every movement step and the acceleration reference is such that the surface elevation oscillation between the movements is decreased as the movement time is decreased.

4.10 Conclusions

Several different methods for calculation of horizontal acceleration references have been developed and evaluated. All methods are based on the model (3.39) and optimal control techniques. Evaluation of the methods has been performed in the experimental setup presented in Chapter 2 where the surface elevation in the container can be measured.

In Section 4.4 the minimum time optimal control problem is solved with constraints in the maximum allowed acceleration u_{max} and surface elevation s_{max}. The problem is solved numerically for different values of u_{max}. The resulting acceleration reference is switching between four different levels, $\pm u_{max}$ and $\pm u_{con}$ when $u_{max} \geq u_{con}$ and between $\pm u_{max}$ otherwise, where u_{con} is the constant acceleration needed to keep the surface elevation at the constraint. The switching times are calculated analytically for the case when $u_{max} \geq u_{con}$ and $\zeta = 0$.

The experimental evaluation of the minimum time acceleration reference reveals that the method only works for small values of u_{max} and s_{max}. Insight into why it works only for small amplitudes can be obtained by studying the stored internal slosh. During the movement there are very large peaks in the stored internal slosh especially if u_{max} is large. This indicates that there is a large amount of energy pumped in and removed from the system. This pumping of energy in and out of the system requires a very accurate model to be successful.

One way to limit the stored internal slosh is to add a constraint on the maximum allowed stored internal slosh i_{max} and solve for the minimum time acceleration reference. This is done in Section 4.5 where the problem is solved numerically for different values of u_{max} and i_{max}. This also results in a switching acceleration reference but the acceleration reference also switches to $u_i(t)$ to keep the stored internal slosh on the constraint, if $\zeta = 0$ we get $u_i(t) = 0$ since no energy is dissipated from the system. The switching times are calculated analytically for the case when $u_{max} \geq u_{con}$, $i_{max} = s_{max}$ and $\zeta = 0$. The movement time is only slightly increased compared to the original minimum time method.

Experimental evaluation of the modified minimum time method shows that larger values of u_{max} and s_{max} can be used before the performance degrades. However, the largest value of s_{max} that gives acceptable performance is still quite far from the maximum allowed s_{max} and the resulting

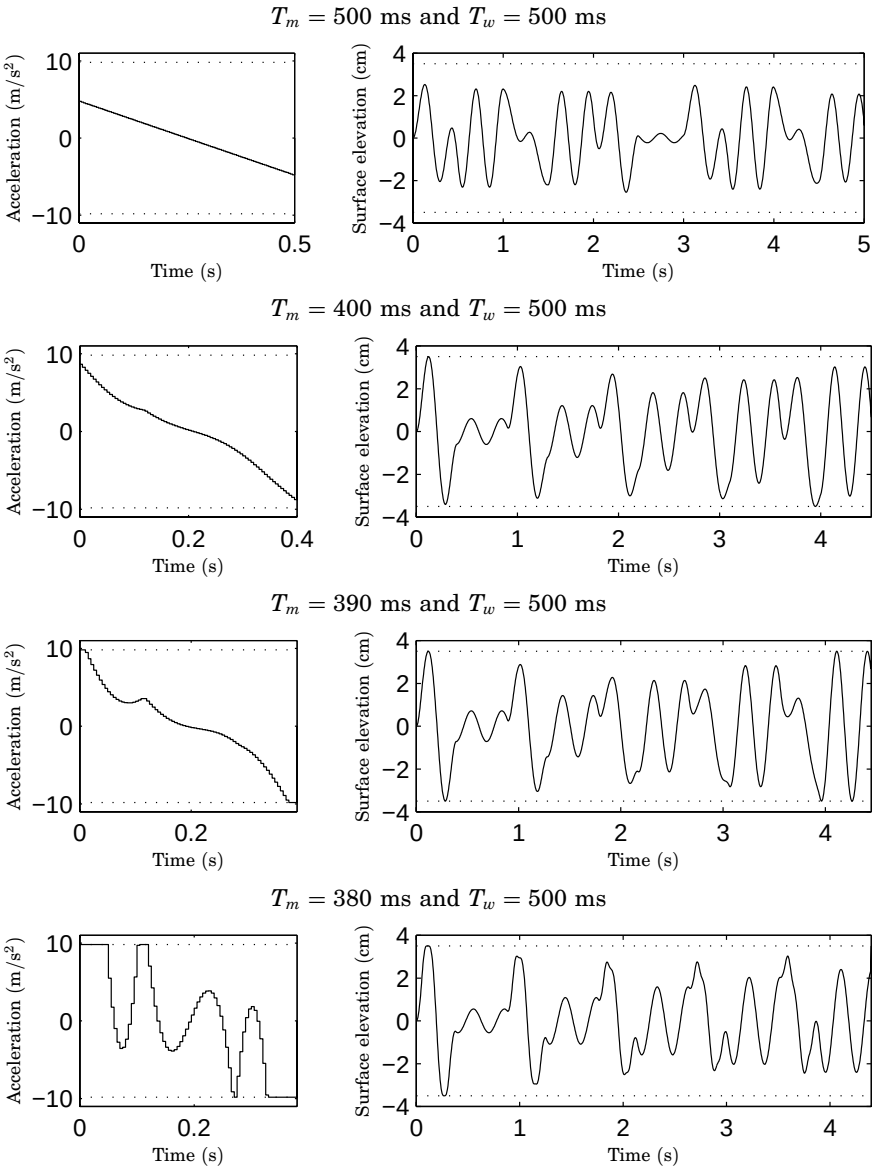

Figure 4.16 Simulation of the minimum energy discrete time optimal control problem when five movements are considered. The waiting time is $T_w = 500$ ms and the movement distance is 0.2 m. As the movement time is decreased the surface elevation is not at rest in between the movements and it is possible to move the container faster than when it is required that the surface should be at rest.

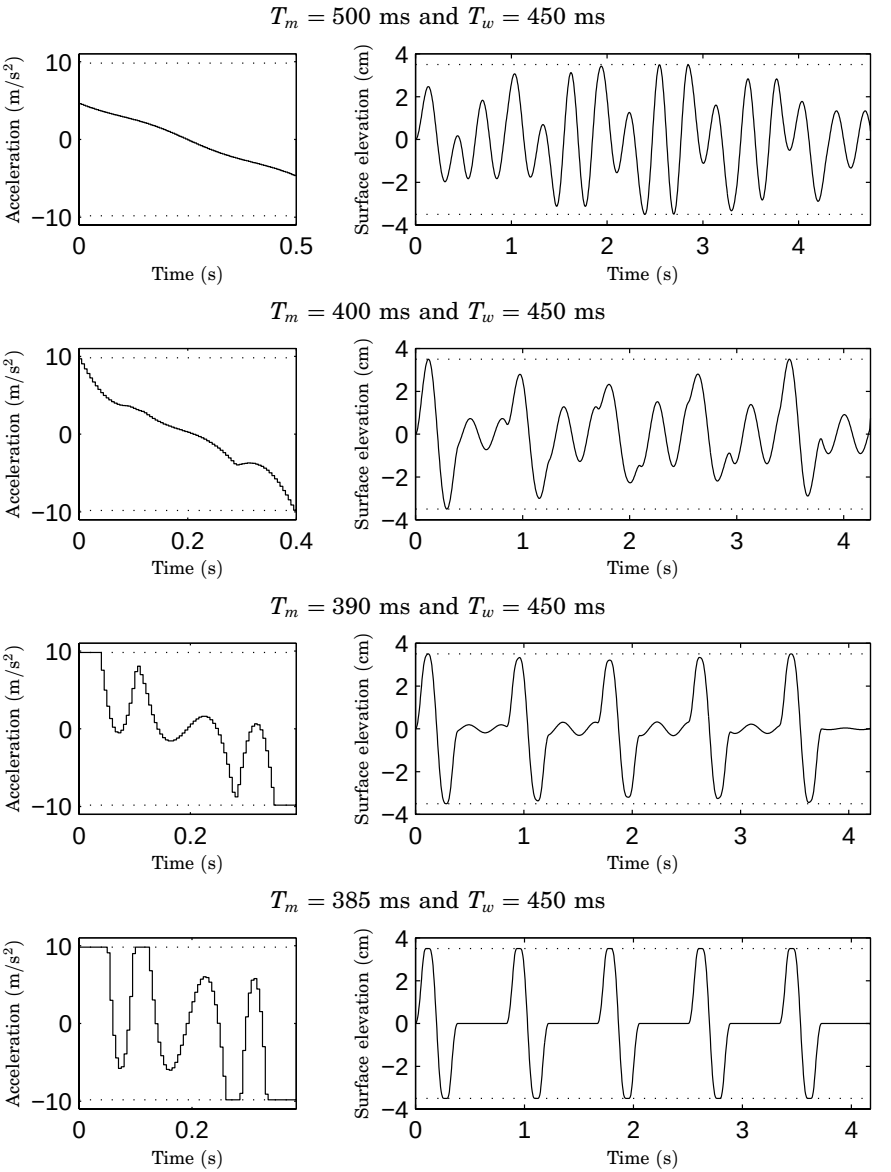

Figure 4.17 Same as Figure 4.16 but with $T_w = 450$ ms. As the movement time is decreased the surface elevation oscillation between the movements is decreased and at the minimum movement time the surface is at rest between the movements.

movement time is too long.

A natural thing to do when controlling something more or less unknown is to be cautious. This can be introduced in the optimal control problem by minimizing the control effort which is presented in Section 4.6. The movement time obtained from the minimum time solution T_{opt} is increased with Δ and a fixed time optimal control problem is solved with the same constraints but with the integral of u^2 as the cost. The problem is solved numerically for several values of Δ. This shows that a increase in Δ results in acceleration references that become smoother and with smaller maximum amplitudes.

The experimental evaluation shows that it is possible to move the container faster and with a larger value of s_{max} without performance degradation than the minimum time methods. However, to achieve this the oscillation frequency ω of the model needs to be adjusted depending on the slosh amplitude. The higher slosh amplitude the lower frequency. This is natural since the oscillation frequency is amplitude dependent, see Section 3.3.

An analytical solution to the minimum energy problem can easily be obtained if the constraints are modified. In Section 4.7 the control constraint is removed and the surface elevation constraint is replaced by a quadratic penalty on the surface elevation and rate of change of the surface elevation. This can be justified by the fact that as Δ is increased neither the control nor the surface elevation constraint is active.

In Section 4.8 some implementation issues are discussed. Most of the acceleration references in this chapter are given as a continuous function that should be implemented in a computer. Therefore, the acceleration references need to be discretized. It is very important that the motion constraints are fulfilled for the discretized acceleration reference. A simple algorithm that solves this problem is presented in Algorithm 4.1.

Section 4.9 presents a method to solve the minimum energy problem in discrete time using a discrete time model, which can be obtained by zero-order-hold sampling of the model in (3.39), and quadratic programming. A method to solve the global optimal control problem during a series of movements using quadratic programming is also presented. Numerical solutions to the global problem show that depending on the waiting time between the movements the solutions are very different. This proves that the only way to obtain an acceleration reference that works for all waiting times is to require that there is no surface oscillation after each movement step.

5

Iterative methods

In the previous chapter optimal control techniques were used to calculate acceleration references using a simple model describing the slosh. The experimental evaluations of the calculated references showed that the model parameters needed to be adjusted for the minimum energy approaches to work. For the minimum time approaches the model was only valid for small surface elevation oscillations. Better control can be obtained if a more accurate model is used. However, a more accurate model is probably of higher order and nonlinear which leads to much harder optimal control problems.

The traditional way to handle model uncertainty is to use feedback. In this case it is not possible to use direct feedback in the control loop since measurement of the slosh in the machine is not cost realistic. It is however possible to measure the surface elevation in the experimental testbed. In Section 3.3 it is shown that the response to an acceleration reference is very repeatable and there are almost no disturbances except measurement faults and noise. Therefore, the control error from an experiment can be used to modify the acceleration reference to be used in the next experiment. The procedure is then repeated until the desired performance is obtained. This methodology is called iterative learning control (ILC) and is described in Section 5.1.

Two different iterative methods are developed for this application, and are described in the sections 5.3 and 5.4. The framework used in the ILC approaches is described in 5.2. The stability, the stationary solution and the noise properties are calculated numerically for both algorithms in Section 5.5 and in Section 5.6 the algorithms are evaluated in simulations with both a linear and a nonlinear process model. Section 5.7 presents experimental results for both algorithms.

The iterative methods presented in this chapter have been found to be a practical and efficient way to generate good acceleration references. The methods does only need a rather crude model of the slosh and are sim-

ple to tune. More conclusions and comparisons between the two different methods are given in Section 5.8.

5.1 Iterative Learning Control

Iterative learning control (ILC) is a method to learn how to follow a trajectory. The method works in an iterative manner where the control error from previous iterations is used to refine the control. Necessary conditions for the method are that the trajectory always starts in the same state and that the major disturbances are repeated each iteration.

The learning signal is introduced either directly into the system as the command signal or control signal, or indirectly as a correction of some other signal, for instance the control signal in a feedback loop. The learning signal $u_k(t)$ at iteration k is in the standard formulation calculated as follows

$$u_k(t) = Q(q)\big(u_{k-1}(t) + L(q)(r(t) - y_{k-1}(t))\big) \tag{5.1}$$

where $r(t)$ is the desired trajectory and $y_{k-1}(t)$ is the response to the input $u_{k-1}(t)$, $Q(q)$ and $L(q)$ are linear time invariant filters. Since the calculation is done off-line the filters need not be causal and generally are not. The design of the filters are usually heuristic but model based approaches are also common.

The update law or learning law in (5.1) is called a first order ILC since only data from the previous iteration is used. Higher order ILCs can also be used that use data from several iterations.

For more information about ILC and further details see [Moore, 1993; Bien and Xu, 1998].

In this application of ILC the learning signal $u(t)$ is the acceleration reference. The specifications on the movement gives the following constraints on $u(t)$

$$\int_0^T u(t)\ dt = 0, \quad \int_0^T \int_0^t u(s)\ dsdt = L \tag{5.2}$$

where T is the movement time and L is the movement distance. The constraints state that the velocity is zero after the movement and that the movement distance is L. These constraints make it hard to choose time-invariant filters $Q(q)$ and $L(q)$ in (5.1).

5.2 The ILC framework

The control signal and the surface elevation measurements are collected in vectors as in Section 4.9, this gives

$$\begin{aligned} U &= [\, u(0) \quad u(h) \quad \dots \quad u((N-1)h) \,]^T \\ Y^b &= [\, y^b(h) \quad y^b(2h) \quad \dots \quad y^b((N+M)h) \,]^T \\ Y^f &= [\, y^f(h) \quad y^f(2h) \quad \dots \quad y^f((N+M)h) \,]^T \end{aligned}$$

where the sampling period h is chosen as $T = Nh$, $y^b(t)$ is the surface elevation on the backward side of the container and $y^f(t)$ on the forward side with respect to the direction of movement. The surface elevation is stored for M additional samples.

An approximation of the behavior is given by the linear discrete time transfer operator $G(q)$, which can be obtained either from system identification or by sampling the model in (3.39). This gives the following approximate surface elevation when the acceleration reference $u(t)$ is applied

$$\hat{y}^b(t) = G(q)u(t), \quad \hat{y}^f(t) = -G(q)u(t)$$

In the same way as in Section 4.9 the following matrix is introduced

$$G = \begin{bmatrix} g(h) & 0 & \dots & 0 \\ g(2h) & g(h) & \dots & 0 \\ \vdots & \vdots & \ddots & \vdots \\ g(Nh) & g((N-1)h) & \dots & g(h) \\ \vdots & \vdots & & \vdots \\ g((N+M)h) & g((N+M-1)h) & \dots & g((M+1)h) \end{bmatrix}$$

where $g(t)$ is the pulse response of $G(q)$. The approximate surface elevation can now be expressed by

$$\hat{Y}^b = GU, \quad \hat{Y}^f = -GU$$

The motion constraints in (5.2) can also be written as a matrix equation. This gives

$$CU = \begin{bmatrix} h & h & \dots & h \\ h^2(N-\frac{1}{2}) & h^2(N-\frac{3}{2}) & \dots & \frac{h^2}{2} \end{bmatrix} U = \begin{bmatrix} 0 \\ L \end{bmatrix}$$

5.3 Constrained Iterative Learning Control (CILC)

The following algorithm is similar to algorithms presented in [Bien and Xu, 1998; Frueh and Phan, 1998; Gunnarsson and Norrlöf, 1999].

A reference $r(t)$ for the surface elevation on the backward side of the container, $-r(t)$ for the forward side, and an initial acceleration reference $u_0(t)$ is calculated using some of the methods presented in Chapter 4. The acceleration reference and the surface elevation reference is sampled with sampling period h and the surface elevation reference is augmented with M zeros giving

$$R = [\, r(h) \quad r(2h) \quad \dots \quad r(Nh) \quad 0 \quad \dots \quad 0 \,]^T$$

This gives the control errors

$$E^b = R - Y^b, \quad E^f = -R - Y^f$$

The objective is to find an acceleration reference U which solves the following minimization problem

$$\begin{aligned} &\min_U \; {E^b}^T W_b E^b + {E^f}^T W_f E^f + U^T W_u U \\ &\text{subject to: } CU = \begin{bmatrix} 0 \\ L \end{bmatrix} \end{aligned} \tag{5.3}$$

where the weighting matrices W_b and W_f with size $(N+M) \times (N+M)$ and W_u with size $N \times N$ are introduced as tuning parameters.

The minimization can be performed in an iterative manner. Assume that an experiment has been performed with the input U_k and the surface elevation responses Y_k^b and Y_k^f have been measured on the real system. In the next iteration the input

$$U_{k+1} = U_k + \Delta \tag{5.4}$$

will be applied. A prediction of the surface elevation responses in the next iteration is given by

$$\hat{Y}_{k+1}^b = Y_k^b + G\Delta, \quad \hat{Y}_{k+1}^f = Y_f^b - G\Delta$$

which gives the following predicted errors

$$\hat{E}_{k+1}^b = E_k^b - G\Delta \tag{5.5}$$

$$\hat{E}_{k+1}^f = E_k^f + G\Delta \tag{5.6}$$

If U_k satisfies the constraints then $U_{k+1} = U_k + \Delta$ also satisfies the constraints if $C\Delta = 0$.

The minimization problem in (5.3) can now be solved in an iterative manner by finding the Δ which solves

$$\begin{aligned} &\min_{\Delta} \; {E_{k+1}^b}^T W_b E_{k+1}^b + {E_{k+1}^f}^T W_f E_{k+1}^f + {U_{k+1}}^T W_u U_{k+1} \\ &\text{subject to: } C\Delta = 0 \end{aligned} \tag{5.7}$$

All Δ that satisfy the constraints are given by $K\theta$ where K is the kernel of C and θ is an arbitrary vector with length $N-2$. Insertion of (5.4), (5.5), (5.6) and $\Delta = K\theta$ in (5.7) gives

$$\begin{aligned} \min_{\theta} \; &(E_k^b - GK\theta)^T W_b (E_k^b - GK\theta) + \\ &(E_k^f + GK\theta)^T W_f (E_k^f + GK\theta) + \\ &(U_k + K\theta)^T W_u (U_k + K\theta) \end{aligned} \tag{5.8}$$

with the $N \times (N-2)$ matrix

$$K = \begin{bmatrix} 1 & 0 & \dots & 0 & 0 \\ -2 & 1 & \dots & 0 & 0 \\ 1 & -2 & \dots & 0 & 0 \\ \vdots & \vdots & \ddots & \vdots & \vdots \\ 0 & 0 & \dots & -2 & 1 \\ 0 & 0 & \dots & 1 & -2 \\ 0 & 0 & \dots & 0 & 1 \end{bmatrix}$$

which is one representation of the kernel of C.

The objective function is quadratic in θ and there are no constraints. The minimizing θ is given by

$$\theta = \mathcal{M} K^T (G^T (W_b E_k^b - W_f E_k^f) - W_u U_k) \tag{5.9}$$

where

$$\mathcal{M} = \left[K^T (G^T (W_b + W_f) G + W_u) K \right]^{-1}$$

The update law is now given by $\Delta = K\theta$, (5.4) and (5.9) and can be written as

$$U_{k+1} = Q U_k + L_b E_k^b + L_f E_k^f \tag{5.10}$$

with

$$Q = I - K\mathcal{M}K^T W_u$$
$$L_b = K\mathcal{M}K^T G^T W_b$$
$$L_f = -K\mathcal{M}K^T G^T W_f$$

The matrices Q, L_b and L_f are constant between the iterations and do not depend on the experimental data and need only to be calculated once. The matrix multiplications correspond to linear filtering of the signals in the time domain, possibly time-varying and non causal and can be written as

$$u_{k+1}(t) = Q(t,q)u_k(t) + L_b(t,q)e_k^b(t) + L_f(t,q)e_k^f(t)$$

which has almost the same structure as the standard version of the update law in (5.1). This gives the following algorithm

ALGORITHM 5.1
Constrained iterative learning control algorithm:

1. Calculate $r(t)$ and $u_0(t)$ using some of the methods in Chapter 4 and set $k = 0$.
2. Calculate the matrices Q, L_b and L_f.
3. Perform an experiment with $u_k(t)$ to obtain $e_k^b(t)$ and $e_k^f(t)$. Stop if performance is satisfactory.
4. Calculate $u_{k+1}(t)$ using (5.10) and increase k by one.
5. Go to step 3.

□

Analysis of the CILC algorithm

A simple analysis of Algorithm 5.1 can be done if the system is described by a linear model. The linear system is described by a matrix P in the same way as the model of the system is described in the update law by the matrix G. This gives the following description of the controlled system

$$Y_k^b = PU_k, \quad Y_k^f = -PU_k$$

and the measured control error

$$E_k^b = R - PU_k - V_k^b, \quad E_k^f = -R + PU_k - V_k^f \tag{5.11}$$

where V^* are vectors containing measurement noise that is added to the measurements.

The iterative process can now be described as a linear system. If the state is chosen as U_k a state space description is easily found using (5.10) and the control errors above. This yields a system of order N. However, this is not a minimal state space representation since

$$U_k = K\theta_k + K\theta_{k-1} + \cdots + K\theta_1 + U_0 = K\Theta_k + U_0$$

where

$$\Theta_{k+1} = \Theta_k + \theta_k$$

is the sum of all updates and is of size $N-2$. This shows that U_k can be described using $N-2$ states. Therefore a state space representation with the state Θ_k will be derived.

The state space representation is obtained from (5.9) which gives θ and the control error given in (5.11). This gives the following state space description of the iterative process where Θ_k is the state, the reference R and U_0 are the inputs, and U_k and the surface elevations Y_k^* are the outputs:

$$\begin{aligned}\Theta_{k+1} = (I - \mathcal{M}K^T(G^T(W_b + W_f)P + W_u)K)\Theta_k - \\ \mathcal{M}K^T(G^T(W_b + W_f)P + W_u)U_0 + \\ \mathcal{M}K^TG^T(W_b(R - V_k^b) + W_f(R + V_k^f))\end{aligned}$$

$$\begin{bmatrix} U_k \\ Y_k^b \\ Y_k^f \end{bmatrix} = \begin{bmatrix} I \\ P \\ -P \end{bmatrix} (K\Theta_k + U_0)$$

The iterative process is hence stable if the following matrix has all eigenvalues inside the unit circle

$$\mathcal{A} = I - \mathcal{M}K^T(G^T(W_b + W_f)P + W_u)K \tag{5.12}$$

Note that if there are no modeling errors, i.e. $P = G$, or if there is no penalty on the control errors, i.e. $W_b = W_f = 0$, then $\mathcal{A} = 0$ and all eigenvalues are in the origin. Hence, the iteration process converges in one iteration since $\mathcal{A} = 0$.

It can easily be seen that the constraint fulfillment is conserved in the iterations since

$$CU_k = \underbrace{CK}_{0}\Theta_k + CU_0 = CU_0$$

If the system is stable and there is no measurement noise then the iteration will converge to a steady state since the inputs are constant.

The steady state is obtained by setting $\Theta = \Theta_{k+1} = \Theta_k$ and solving for Θ. The steady state is given by the solution of

$$K^T(G^T(W_b + W_f)P + W_u)K\Theta = \\ -K^T(G^T(W_b + W_f)P + W_u)U_0 + K^T G^T(W_b + W_f)R \quad (5.13)$$

The noise properties of the algorithm can be studied by calculation of the variance of U_k and Y_k^* when the measurement noise is white noise with zero mean and variance σ^2. The variance is calculated using the H_2-norm of the transfer function from the disturbance input V_k to the outputs U_k and Y_k. A state space representation of the system is

$$\begin{aligned} \Theta_{k+1} &= \mathcal{A}\Theta_k + \mathcal{B}V_k \\ U_k &= C_u\Theta_k \\ Y_k &= C_y\Theta_k \end{aligned}$$

with

$$\mathcal{B} = [-\mathcal{F}K^T G^T W_b \quad \mathcal{F}K^T G^T W_f\,], \quad V_k = \begin{bmatrix} V_k^b \\ V_k^f \end{bmatrix}, \quad C_u = K, \quad C_y = PK$$

Only one of the surface elevation outputs are considered. Since the only difference between them is the sign, the variance of Y_k^b will be equal to the variance of Y_k^f. With $E(V_k V_k^T) = \sigma^2 I$ we get

$$\begin{aligned} \sigma_U^2 &= E(U^T U) = ||C_u(qI - \mathcal{A})^{-1}\mathcal{B}||_2^2\sigma^2 \\ \sigma_Y^2 &= E(Y^T Y) = ||C_y(qI - \mathcal{A})^{-1}\mathcal{B}||_2^2\sigma^2 \end{aligned} \quad (5.14)$$

in stationarity.

Numerical calculation of the stability, of the stationary solution and of th noise properties are given in Section 5.5.

5.4 Iterative Optimal Control (IOC)

The algorithm presented in Section 5.3 tries to shape the input such that the response follows a desired trajectory. The desired trajectory is calculated using a simplified linear model of the system. If there are large modeling errors the desired trajectory is not optimal and may even be infeasible. Therefore an algorithm which solves the underlying optimal control problem using data from experiments in an iterative manner will

be derived. A similar approach is presented in [Roberts, 1993] where a general optimal control problem is solved in an iterative manner using data from experiments on the real process with both model mismatch and approximate objective functions.

The algorithm is based on the discrete time minimum energy problem in Section 4.9. Since a linear model of the slosh is used the surface elevation is symmetric, see Section 5.2. This will give rise to problems if both the surface elevation on the backward side and on the forward side are included in the optimal control problem. If there are hard constraints on the surface elevation the problem will be infeasible if the measurements of the surface elevation are not exactly symmetric at the constraint. Therefore the terminal constraints on the surface elevation are replaced with a penalty of the surface elevation after the movement has been performed over M samples.

This gives the optimal control problem

$$\begin{aligned}
&\min_{u(t)} \ \rho \sum_{k=0}^{N-1} u(kh)^k + \sum_{k=N+1}^{N+M} \left(y^b(kh)^2 + y^f(kh)^2 \right) \\
&\text{subject to: } |u(kh)| \leq u_{max}, \ k \in [0, N-1] \\
&\qquad\qquad u(kh) = 0, \ k \in [N, \infty] \\
&\qquad\qquad y^b(kh) \leq s_{max}, \ y^f(kh) \leq s_{max}, \ k \in [1, N] \\
&\qquad\qquad v(Nh) = 0 \\
&\qquad\qquad p(Nh) = L
\end{aligned}$$

where the parameter ρ is used as a tuning parameter, v is the velocity and p is the position of the container.

The framework presented in Section 5.2 and the following decomposition of the matrix G and the vectors Y^*

$$G = \begin{bmatrix} G_1 \\ G_2 \end{bmatrix}, \qquad Y^* = \begin{bmatrix} Y_1^* \\ Y_2^* \end{bmatrix}$$

where G_1 is the N upper rows of G and G_2 the M lower rows and Y_1^* is the N first rows of Y^* and Y_2^* is the M last rows allows the problem to be written as

$$\begin{aligned}
&\min_{U} \ \rho U^T U + {Y_2^b}^T Y_2^b + {Y_2^f}^T Y_2^f \\
&\text{subject to: } |U| \leq U_{max} \\
&\qquad\qquad Y_1^b \leq S_{max}, \ Y_1^f \leq S_{max} \\
&\qquad\qquad CU = \begin{bmatrix} 0 \\ L \end{bmatrix}
\end{aligned}$$

Similar to as in Section 5.3 this can be solved in an iterative manner. An experiment is performed with the input U_k, and Y_k^b and Y_k^f are obtained. In the next iteration the input U_{k+1} will be applied. A linear approximation of the response to U_{k+1} is given by

$$\hat{Y}_{k+1}^b = Y_k^b + G(U_{k+1} - U_k) \tag{5.15}$$

$$\hat{Y}_{k+1}^f = Y_k^f - G(U_{k+1} - U_k) \tag{5.16}$$

The optimal control problem for iteration $k+1$ is

$$\begin{aligned}
&\min_{U_{k+1}} \ \rho {U_{k+1}}^T U_{k+1} + {Y_{2\,k+1}^b}^T Y_{2\,k+1}^b + {Y_{2\,k+1}^f}^T Y_{2\,k+1}^f \\
&\text{subject to: } |U_{k+1}| \leq U_{max} \\
&\qquad Y_{1\,k+1}^b \leq S_{max},\ Y_{1\,k+1}^f \leq S_{max} \\
&\qquad C U_{k+1} = \begin{bmatrix} 0 \\ L \end{bmatrix}
\end{aligned}$$

Insertion of (5.15) and (5.16) gives

$$\begin{aligned}
&\min_{U_{k+1}} \ {U_{k+1}}^T (\rho I + 2G_2^T G_2) U_{k+1} + 2(Y_{2\,k}^b - Y_{2\,k}^f - 2G_2 U_k)^T G_2 U_{k+1} \\
&\text{subject to: } |U_{k+1}| \leq U_{max} \\
&\qquad G_1 U_{k+1} \leq S_{max} - Y_{1\,k}^b - G_1 U_k \\
&\qquad -G_1 U_{k+1} \leq S_{max} - Y_{1\,k}^f + G_1 U_k \\
&\qquad C U_{k+1} = \begin{bmatrix} 0 \\ L \end{bmatrix}
\end{aligned} \tag{5.17}$$

where all terms that do not depend on U_{k+1} have been removed from the objective function. This is a standard quadratic program which can be solved using any numerical solver. This gives the following algorithm

ALGORITHM 5.2
Iterative optimal control algorithm:

1. Set $u_0(t) = 0$, $y_0^b(0) = y_0^f(t) = 0$ and $k = 0$.
2. Calculate $u_{k+1}(t)$ by solving the quadratic program in (5.17) and increase k by one.
3. Perform an experiment with $u_k(t)$ to obtain $y_k^b(t)$ and $y_k^f(t)$. Stop if performance is satisfactory.
4. Go to step 2.

□

Analytical solution to the quadratic program

If the constraint on the control signal and on the surface elevation is removed the problem is possible to solve analytically. The minimization problem in (5.17) now becomes

$$\begin{aligned}&\min_{U_{k+1}} \; {U_{k+1}}^T(\rho I + 2G_2^T G_2)U_{k+1} + 2(Y_{2\,k}^b - Y_{2\,k}^f - 2G_2U_k)^T G_2 U_{k+1}\\ &\text{subject to: } CU_{k+1} = \begin{bmatrix}0\\ L\end{bmatrix}\end{aligned}$$

With

$$\begin{aligned}&H = 2(\rho I + 2G_2^T G_2), \quad c = 2G_2^T(Y_{2\,k}^b - Y_{2\,k}^f - 2G_2U_k)\\ &b = \begin{bmatrix}0\\ L\end{bmatrix}, \quad x = U_{k+1}\end{aligned} \tag{5.18}$$

the problem can be written on the form

$$\begin{aligned}&\min_x \; \frac{1}{2}x^T H x + c^T x\\ &\text{subject to: } Cx = b\end{aligned}$$

This can easily be solved using the Karush-Kuhn-Tucker (KKT) conditions. The Lagrangian for the problem is

$$L(x, v) = \frac{1}{2}x^T H x + c^T x + v^T(Cx - b)$$

where v is a vector of Lagrange variables. Differentiation of L with respect to x gives

$$\frac{dL(x, v)}{dx} = Hx + c + C^T v$$

The KKT conditions become

$$\begin{cases}Hx + c + C^T v = 0\\ Cx - b = 0\end{cases}$$

which gives the following matrix representation

$$\begin{bmatrix}H & C^T\\ C & 0\end{bmatrix}\begin{bmatrix}x\\ v\end{bmatrix} = \begin{bmatrix}-c\\ b\end{bmatrix}$$

If H is invertible we have

$$\begin{bmatrix} H & C^T \\ C & 0 \end{bmatrix}^{-1} = \begin{bmatrix} H^{-1} - H^{-1}C^T\widetilde{H}CH^{-1} & H^{-1}C^T\widetilde{H} \\ \widetilde{H}CH^{-1} & -\widetilde{H} \end{bmatrix}$$

where $\widetilde{H} = (CH^{-1}C^T)^{-1}$. This gives

$$x = (H^{-1}C^T\widetilde{H}CH^{-1} - H^{-1})c + H^{-1}C^T\widetilde{H}b$$

where the experimental data appear linearly in c. This gives that the update law can be written on the form

$$U_{k+1} = QU_k + L_bY^b_{2\,k} + L_fY^f_{2\,k} + U_c$$

with

$$\begin{aligned} Q &= 4\mathcal{M}G_2^TG_2 \\ L_b &= -2\mathcal{M}G_2^T \\ L_f &= 2\mathcal{M}G_2^T \\ U_c &= H^{-1}C^T\widetilde{H}\begin{bmatrix} 0 \\ L \end{bmatrix} \end{aligned}$$

where

$$\mathcal{M} = H^{-1} - H^{-1}C^T\widetilde{H}CH^{-1}$$

and H is given in (5.18).

Analysis of the IOC algorithm

A simple analysis of Algorithm 5.2 can be done if the system is described by a linear model. The linear system is described by a matrix P in the same way as the model of the system is described in the update law by the matrix G. This gives the following description of the controlled system

$$Y_k^b = PU_k, \quad Y_k^f = -PU_k$$

and the measurements

$$\widetilde{Y}_k^b = Y_k^b + V_k^b, \quad \widetilde{Y}_k^f = Y_k^f + V_k^f$$

where V^* are vectors containing measurement noise that is added in the measurement.

This gives the following state space description of the iterative process where U_k is the state, U_c is a constant input and Y_k^* are the outputs.

$$U_{k+1} = 4\mathcal{M}G_2^T(G_2 - P_2)U_k + 2\mathcal{M}G_2^T(V_{2\,k}^f - V_{2\,k}^b) + U_c$$
$$\begin{bmatrix} Y_k^b \\ Y_k^f \end{bmatrix} = \begin{bmatrix} P \\ -P \end{bmatrix} U_k$$

The iterative process is stable if the following matrix has all eigenvalues inside the unit circle.

$$\mathcal{A} = 4\mathcal{M}G_2^T(G_2 - P_2) \tag{5.19}$$

If the matrix G is constructed using the pulse response from a linear system of order n then the rank of G_2 is at most n (Kronecker's theorem see for example page 210 in [Young, 1988]). The rank of $\mathcal{A}$ is smaller than or equal to the rank of G_2 this means that at least $N - n$ eigenvalues of $\mathcal{A}$ will be in the origin. If $P_2 = G_2$ then all eigenvalues are in the origin.

It is easily seen that the constraint is conserved during the iterations since

$$C\mathcal{M} = CH^{-1} - \underbrace{CH^{-1}C^T}_{\widetilde{H}^{-1}}\widetilde{H}CH^{-1} = 0$$

and

$$CU_c = \underbrace{CH^{-1}C^T}_{\widetilde{H}^{-1}}\widetilde{H}\begin{bmatrix} 0 \\ L \end{bmatrix} = \begin{bmatrix} 0 \\ L \end{bmatrix}$$

If the system is stable and there is no measurement noise then the iteration will converge to a steady state since the input is constant. The steady state is obtained by setting $U = U_{k+1} = U_k$ and solving for U. The steady state is given by the solution of

$$(I - 4\mathcal{M}G_2^T(G_2 - P_2))U = U_c \tag{5.20}$$

The noise properties of the algorithm are studied in the same way as for the CILC algorithm in Section 5.3 by calculating the variance of U_k and Y_k^* when the measurement noise is white noise with zero mean and variance σ^2. The variance is calculated using the H_2-norm of the transfer function from the disturbance input to the output. A state space representation of the system is

$$U_{k+1} = \mathcal{A}U_k + \mathcal{B}V_k$$
$$Y_k = C_y U_k$$

with

$$\mathcal{B} = [\,0 \quad -2\mathcal{M}G_2^T \quad 0 \quad 2\mathcal{M}G_2^T\,], \quad V_k = \begin{bmatrix} V_{k\,1}^b \\ V_{k\,2}^b \\ V_{k\,1}^f \\ V_{k\,2}^f \end{bmatrix}, \quad C_y = P$$

Only one of the surface elevation outputs are considered. Since the only difference between them is the sign, the variance of Y_k^b will be equal to the variance of Y_k^f. With $E(V_k V_k^T) = \sigma^2 I$ we get

$$\begin{aligned} \sigma_U^2 &= E(U^T U) = ||(qI - \mathcal{A})^{-1}\mathcal{B}||_2^2 \sigma^2 \\ \sigma_Y^2 &= E(Y^T Y) = ||C_y(qI - \mathcal{A})^{-1}\mathcal{B}||_2^2 \sigma^2 \end{aligned} \tag{5.21}$$

in stationarity.

Numerical calculation of the stability, of the stationary solution and of the noise properties are given in Section 5.5.

5.5 Numerical analysis

The stability, the stationary solutions and the noise sensitivity of the algorithms are analyzed using numerical calculations when the process is described by a linear system.

The model used in the algorithms is given in continuous time by the transfer operator

$$G_c(p) = \frac{a}{2g} \frac{\omega_m^2}{p^2 + \omega_m^2}$$

with $a = 0.07$ m and $w_m = 21.0$ rad/s which are the theoretical values given in Section 3.1.

The process is described in continuous time by the transfer operator

$$P_c(p) = \frac{a_p}{2g} \frac{\omega_p^2}{p^2 + 2\zeta_p \omega_p p + \omega_p^2}$$

where the gain can be changed through a_p, damping is added with ζ_p and the oscillation frequency can be modified using ω_p.

Zero-order-hold sampling of $G_c(p)$ and $P_c(p)$ with the sampling period $h = 0.01$ s gives the discrete time transfer operators $G_d(q)$ and $P_d(q)$ which are used to construct the matrices G and P as described in Section 5.2. The movement time is chosen as 0.46 s which gives $N = 46$ and M is chosen as 20. The variance of the measurement noise is chosen as $\sigma^2 = 10^{-6}$ which is in the same range as the measurement noise encountered in the experimental setup.

The Constrained Iterative Learning Control algorithm (CILC)

The stability, the stationary solution and the noise properties of the CILC algorithm derived in Section 5.3 is calculated numerically.

Stability First the root locus is studied when the parameters in the process model are changed with the weighting matrices $W_u = 10^{-5}I$ and $W_b = W_f = I$. The parameters of the process model are set to the same values as the model used in the update law, i.e. $\omega_p = \omega_m = 21.0$ rad/s, $\zeta_p = 0$ and $a_p = a_m = 0.07$ m. The eigenvalues of the matrix $\mathcal{A}$ in (5.12) are then plotted as one of the parameters is changing. The eigenvalues are calculated using the Matlab function `eig`.

Figures 5.1, 5.2 and 5.3 show the eigenvalues when ω_p, ζ_p and a_p are varying. The figures show that the eigenvalues move outside the unit circle if ω_p and a_p is sufficiently far from ω_m and a_m and that the stability is not affected by ζ_p.

In Figure 5.4 the eigenvalues are shown for 500 random parameters and four different values of the control cost W_u. The parameters are uniformly distributed within the following intervals, $\omega_p \in [17, 21]$, $\zeta_p \in [0, 0.1]$ and $a_p \in [0.06, 0.08]$. The figure shows that the eigenvalues are moved further from the origin as W_u is decreased and hence the robustness to model errors is also decreased.

Stationary solution To evaluate the influence of the weighting matrices on the final result the stationary solution is calculated with the weighting matrices $W_u = \rho I$ and $W_b = W_f = I$ for different values of ρ.

The surface elevation reference and initial control signal is calculated using the modified minimum energy strategy presented in Section 4.7.

Figure 5.5 shows

$$U^T U = \sum_{k=0}^{N-1} u(kh)^2 \quad \text{and} \quad E^T E = \sum_{k=1}^{N+M} e^b(kh)^2$$

as a function of ρ. Only the error on one side is considered since $e^f(t) = -e^b(t)$. The figure shows $U^T U$ and $E^T E$ when the model in the update law and the process are equal and for 20 random processes with parameters in the intervals, $\omega_p \in [17, 21]$, $\zeta_p \in [0, 0.1]$ and $a_p \in [0.06, 0.08]$.

The figure shows that only a small decrease of the $E^T E$ is obtained if $\rho < 10^{-6}$ compared to $\rho = 10^{-5}$ and that the control signal U becomes very large for small values of ρ. For $\rho > 10^{-6}$ there is only a slight decrease in the control signal and there is no increase in the control error if $\rho > 10^{-3}$. Therefore a suitable choice is $\rho = 10^{-5}$. The figure also shows that the achievable minimum error is increased when there is a mismatch

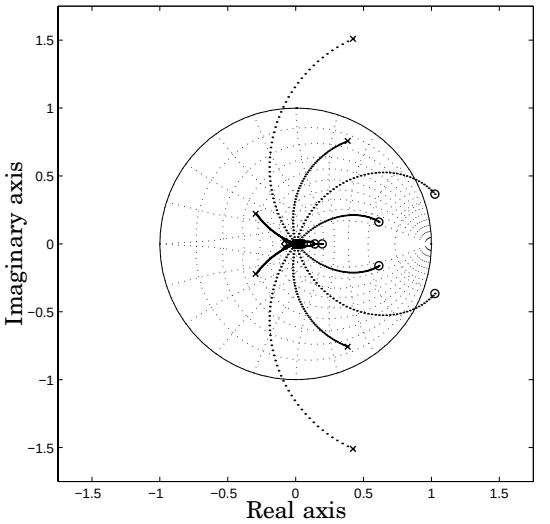

Figure 5.1 The eigenvalues of $\mathcal{A}$ in (5.12) for the CILC algorithm when ω_p is varying from 13 rad/s ($\circ$) to 29 rad/s ($\times$). If ω_p is sufficiently far from $\omega_m = 21$ rad/s the system becomes unstable.

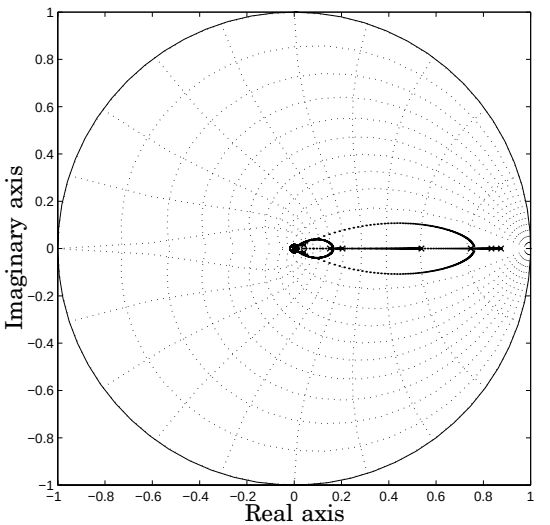

Figure 5.2 The eigenvalues of $\mathcal{A}$ in (5.12) for the CILC algorithm when ζ_p is varying from 0 ($\circ$) to 1 ($\times$). The system is stable for all values of ζ_p.

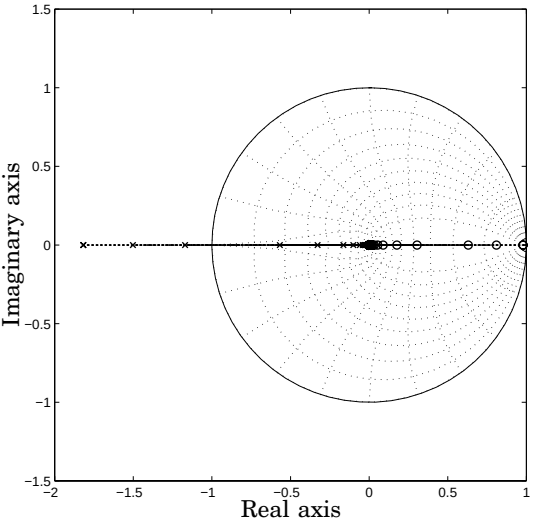

Figure 5.3 The eigenvalues of $\mathcal{A}$ in (5.12) for the CILC algorithm when a_p is varying from 0 m ($\circ$) and 0.2 m ($\times$). The system becomes unstable if a_p is sufficiently larger than $a_m = 0.07$ m.

between the model in the update law and the process and that the control signal does not become large if the model and process are equal.

In Figure 5.6 the stationary solution is shown for some values of ρ for a process with the parameters $\omega_p = 0.9\omega_m$, $\zeta_p = 0.01$ and $a_p = 1.1a_m$. The figure shows that as ρ is decreased there is a chattering behavior in the control signal and the amplitude becomes very large. The output of the system is very close to the reference for all $\rho \leq 10^{-5}$.

Since the main objective is to make the residual slosh small the weighting matrices W_b and W_f can be modified to penalize the surface elevation more in the M last samples. Figure 5.7 shows the M last samples when $W_b = W_f = I$ and when $W_b = W_f = \text{diag}(I_{46}, 10I_{20})$, where the penalty on the last M samples is 10 instead of 1. The figure shows that the residual slosh is considerably decreased.

Noise The noise properties of the CILC algorithm is examined by calculating the control signal variance σ_u^2 and the output variance σ_y^2 in (5.14) for different values of the control weight $W_u = \rho I$ with $W_b = W_f = I$. Figure 5.8 shows the variances σ_u^2 and σ_y^2 for different values of ρ. The H_2-norm is calculated using the Matlab function `norm` for linear time invariant systems.

The variances are calculated when the process is equal to the model

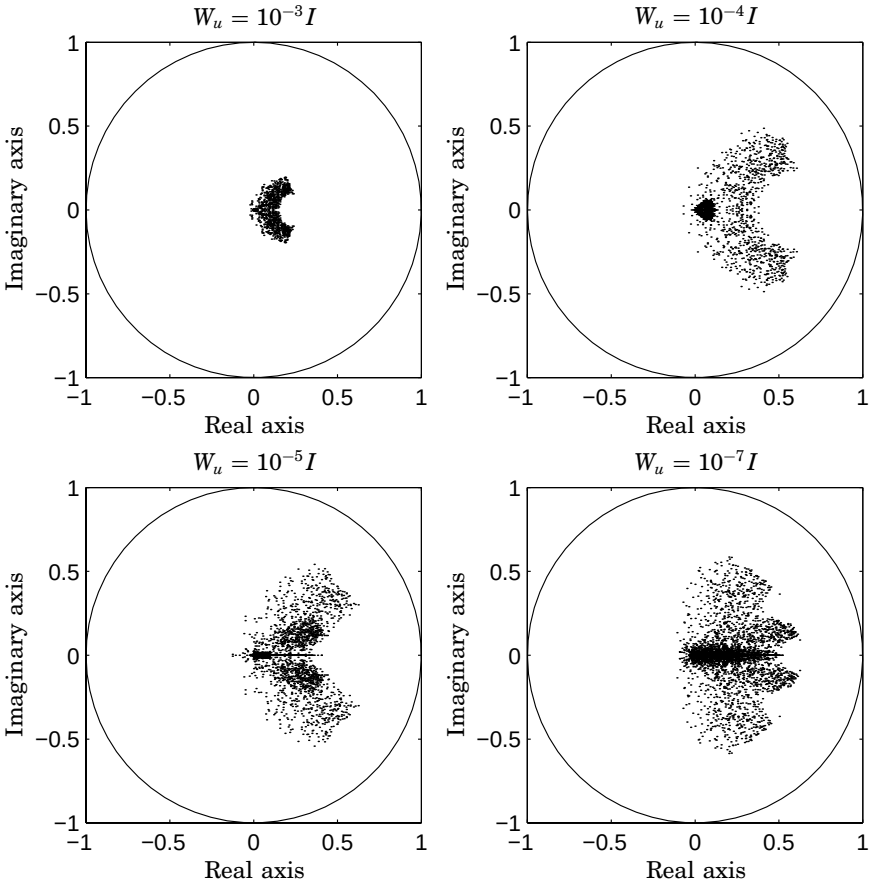

Figure 5.4 The eigenvalues of $\mathcal{A}$ in (5.12) for the CILC algorithm for 500 random systems with uniformly distributed parameters in the intervals $\omega_p \in [17, 21]$, $\zeta_p \in [0, 0.1]$ and $a_p \in [0.06, 0.08]$ for four values of W_u. The system is stable for all of the 500 random random processes but the eigenvalues are further from the origin as W_u is decreased.

used in the update law and for 10 random processes with parameters in the intervals $\omega_p \in [17, 21]$, $\zeta_p \in [0, 0.1]$ and $a_p \in [0.06, 0.08]$. The figure shows that the noise gives a very large variance in the control signal for small values of ρ. For large values of ρ the variances decrease rapidly. Note that the variances do not change much due to the mismatch between the model in the update law and the actual process.

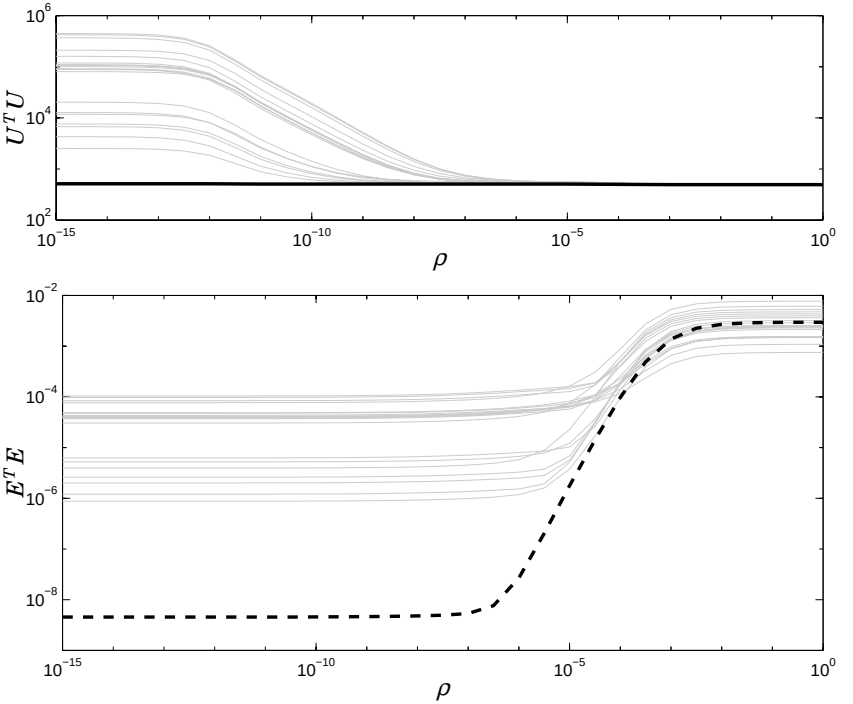

Figure 5.5 The magnitude of the control signal and the control error for different values of ρ with the CILC algorithm. The thick lines are for the case when the model in the update law and the process are equal and the gray lines are for 20 random processes with parameters in the intervals, $\omega_p \in [17, 21]$, $\zeta_p \in [0, 0.1]$ and $a_p \in [0.06, 0.08]$. The figure indicates that $\rho = 10^{-5}$ is a suitable choice.

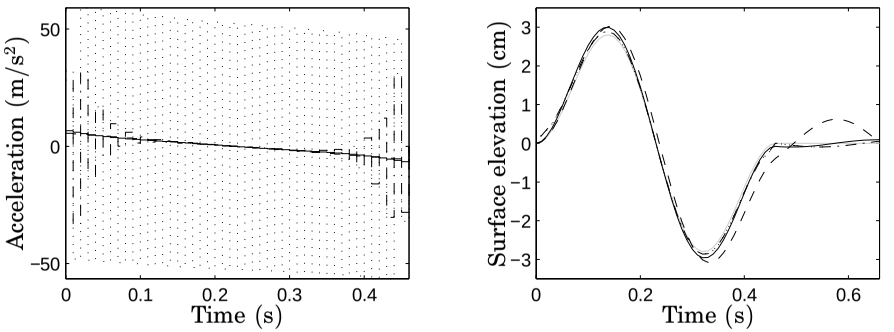

Figure 5.6 The stationary solution of the CILC algorithm given in (5.13) for a process with the parameters $\omega_p = 0.9\omega_m$, $\zeta_p = 0.01$ and $a_p = 1.1a_m$ when $\rho = 1$ (dashed), $\rho = 10^{-5}$ (solid), $\rho = 10^{-10}$ (dash-dotted) and $\rho = 10^{-15}$ (dotted). The reference is the solid gray line. The figure shows that for $\rho \leq 10^{-10}$ there is a chattering behavior in the control signal and that the output is close to the reference for $\rho \leq 10^{-5}$.

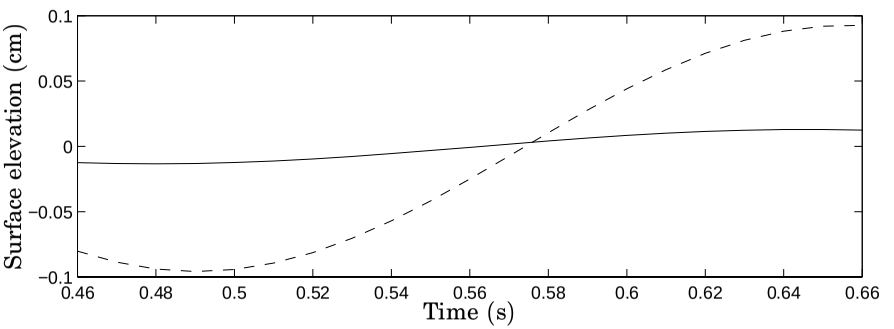

Figure 5.7 The stationary solution of the CILC algorithm given in (5.13) for a process with the parameters $\omega_p = 0.9\omega_m$, $\zeta_p = 0.01$ and $a_p = 1.1a_m$ when $W_u = 10^{-5}$, $W_b = W_f = I$ (dashed) and $W_b = W_f = \mathrm{diag}(I_{46}, 10I_{20})$ (solid). The figure shows that the residual slosh is considerably decreased with the new weighting matrices.

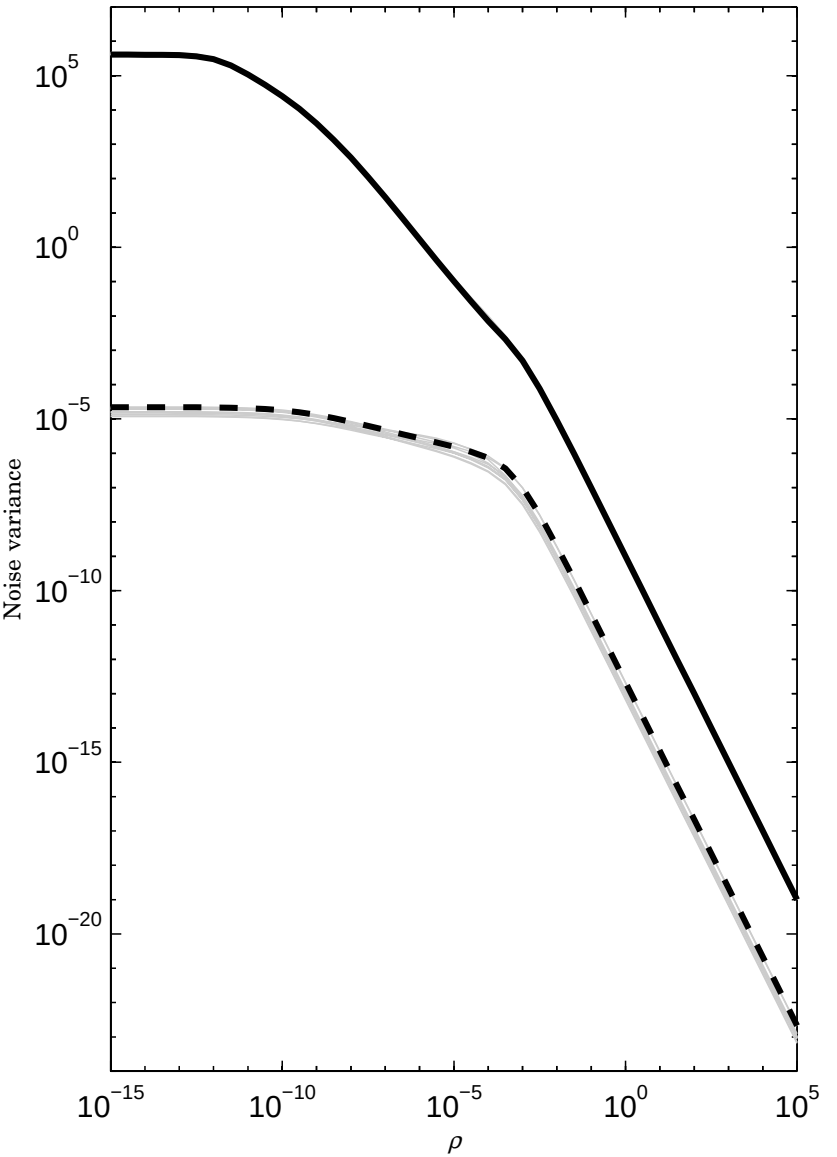

Figure 5.8 Noise variances for the CILC algorithm with respect to $W_u = \rho I$. The thick lines are σ_u^2 (solid) and σ_y^2 (dashed) when the process and the model in the update law are equal. The grey lines are the variances for 10 random processes with parameters in the intervals $\omega_p \in [17, 21]$, $\zeta_p \in [0, 0.1]$ and $a_p \in [0.06, 0.08]$. The variances seem to be insensitive to model mismatch.

The Iterative Optimal Control algorithm (IOC)

The stability, the stationary solution and the noise properties of the IOC algorithm derived in Section 5.4 is calculated numerically.

Stability The eigenvalues of the matrix $\mathcal{A}$ in (5.19) are plotted as one of the parameters in the process model varies and the others are equal to the parameters in the update law. Since the model used in the update law is of second order all eigenvalues but two will be located in the origin. These will not be drawn in the root locus plots. The eigenvalues are calculated using the Matlab function `eig`.

Figures 5.9, 5.10 and 5.11 show the two eigenvalues when the parameters are varying. The figures show that the eigenvalues move outside the unit circle if ω_p and a_p are sufficiently far from ω_m and a_m and that the stability is not affected by ζ_p.

In Figure 5.12 the eigenvalues for 500 random parameters and four different values on the control cost are shown. The parameters are uniformly distributed with the following intervals, $\omega_p \in [17, 21]$, $\zeta_p \in [0, 0.1]$ and $a_p \in [0.06, 0.08]$. The figure shows that the eigenvalues are moved further from the origin as W_u is decreased and hence the robustness to model errors is also decreased. For $\rho \leq 10^{-5}$ the iteration process becomes unstable for some of the parameter values. Compared to the eigenvalues for the CILC algorithm in Figure 5.4 the eigenvalues are further from the origin for the IOC algorithm.

Stationary solution To evaluate the influence of the control cost on the final result the stationary solution is calculated for different values of ρ. Figure 5.13 shows

$$U^T U = \sum_{k=0}^{N-1} u(kh)^2 \quad \text{and} \quad Y_2^T Y_2 = \sum_{k=N+1}^{N+M} y^b(kh)^2$$

as a function of ρ, only the output on one side is considered since $y^f(t) = -y^b(t)$. The figure shows $U^T U$ and $Y_2^T Y_2$ when the model in the update law and the process are equal and for 20 random processes with parameters in the intervals, $\omega_p \in [17, 21]$, $\zeta_p \in [0, 0.1]$ and $a_p \in [0.06, 0.08]$. The figure shows that the residual slosh decreases when ρ is decreased and that there is a slight increase in the control signal when $\rho \leq 10^{-4}$. The increase in the control signal is larger if there are modeling errors.

In Figure 5.14 the stationary solution is shown for some values of ρ for a process with the parameters $\omega_p = 0.9\omega_m$, $\zeta_p = 0.01$ and $a_p = 1.1a_m$. The figure shows that the residual slosh is almost zero for $\rho \leq 10^{-5}$.

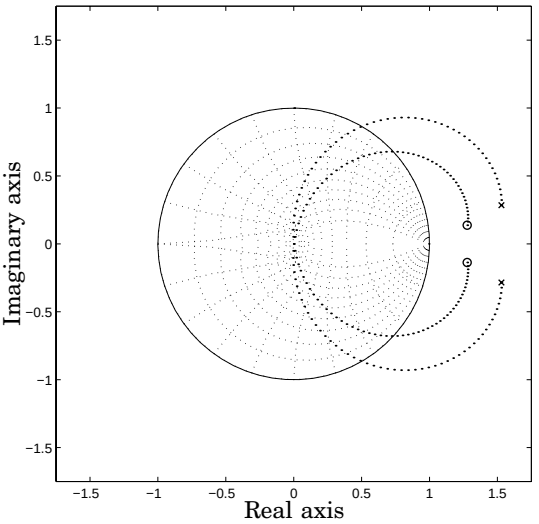

Figure 5.9 The eigenvalues of $\mathcal{A}$ in (5.19) for the IOC algorithm when ω_p is varying from 13 rad/s ($\circ$) to 29 rad/s ($\times$). The system becomes unstable if ω_p is sufficiently far from $\omega_m = 21$ rad/s.

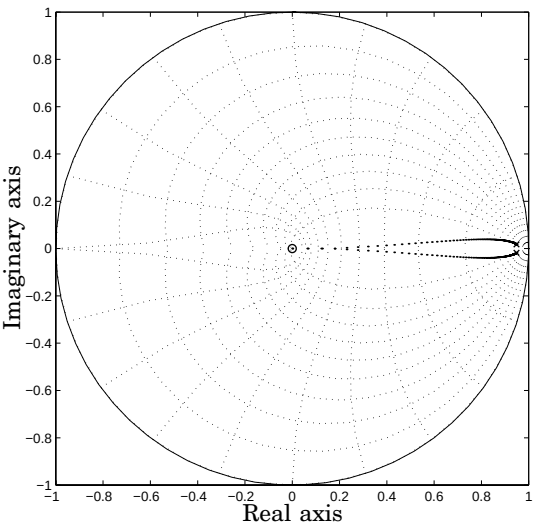

Figure 5.10 The eigenvalues of $\mathcal{A}$ in (5.19) for the IOC algorithm when ζ_p is varying from 0 ($\circ$) to 1 ($\times$). The system is stable for all values of ζ_p.

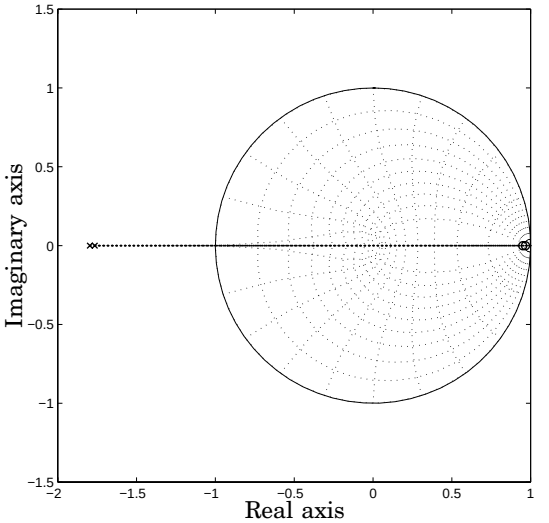

Figure 5.11 The eigenvalues of $\mathcal{A}$ in (5.19) for the IOC algorithm when a_p is varying from 0 m ($\circ$) and 0.2 m ($\times$). When a_p is sufficiently large the system becomes unstable.

Noise Similarly as with the CILC algorithm the noise properties of the IOC algorithm are examined by calculating the control signal variance σ_u^2 and the output variance σ_y^2 in (5.21) for different values of the control cost ρ. Figure 5.15 shows the variances σ_u^2 and σ_y^2 for different values of ρ. The H_2-norm is calculated using the Matlab function `norm` for linear time invariant systems.

The variances are calculated when the process is equal to the model used in the update law and for 10 random processes with parameters in the intervals $\omega_p \in [17, 21]$, $\zeta_p \in [0, 0.1]$ and $a_p \in [0.06, 0.08]$. The figure shows that the variance approaches a constant value as ρ is decreased. For large values of ρ the variances decrease rapidly. It can also be seen that the variances change much due to the mismatch between the model in the update law and the actual process for small values of ρ.

5.6 Evaluation using simulation

The CILC and IOC algorithms described in previous sections are evaluated in simulations.

The model used in the algorithms is given in continuous time by the

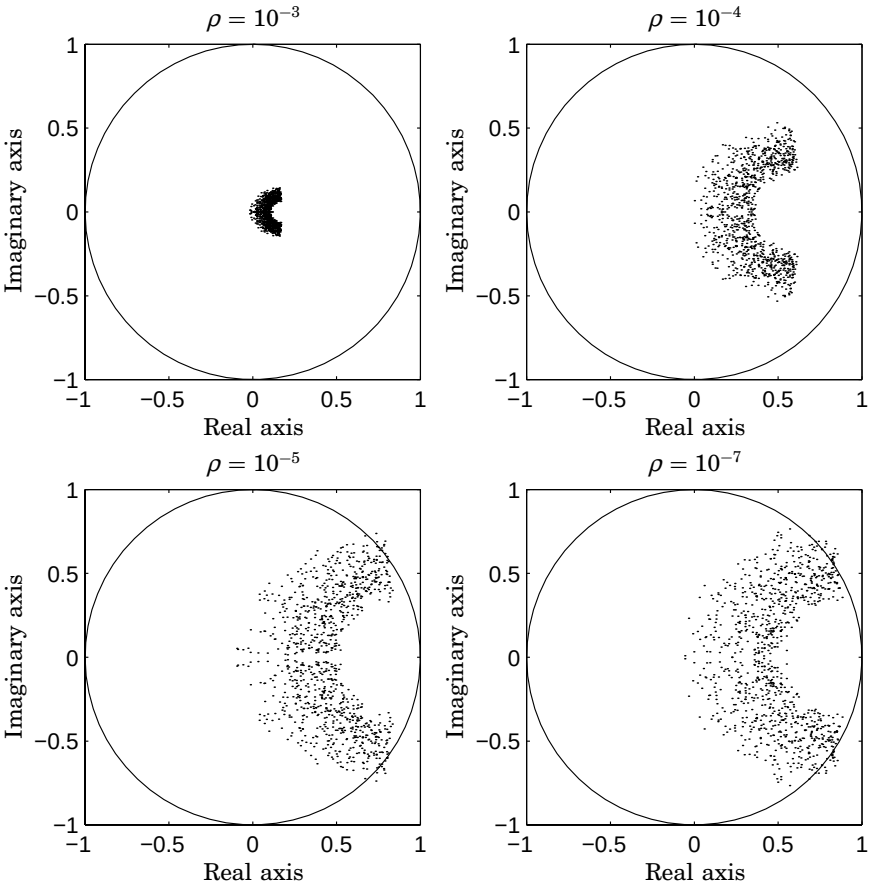

Figure 5.12 The eigenvalues of $\mathcal{A}$ in (5.19) for the IOC algorithm for 500 random systems with uniformly distributed parameters in the intervals $\omega_p \in [17, 21]$, $\zeta_p \in [0, 0.1]$ and $a_p \in [0.06, 0.08]$ for four values of ρ. The system becomes unstable for some of the random processes when $\rho \leq 10^{-5}$. Compare with Figure 5.4 for the CILC algorithm.

transfer operator

$$G_c(p) = \frac{a_m}{2g} \frac{\omega_m^2}{p^2 + \omega_m^2}$$

with $a_m = 0.07$ m and $w_m = 21.0$ rad/s which are the theoretical values given in Section 3.1. This is the same model that was used in the numerical analysis in Section 5.5. The movement time is 0.46 s which gives $N = 46$ and M is chosen as 20.

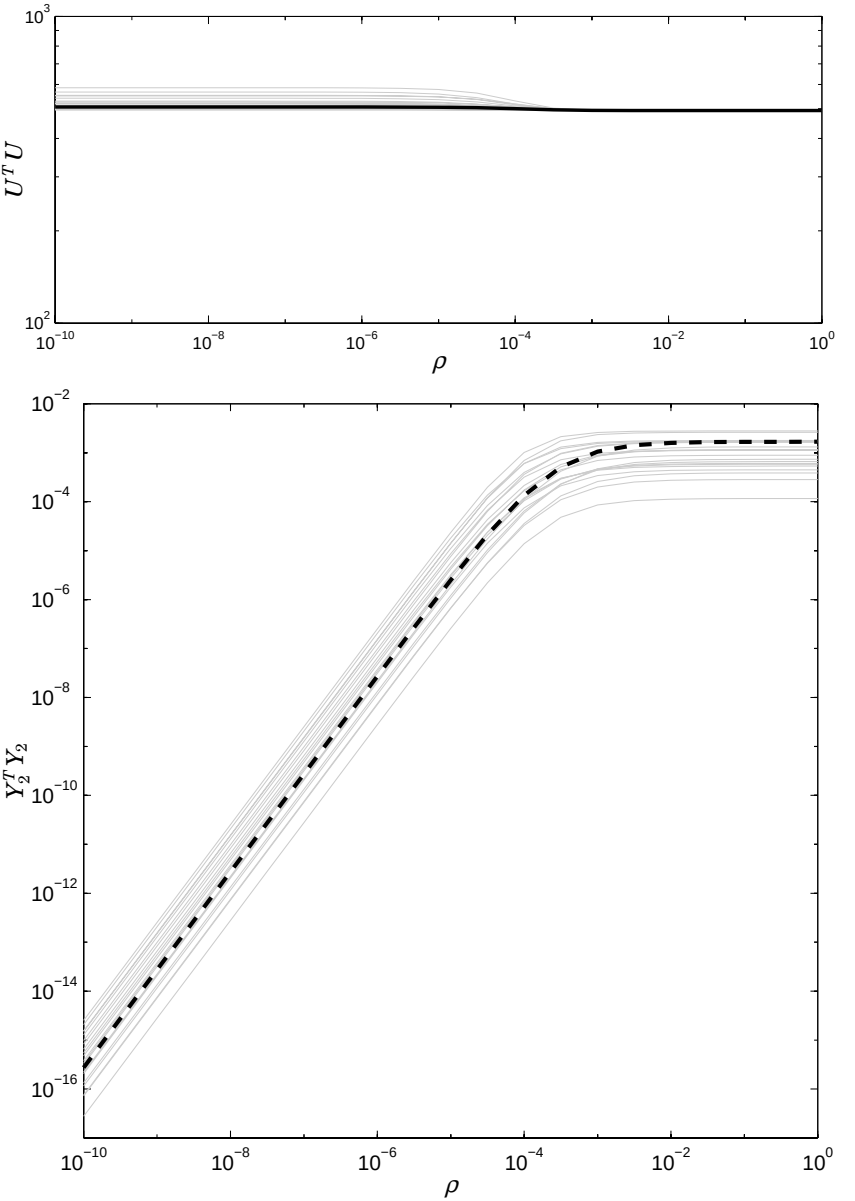

Figure 5.13 The magnitude of the control signal and the residual slosh for different values of the control penalty ρ with the IOC algorithm. The thick lines are for the case when the model in the update law and the process are equal and the gray lines are for 20 random processes with parameters in the intervals, $\omega_p \in [17, 21]$, $\zeta_p \in [0, 0.1]$ and $a_p \in [0.06, 0.08]$.

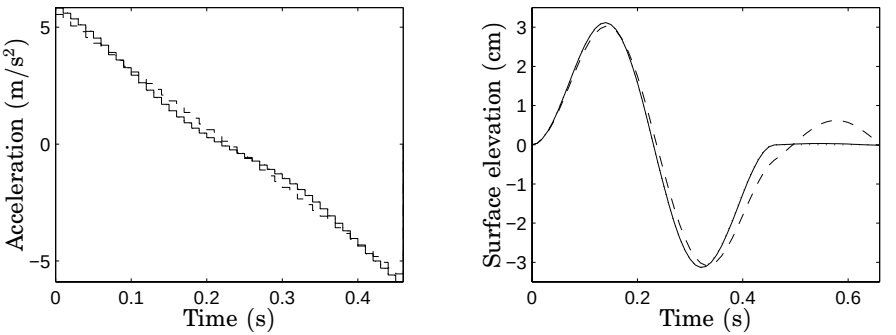

Figure 5.14 The stationary solution of the IOC algorithm given in (5.20) for a process with the parameters $\omega_p = 0.9\omega_m$, $\zeta_p = 0.01$ and $a_p = 1.1a_m$ when $\rho = 1$ (dashed), $\rho = 10^{-5}$ (solid) and $\rho = 10^{-10}$ (dotted). The stationary solutions are very close for $\rho = 10^{-5}$ and $\rho = 10^{-10}$. Compared to Figure 5.6 there is no problem with chattering in the control signal as ρ is decreased.

Process models

Two process models are used in the evaluation; one linear and one nonlinear. The nonlinear model is designed to mimic some of the nonlinear behavior experienced in the real process, see Section 3.3, but there is no direct physical interpretation of the model.

Linear process model The linear model is given in continuous time by the transfer operator

$$P_c(p) = \frac{a_p}{2g}\frac{\omega_p^2}{p^2 + 2\zeta_p\omega_p p + \omega_p^2}$$

with $\omega_p = 0.9\omega_m$, $\zeta_p = 0.01$ and $a_p = 1.1a_m$. Hence, the gain of the process is increased and the oscillation frequency is decreased compared to the model used in the update law. Damping is also added to the process model. The surface elevation measurements are given by

$$\begin{aligned} y^b(t) &= P_c(p)u(t) + v^b(t) \\ y^f(t) &= -P_c(p)u(t) + v^f(t) \end{aligned}$$

where v^* are discrete time white noise with variance 10^{-6}. This is the same model structure and noise variance that were used when evaluating the stability, the stationary solution and the noise properties in Section 5.5.

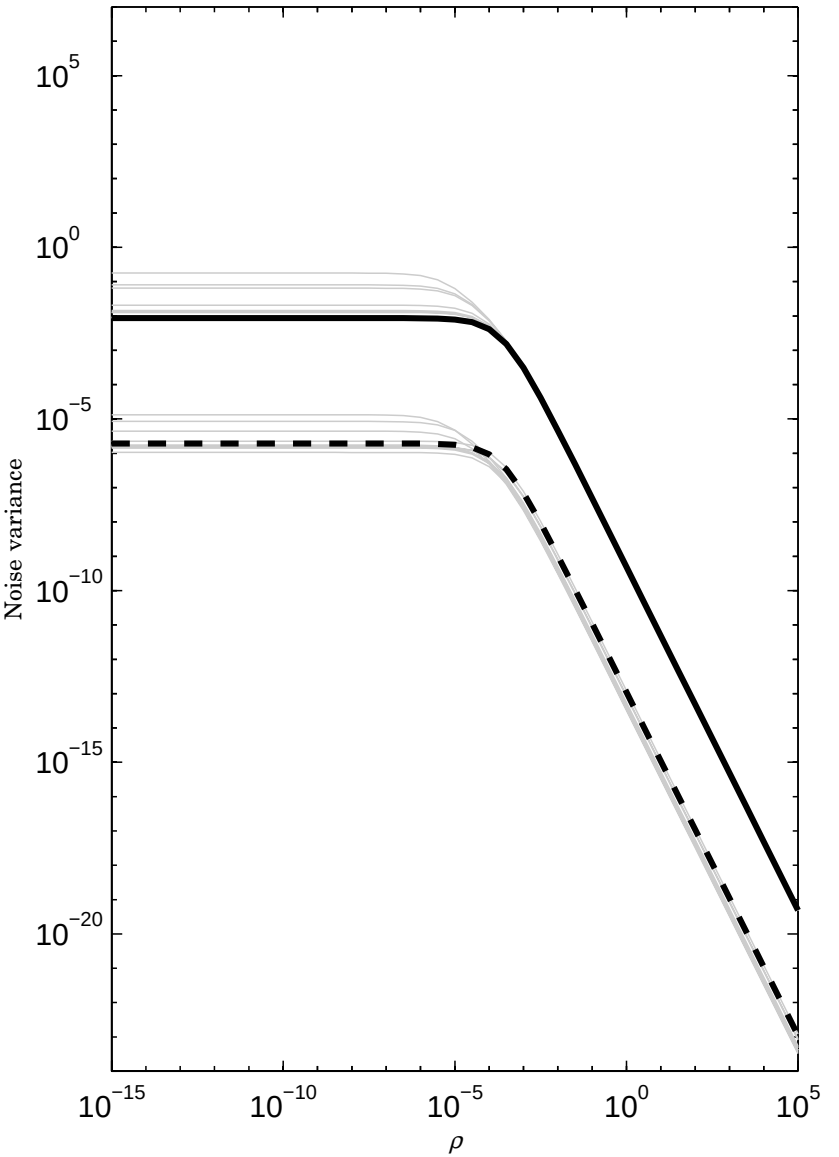

Figure 5.15 Variances for the IOC algorithm with respect to ρ. The thick lines are σ_u^2 (solid) and σ_y^2 (dashed) when the process and the model in the update law are equal. The grey lines are the variances for 10 random processes with parameters in the intervals $\omega_p \in [17, 21]$, $\zeta_p \in [0, 0.1]$ and $a_p \in [0.06, 0.08]$. Compared to the variances for the CILC algorithm in Figure 5.8, σ_u^2 is considerably smaller for small values of ρ.

Nonlinear process model The nonlinear process model is given in continuous time by the state space description

$$\begin{aligned}
\dot{x}_1(t) &= -2\zeta_p\omega_m x_1(t) - \omega_m^2 \frac{\tanh 30x_2(t)}{30} + \frac{a_m\omega_m}{2g}u(t) \\
\dot{x}_2(t) &= x_1(t) \\
y^b(t) &= \frac{4}{5}x_2(t) + 7x_2^2(t) + v^b(t) \\
y^f(t) &= -\frac{4}{5}x_2(t) + 7x_2^2(t) + v^f(t)
\end{aligned}$$

where ω_m, ζ_p, a_m and v^* are the same as previously. The term $\frac{\tanh 30x_2(t)}{30}$ gives an amplitude dependent oscillation frequency and the quadratic term in the output gives asymmetric oscillation. These are behaviors that have been observed in real slosh, see Section 3.3. This model is only designed to mimic these phenomena and has no direct physical meaning.

The Constrained Iterative Learning Control algorithm (CILC)

The CILC algorithm is evaluated on the linear process model given above. The initial acceleration reference and the surface elevation reference are calculated using the minimum energy approach presented in Section 4.7 and the same model as used in the update law.

The weighting matrices are chosen as proposed in Section 5.5, $W_u = 10^{-5}I$ and $W_b = W_f = \text{diag}(I_{46}, 10I_{20})$. Figure 5.16 shows the cost

$$J = {E^b}^T W_b E^b + {E^f}^T W_f E^f + U^T W_u U$$

for the ten first iterations. The figure shows that the cost decreases rapidly during the four first iterations and then remains on a constant level.

In Figure 5.17 the surface elevation on the backward side of the container is shown for the ten first iterations. After four iterations the surface elevation is very close to the reference and does not change much as the iterations are continued.

Figure 5.18 shows the acceleration and the surface elevation on the backward side for the initial trajectory and after five iterations. It also shows the surface elevation reference and the simulated measured surface elevation. It is shown in the figure that the surface elevation is close to the reference after five iterations and the biggest difference is a slightly larger amplitude of the resulting surface elevation. This is due to that the gain is higher in the linear process model which makes the calculated reference infeasible.

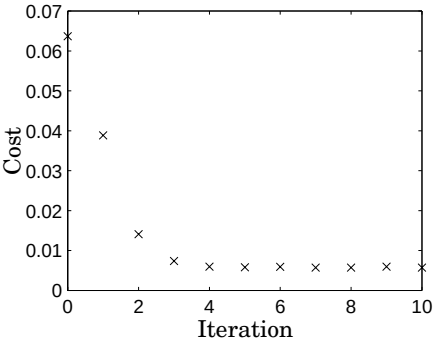

Figure 5.16 The cost for the CILC algorithm for the ten first iterations in the simulation with the linear process model. The cost decreases rapidly during the four first iterations.

A more realistic test of the CILC algorithm is to use the nonlinear process model which emulates some of the behaviors encountered in reality. The algorithm is used with the same weights as used with the linear process model. Figure 5.19 shows the initial and resulting surface elevation after 5 iterations. The figure illustrates the main drawback with the CILC algorithm, the problem with infeasible reference trajectories. The resulting surface elevation is very far from the reference during the peak and the crest of the wave. This is due to the asymmetry in the oscillation. The convergence is also slightly slower compared to the linear process model.

The main objectives are to keep the maximum surface elevation and the residual slosh small. The asymmetry in the oscillation causes the maximum surface elevation to increase since the algorithm tries to make the surface elevations to follow the reference. Since there is a coupling between the surface elevation on the forward and on the backward side of the container the peak on the forward side cannot be lowered without raising the crest on the backward side. It is more important to lower the maximum surface elevation than to increase the crests and therefore the weighting matrices W_b and W_f are modified to neglect the errors when the reference is negative.

To handle the asymmetric oscillation the following weighting matrices are therefore used

$$W_b = \text{diag}(I_{23}, 0_{23}, 10I_{20}), \quad W_f = \text{diag}(0_{23}, I_{23}, 10I_{20}) \tag{5.22}$$

and $W_u = 10^{-5}I$ where 0_n is an $n \times n$ zero matrix. The results using the modified weighting matrices are shown in Figure 5.20. The figure shows

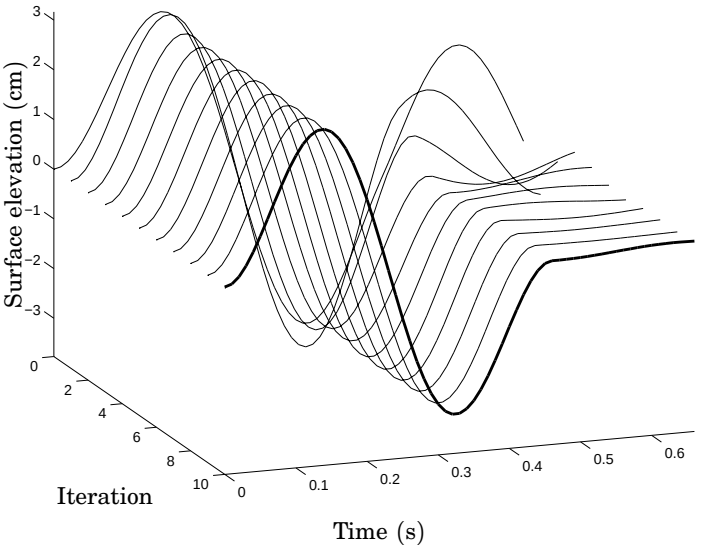

Figure 5.17 The surface elevation of the backward side of the container for the ten first iterations when the CILC algorithm is simulated with the linear process model. The surface elevation converges to a steady state in four iterations.

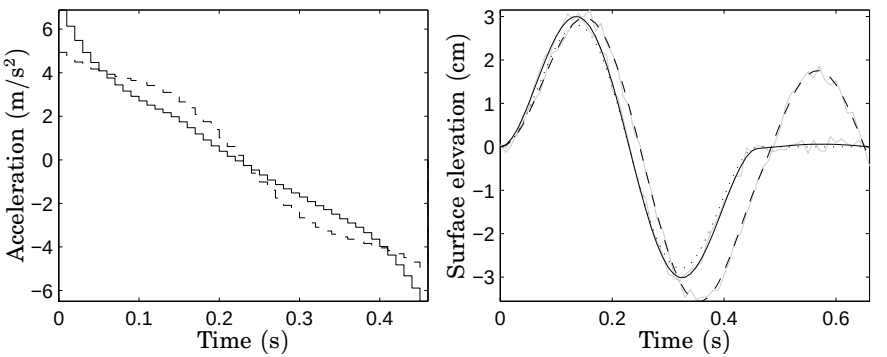

Figure 5.18 The acceleration reference (left) and surface elevation (right) before the iteration is started (dashed) and after five iterations (solid) when the CILC algorithm is simulated with the linear process model. The surface elevation reference (dotted) and the simulated measurement (grey) are also shown. The surface elevation after five iterations is close to the reference and there is very little noise visible in the surface elevation.

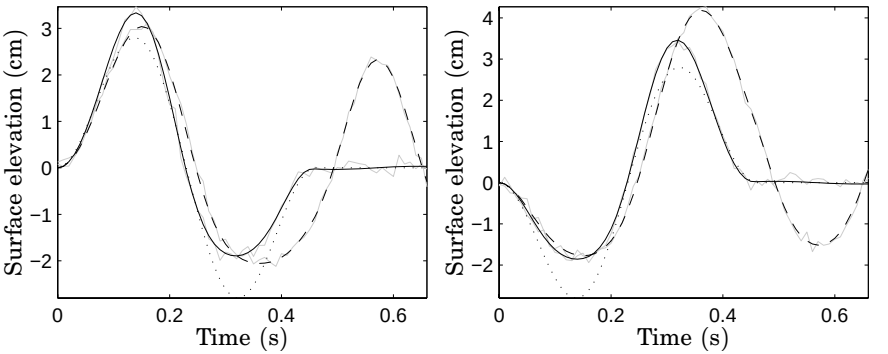

Figure 5.19 The surface elevation on the backward (left) and on the forward (right) side of the container before the iteration is started (dashed) and after five iterations (solid) when the CILC algorithm is simulated with the nonlinear process model. The surface elevation reference (dotted) and the simulated measurement (grey) are also shown. The asymmetric oscillation amplitude causes a large difference between the reference and the resulting surface elevation after five iterations.

that the maximum surface elevation is reduced to the same level as in the simulation with the linear process model. This shows that it is possible to compensate for nonlinearities by modifying the weighting matrices.

The simulations have shown that the CILC algorithm is able to handle the nonlinearities and that it is not affected by the measurement noise with this choice of the weighting matrices.

The Iterative Optimal Control algorithm (IOC)

In the same way as the CILC algorithm was evaluated the IOC algorithm is now simulated using a linear process model. The control cost is chosen as $\rho = 10^{-5}$ as proposed in Section 5.5. The maximum control is $u_{max} = 10$ m/s^2 and the maximum allowed surface elevation is $s_{max} = 3.5$ cm. Figure 5.21 shows the actual cost and the predicted cost for ten iterations, where the actual cost, J^a, is calculated using the actual surface elevation and predicted cost, J^p, is calculated using the predicted surface elevation. The cost is calculated using

$$\begin{aligned} J_k^a &= \rho U_k^T U_k + Y_{2\,k}^{b\,T} Y_{2\,k}^b + Y_{2\,k}^{f\,T} Y_{2\,k}^f \\ J_k^p &= \rho U_k^T U_k + \hat{Y}_{2\,k}^{b\,T} \hat{Y}_{2\,k}^b + \hat{Y}_{2\,k}^{f\,T} \hat{Y}_{2\,k}^f \end{aligned} \tag{5.23}$$

with

$$\hat{Y}_{2\,k}^b = \widetilde{Y_{2\,k-1}^b} + G_2(U_k - U_{k-1}), \quad \hat{Y}_{2\,k}^f = \widetilde{Y_{2\,k-1}^f} - G_2(U_k - U_{k-1})$$

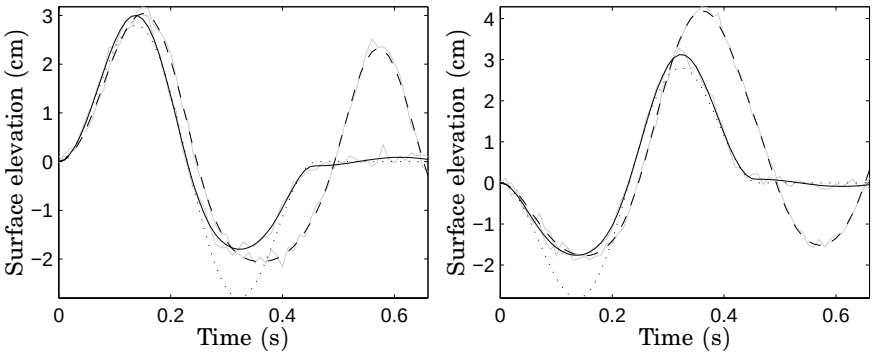

Figure 5.20 The surface elevation on the backward (left) and on the forward (right) side of the container before the iteration is started (dashed) and after five iterations (solid) when the CILC algorithm is simulated with the nonlinear process model and the modified weighting matrices given in (5.22). The surface elevation reference (dotted) and the simulated measurement (grey) are also shown. Compared to Figure 5.19 the maximum surface elevation is reduced.

where $\widetilde{Y}$ is the simulated surface elevation measurement and $\hat{Y}$ is the predicted surface elevation.

The figure shows that the actual cost decreases rapidly and the predicted and actual cost are very close after five iterations. The figure shows also that when the iterations have converged the predicted cost is occasionally larger than the actual cost. This is because the noise is include in the measurement of the surface elevation from the previous iteration in the prediction.

Figure 5.22 shows the surface elevation on the backward side of the container for the ten first iterations. The residual slosh decreases fast in the first five iterations and then the surface elevation does not change much.

The true optimal control signal is easy to calculate for the linear process model and is compared with the result of the IOC algorithm in Figure 5.23. The figure shows that the IOC algorithm converges to a steady state very close to the true optimal solution.

The IOC algorithm is also tested with the nonlinear process model to see how the nonlinearities are handled. Figure 5.24 shows the actual and predicted cost for the ten first iterations. The actual cost decreases rapidly during the five first iterations and then the actual cost and predicted cost are very close.

The surface elevation on both sides of the container is shown for the ten first iterations in Figure 5.25 for the nonlinear model. The figure shows

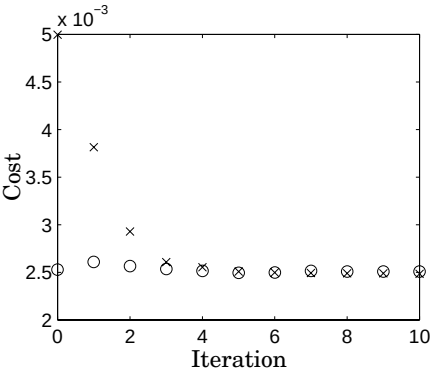

Figure 5.21 The actual (×) and predicted (∘) cost for the ten first iterations with the IOC algorithm and the linear process model. The actual cost decreases fast in the five first iterations and then the predicted and actual cost are very close.

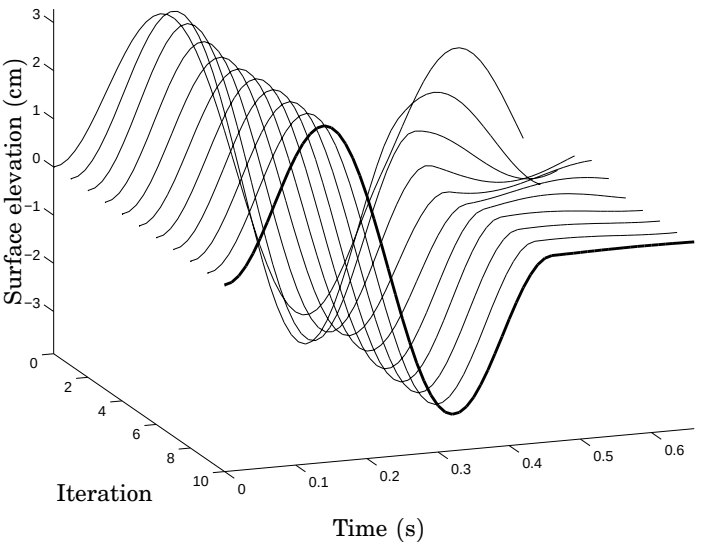

Figure 5.22 The surface elevation on the backward side of the container for the ten first iterations when the IOC algorithm is simulated with the linear process model. The residual slosh decreases fast and the surface elevation converges to a steady state in six iterations.

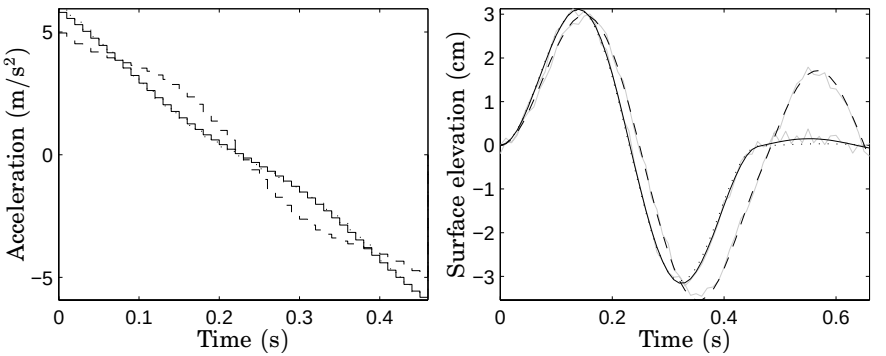

Figure 5.23 The acceleration reference (left) and surface elevation (right) before the iteration is started (dashed) and after six iterations (solid) when the IOC algorithm is simulated with the linear process model. The true optimal solution (dotted) and the measured surface elevation (grey) are also shown. The figure shows that the result of the IOC algorithm is very close to the true optimal solution.

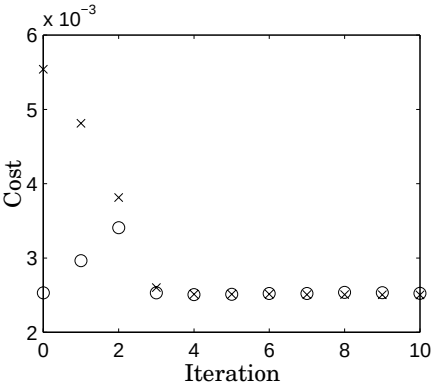

Figure 5.24 The actual (×) and predicted (∘) cost for the ten first iterations with the IOC algorithm and the nonlinear process model. The actual cost decreases fast in the five first iterations and then the predicted and actual cost are very close.

that the residual slosh is very large in the first iteration but decreases rapidly and is almost zero after six iterations. The maximum surface elevation on the forward side of the container is also very large in the first iterations but is decreased to a normal level in 2 iterations.

In the simulations with the IOC algorithm neither the control nor the surface elevation constraints are active when the iterations have con-

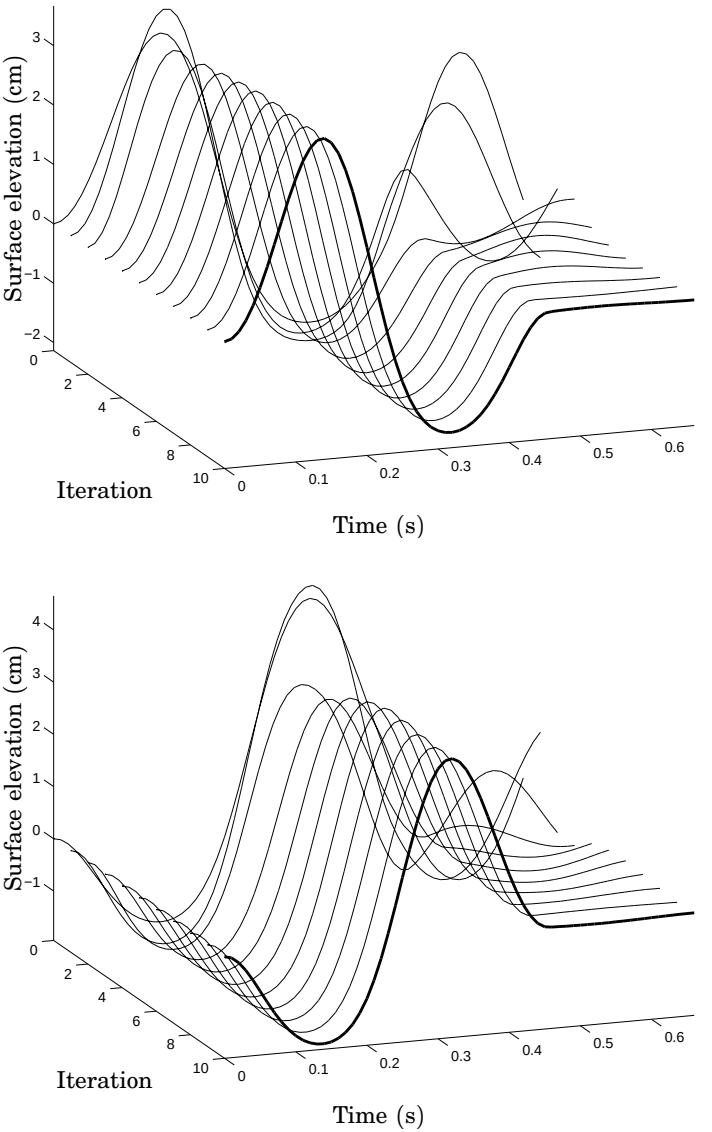

Figure 5.25 The surface elevation on the backward (upper) and on the forward (lower) side of the container for the ten first iterations when the IOC algorithm is simulated with the nonlinear process model. The residual slosh decreases fast and the surface elevation converges to a steady state in six iterations.

verged. This corresponds to the case that was analyzed in Section 5.4 and Section 5.5. To examine the behavior of the algorithm in the case of active constraints the movement time is decreased to 420 ms which gives $N = 42$, $M = 20$ and the algorithm is simulated with the nonlinear process model. To obtain the same levels of residual slosh as in the previous simulations the control cost had to be decreased to $\rho = 10^{-7}$.

Figure 5.26 shows the surface elevation on the backward side of the container for the 20 first iterations for two simulations; one with measurement noise and the other one without. A comparison between the two simulations shows that there is a fluctuation in the surface elevation between the iterations in the simulation with noise that is not present in the noise free simulation. This fluctuation has not been present in the previous simulations with the IOC algorithm. This indicates that the algorithm is more sensitive to noise when the constraints are active. This is quite intuitive, since if the control is calculated to keep the predicted surface elevation on the constraint then in the next iteration when the control is applied a different noise sequence will be present and the constraint will be violated.

This can also be seen by studying the control signal shown in Figure 5.27 for both cases. The figure shows that the control signal is almost bang-bang after the first iteration which is very different from the initial control. This is because there is a very large violation of the surface elevation constraint when the initial control is applied. This shows that there is a very high gain from constraint violations to the control.

The simulations have shown that the IOC algorithm is able to handle the nonlinearities and the measurement noise. Contrary to the CILC algorithm there is no need to alter the parameters of the algorithm to handle nonlinearities and there is no problem with infeasible reference trajectories. There is however some problems with noise if the surface elevation constraints are active because of fluctuations between iterations. This is because there is no noise attenuation in the prediction of the surface elevation in the algorithm.

5.7 Evaluation using experiments

The performance of the CILC and IOC algorithms in reality is evaluated using the experimental setup described in Chapter 2.

Since there is only one surface elevation measurement on one side of the container two experiments with the same acceleration reference is performed to obtain the data needed; one forward and one backward.

The model used in the algorithms is given in continuous time by the

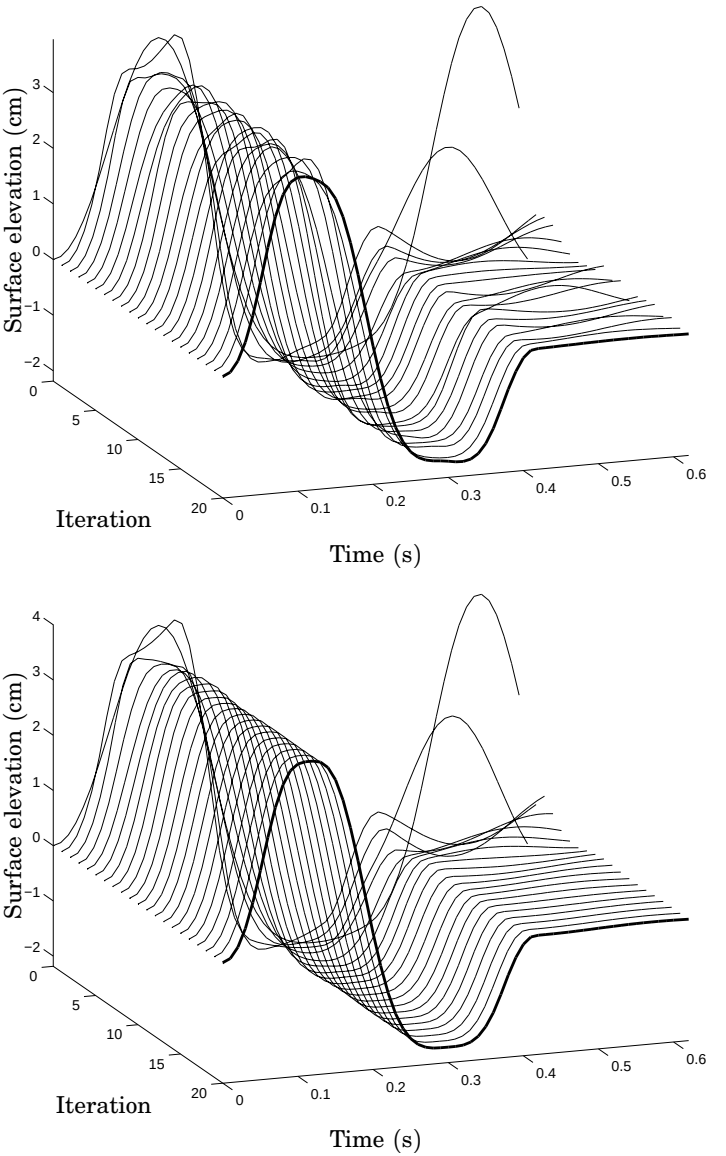

Figure 5.26 Surface elevation on the backward side of the container when the IOC algorithm is simulated using a nonlinear process model for a movement when the constraints are active. The simulation is performed both with measurement noise (upper) and without (lower). The figure shows that there is a fluctuation in the surface elevation between the iterations induced by the noise. However the algorithm is still successful in minimizing the maximum surface elevation and residual slosh.

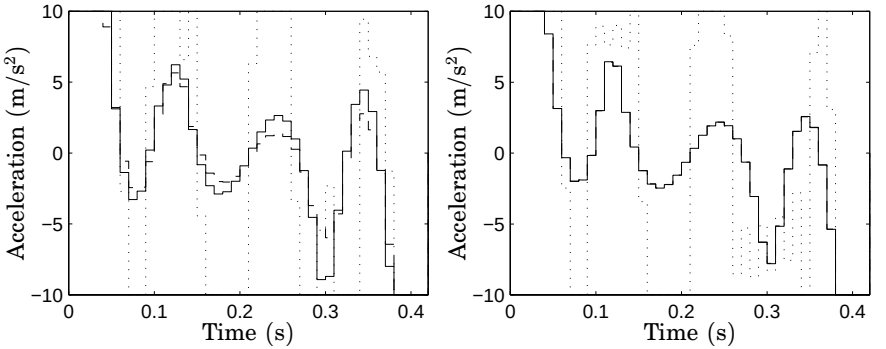

Figure 5.27 The control signal when the IOC algorithm is simulated using the nonlinear process model for a movement when the constraints are active. The simulation is performed both with measurement noise (left) and without (right). The figure shows the control signal after the first iteration (dotted), the 19th (dashed) and the 20th (solid). The control signal after the first iteration is almost bang-bang in both cases and with measurement noise the difference between the 19th and 20th iteration is quite large.

transfer operator

$$G_c(p) = \frac{a_m}{2g} \frac{\omega_m^2}{p^2 + \omega_m^2}$$

with $a_m = 0.07$ m and $\omega_m = 21.0$ rad/s which are the theoretical values given in Section 3.1. The movement time is 0.46 s which gives $N = 46$ and M is chosen as 20. This is the same model and parameters that were used in the numerical analysis in Section 5.5 and in the simulations in Section 5.6.

The Constrained Iterative Learning Control algorithm (CILC)

The following weighting matrices were used when running the CILC algorithm in the experimental setup:

$$W_u = 10^{-5} I, \quad W_b = \text{diag}(I_{23}, 0_{23}, 10 I_{20}), \quad W_b = \text{diag}(0_{23}, I_{23}, 10 I_{20})$$

These are the same weighs that were used in the simulations with the nonlinear process model. The results of the experiments are presented in the figures 5.28, 5.29 and 5.30.

In Figure 5.28 the cost is shown for the ten first iterations. The figure shows that the cost increases in the first iteration but then decreases fast during the next three iterations. After four iterations there is only a slight decrease of the cost.

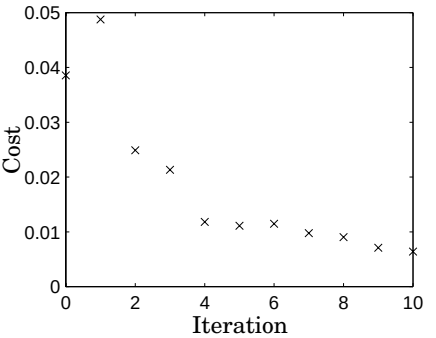

Figure 5.28 The cost for the ten first iterations with the CILC algorithm in the experimental setup. The cost increases in the first iteration but then decreases fast during the next three iterations.

Figure 5.29 shows the acceleration reference and surface elevation response for the initial experiment and after ten iterations. It is seen in the figure that the maximum surface elevation is decreased and that there is almost no residual slosh after ten iterations.

The surface elevation response in all experiments are shown in Figure 5.30. The figure shows that the residual slosh decreases fast and that the maximum slosh is also decreased.

The experiments have shown that the CILC algorithm is successful in reducing the residual slosh in the experimental setup.

The Iterative Optimal Control algorithm (IOC)

The IOC algorithm is evaluated in the experimental setup and the control cost is chosen as $\rho = 10^{-5}$ as in the numerical analysis and in the simulations. The maximum control is set to $u_{max} = 10$ m/s^2 and the maximum allowed surface elevation $s_{max} = 3.5$ cm. The results of the experiments are presented in the figures 5.31, 5.32 and 5.33.

The actual cost, J^a, and predicted cost, J^p, see (5.23), for the twelve first iterations are shown in Figure 5.31. The cost decreases fast in the first iteration then alternates between increase and decrease for a few iterations and then continues to decrease after the fourth iteration. After ten iterations the actual and predicted cost are very close.

In Figure 5.32 the acceleration reference and surface elevation response for the initial experiment and after twelve iterations are shown. The figure shows that there is almost no residual slosh after twelve iterations and that the maximum surface elevation is decreased and that the surface elevation constraint is not violated.

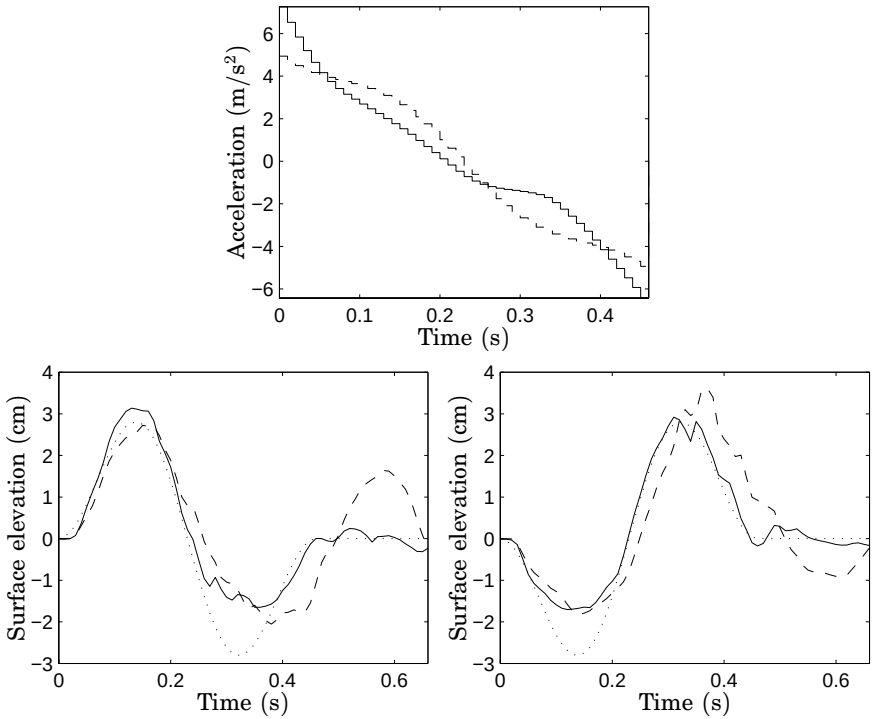

Figure 5.29 The acceleration reference (upper), surface elevation on the backward side (lower left) and on the forward side (lower right) before the iteration is started (dashed) and after ten iterations (solid) when the CILC algorithm is used in the experimental setup. The dotted line shows the surface elevation reference used in the algorithm. The figure shows that the residual slosh is considerably decreased and that the surface elevation is close to the reference when the reference is positive after ten iterations.

The surface elevation response for the twelve first iterations are shown in Figure 5.33. The figure shows that the residual slosh decreases fast in the first iterations and that the maximum surface elevation is also decreased in the first iterations.

The experiments have shown that the IOC algorithm is successful in reducing the residual slosh in the experimental setup.

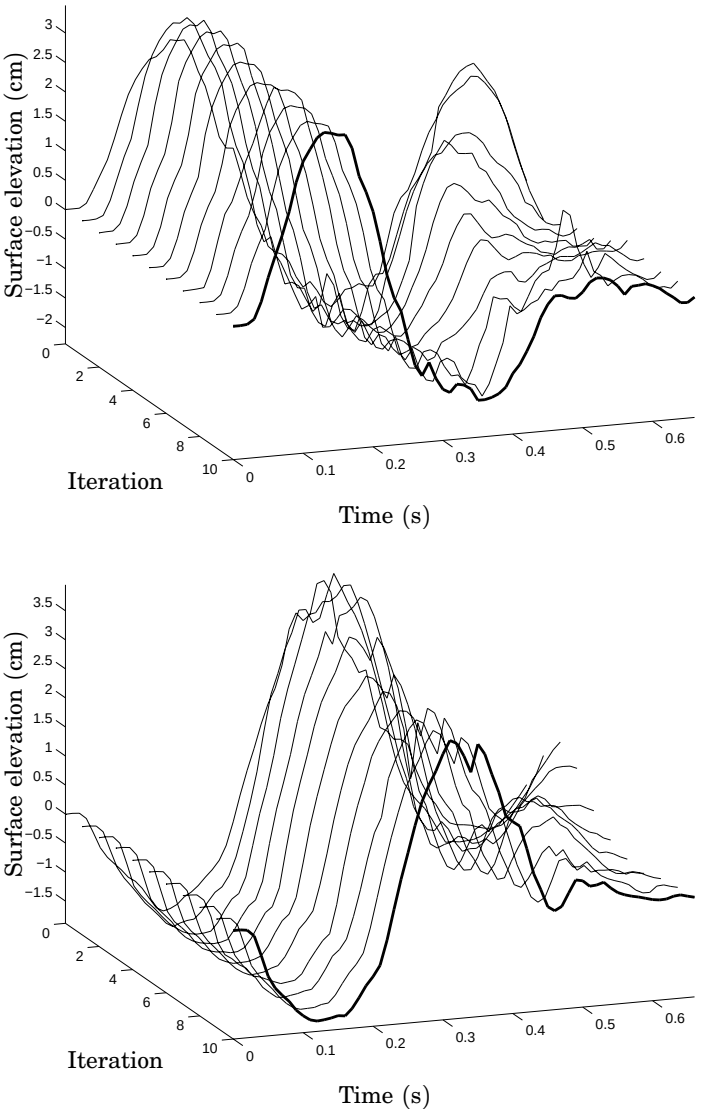

Figure 5.30 The surface elevation on the backward (upper) and on the forward (lower) side of the container for the ten first iterations when the CILC algorithm is used in the experimental setup. The residual slosh decreases fast and the maximum slosh is also decreased.

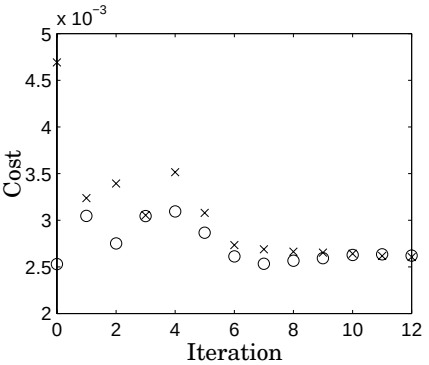

Figure 5.31 The actual (×) and predicted (∘) cost for the twelve first iterations with the IOC algorithm in the experimental setup. The actual cost decreases in the first iteration then jumps around for a few iterations and then continues to decrease after the fourth iteration. After ten iterations the actual and the predicted cost are very close.

5.8 Conclusions

In this chapter two different approaches of Iterative Learning Control (ILC) have been used to find an acceleration reference that fulfills the specifications. Since the learning signal is the acceleration and there are constraints on the final position and velocity the standard formulation of Iterative Learning Control could not be used.

In Section 5.3 the Constrained Iterative Learning Control (CILC) algorithm is presented. The algorithm tries to find an acceleration reference that makes the surface elevation follow a reference while preserving the constraints on terminal position and velocity of the container. The algorithm is based on minimization of a quadratic cost function subject to linear equality constraints. The cost function contains the acceleration and the surface elevation error on both sides of the package. The optimization problem is solved analytically which results in an update law that consists of three time-varying linear filters. Analysis of the algorithm using a linear process model gives stability conditions, the stationary solution and some noise properties.

The CILC algorithm uses a reference for the surface elevation that is derived using some of the methods in Chapter 4. If there are modeling errors when generating the reference it will be non optimal and even infeasible. Therefore, the Iterative Optimal Control (IOC) algorithm is derived was Section 5.4.

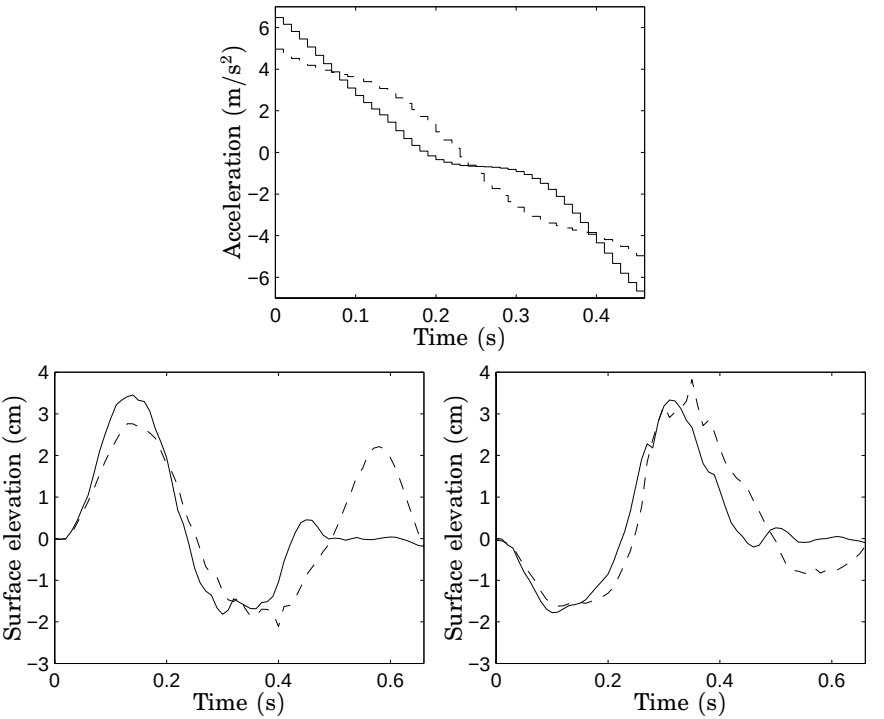

Figure 5.32 The acceleration reference (upper), surface elevation on the backward side (lower left) and on the forward side (lower right) before the iteration is started (dashed) and after ten iterations (solid) when the IOC algorithm is used in the experimental setup. The figure shows that the residual slosh is considerably decreased and that the surface elevation constraint is not violated.

The IOC algorithm is based on the discrete time minimum time optimal control problem in Section 4.9 but the equality constraints on the surface elevation is replaced by a quadratic penalty on the residual slosh. The algorithm is given as a quadratic program that is solved between each experiment. The inequality constraints on the acceleration and surface elevation are removed which enables the optimization problem to be solved analytically. The analytical solution to the quadratic program yields an update law that consists of three time-varying linear filters similarly as the CILC algorithm. Analysis of the algorithm using the analytical solution and a liner process model gives stability conditions, the stationary solution and some noise properties.

Both algorithms use a linear model of the surface elevation response

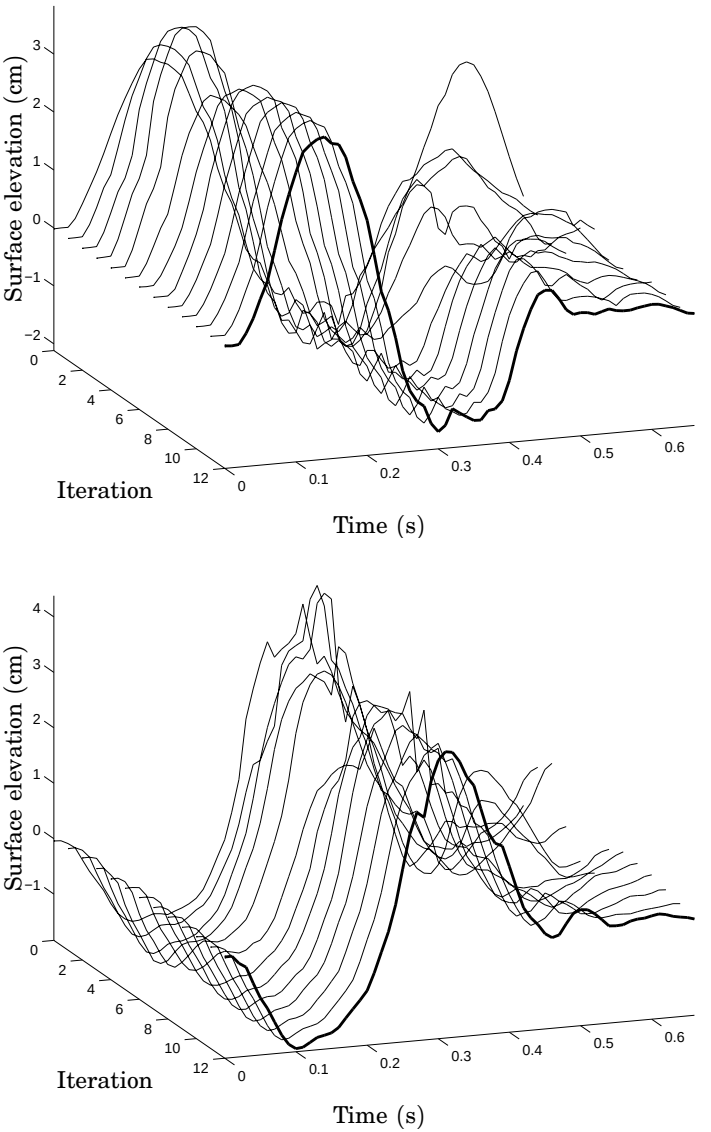

Figure 5.33 The surface elevation on the backward (upper) and forward (lower) side of the container for the the first iterations when the IOC algorithm is used in the experimental setup. The residual slosh decreases fast and the maximum slosh is also decreased.

to acceleration to predict the surface elevation in the next iteration.

In Section 5.5 the eigenvalues are calculated numerically for both algorithms with a linear process model of the same structure as the model in the update law but with parameter mismatch. This shows that if there are sufficiently large parameter mismatch the iterative procedure becomes unstable. The calculation also shows that a larger parameter mismatch can be handled if the penalty on the control is larger and that the CILC algorithm is more robust to model errors than the IOC algorithm. The section also contains numerical calculations of the stationary solutions for different weights in the cost functions and shows that if the control cost is too small in the CILC algorithm the acceleration reference will exhibit a chattering behavior. The examination of the stationary solution gives some insight on how to choose the weights. The numerical calculation of the noise variance shows that the variance increases as the control cost is decreased and for small values of the control cost the variance in the control signal is about 10^7 times larger for the CILC algorithm than for the IOC algorithm.

The algorithms are evaluated using simulations of both a linear and a nonlinear process model in Section 5.6. The simulations show that both methods work well for both the linear and the nonlinear process model. However, the weights in the CILC algorithm needed to be modified such that the surface elevation error is not penalized when the surface elevation reference is negative with the nonlinear process model. This is because the surface oscillation is asymmetric in the nonlinear process model which makes the reference infeasible. These problems were not encountered using the IOC algorithm but the simulations showed that the noise sensitivity was increased if the surface elevation constraints were active.

Evaluation of the algorithms in the experimental setup are made in Section 5.7. The experiments show that both algorithms are successful in finding suitable acceleration references that minimize the residual slosh.

The iterative methods have proven to work very well and have shown that it is possible to find good acceleration references using only a simple model of the slosh phenomenon.

6

Combined horizontal and rotational motion

One way to minimize the surface elevation relative to the container wall is to combine horizontal acceleration with rotation of the container to counteract the motion of the liquid. The use of rotation to obtain slosh free motion is also explored in [Feddema *et al.*, 1997] and [Yano *et al.*, 1999].

The experimental evaluation in Section 3.3 showed that the response to horizontal acceleration and rotational acceleration is linear for small oscillation amplitudes. It was also shown that the oscillation caused by the rotational acceleration can be minimized by choosing the vertical position of the rotational axis properly.

In this chapter the model in (3.40) for simultaneous horizontal and rotational acceleration presented in Section 3.5 is used for synthesis of movements that minimize the maximum surface elevation relative to the container wall.

Section 6.1 shows how the tilt angle that totally counteracts the surface elevation can be calculated if the rotational acceleration does not cause any surface oscillation. In Section 6.2 the problem is approached using optimal control and a minimum energy discrete time optimal control problem is solved using quadratic programming. The obtained horizontal and rotational acceleration references are also evaluated using experiments showing that the method is successful. The conclusions are given in Section 6.3.

6.1 Direct calculation of the tilt angle

If the rotational acceleration does not cause any surface oscillation, i.e. $b_2 = 0$ in (3.40), the tilt angle that gives zero surface elevation relative

to the container wall can easily be calculated. The horizontal acceleration is calculated using any of the methods in Chapter 4 or Chapter 5. The resulting surface elevation $s(t)$ is then obtained by simulating the model in (3.39).

The tilt angle $\theta(t)$ that gives zero surface elevation relative to the container wall is now obtained from

$$\theta(t) = \arctan \frac{2s(t)}{a}$$

where a is the container width. This gives the required rotational acceleration

$$u_r(t) = \frac{d^2\theta(t)}{dt^2} = \frac{2a\frac{d^2s(t)}{dt^2}}{a^2 + 4s(t)^2} - \frac{16a\left(\frac{ds(t)}{dt}\right)^2 s(t)}{(a^2 + 4s(t)^2)^2}$$

where $\frac{d^2s(t)}{dt^2}$ and $\frac{ds(t)}{dt}$ can be obtained from the state equations in (3.39).

It is also possible to calculate the tilt angle that reduces the surface elevation relative to the container wall by a certain amount. By choosing α between 0 and 1 in

$$\theta(t) = \arctan \frac{2\alpha s(t)}{a}$$

the maximum surface elevation can be decreased to a desired level. With $\alpha = 1$ the surface elevation is set to zero and with $\alpha = 0$ the maximum is unchanged and there is no tilting action. The required rotational acceleration is obtained in the same way as previously.

6.2 Optimal control

The direct calculation is only applicable if the rotational acceleration does not excite the surface oscillation. If b_2 in (3.40) is not zero then the rotation will cause surface oscillation. Therefore, when designing the rotational acceleration the surface oscillations need to be taken into account. This can be done by solving an optimal control problem for the horizontal and rotational acceleration.

All optimal control problems that were studied in Chapter 4 can also be studied when the rotational acceleration is added by using the model in (3.40) instead of the model in (3.39) and adding constraints on the terminal angel and angular velocity. Here, only the minimum energy problem will be studied since that approach proved to work well in practice, see Section 4.6.

The following optimal control problem will be studied

$$\min_{u_h,u_r} \int_0^T \rho_h u_h^2(t) + \rho_r u_r^2(t)\ dt$$

subject to: The model in (3.40)

$$|u_h(t)| \leq a_{max}$$
$$|u_r(t)| \leq r_{max}$$
$$|s(t)| \leq s_{max}$$
$$x(0) = [\,0 \quad 0 \quad 0 \quad 0 \quad 0 \quad 0\,]^T$$
$$x(T) = [\,0 \quad 0 \quad 0 \quad L \quad 0 \quad 0\,]^T$$

where T is the movement time and L is the movement distance. The constraints state that there is no surface oscillation in the end of the movement and that the container moves the desired distance and is at rest at the end of the movement.

If the rotational acceleration does not excite the oscillation, i.e. $b_2 = 0$, the maximum surface elevation is set to $s_{max} = 0$, the cost for tilting is set to $\rho_r = 0$, the maximum allowed rotational acceleration is set to $r_{max} = \infty$ and the horizontal acceleration is the minimum energy acceleration reference then the solution to the optimal control problem will be the same as for the direct calculation of the tilt angle described previously.

Similarly as in Section 4.9 this continuous time optimal control problem can be discretized using zero-order-hold sampling of the inputs u_h and u_r. The model in (3.40) is nonlinear in the output. If the model is linearized, the optimal control problem can be formulated as a quadratic programming problem in the same way as in Section 4.9.

By replacing the term $-(a/2)\tan x_6$ with $-(a/2)x_6$ the system becomes linear. This simplification will lead to that $s(t)$ is larger for the linearized model than for the nonlinear model and hence solutions to optimal control problems using the linearized model will tilt the container more than necessary to satisfy the constraint $|s(t)| \leq s_{max}$ for the nonlinear model.

The sampling period h is chosen such that $T = Nh$ and the matrices G^h and G^r are constructed in the same way as in Section 4.9 where G^h contains the pulse response from horizontal acceleration to the surface elevation relative to the container wall and G^r the corresponding response from rotational acceleration.

The control signals are collected in the vector

$$U = [\,u_h(0) \quad \ldots \quad u_h((N-1)h) \quad u_r(0) \quad \ldots \quad u_r((N-1)h)\,]^T$$

and now the response to the horizontal and rotational acceleration can be written as

$$S = GU \quad \text{with} \quad G = [\,G^h \quad G^r\,]$$

since the initial condition is zero. The optimal control problem can now be written as

$$\begin{aligned} \min_U \ & U^T \begin{bmatrix} \rho_h I & 0 \\ 0 & \rho_r I \end{bmatrix} U \\ \text{subject to:} \quad & |U| \leq \begin{bmatrix} A_{max} \\ R_{max} \end{bmatrix} \\ & |GU| \leq S_{max} \\ & CU = [0 \quad 0 \quad 0 \quad L \quad 0 \quad 0]^T \end{aligned} \tag{6.1}$$

where A_{max}, R_{max} and S_{max} are constant vectors with length N. The terminal constraint matrix C is given by

$$C = \begin{bmatrix} g_1^h(Nh) & \dots & g_1^h(h) & g_1^r(Nh) & \dots & g_1^r(h) \\ g_2^h(Nh) & \dots & g_2^h(h) & g_2^r(Nh) & \dots & g_2^r(h) \\ g_3^h(Nh) & \dots & g_3^h(h) & 0 & \dots & 0 \\ g_4^h(Nh) & \dots & g_4^h(h) & 0 & \dots & 0 \\ 0 & \dots & 0 & g_5^r(Nh) & \dots & g_5^r(h) \\ 0 & \dots & 0 & g_6^r(Nh) & \dots & g_6^r(h) \end{bmatrix}$$

where g_i^h is the pulse response from the horizontal acceleration to state i and g_i^r the corresponding response from rotational acceleration.

This is a standard quadratic programming problem that can be solved numerically using any of the numerous solvers available. If the inequality constraints are removed it is also easy to solve analytically.

Numerical solution

A numerical solution for the quadratic program in (6.1) is obtained using the `quadprog` function in Matlab. The problem is solved for different values of ρ_h, s_{max} and b_2 in (3.40) with $\rho_r = 1$. The movement time is $T = 0.5$ s, the movement distance is $L = 0.1$ m and the theoretical model parameters $\omega = 21.0$ rad/s and $\zeta = 0$ are used. The results are shown in the figures 6.1, 6.2 and 6.3.

In Figure 6.1 the rotational acceleration does not excite the oscillation, $b_2 = 0$, and the problem is solved for $s_{max} = [0.012, 0.008, 0.004]$ m and $\rho_h = [1, 10^2, 10^4]$. The figure shows that when $s_{max} = 0.0012$ no tilting of the container is necessary to satisfy the constraints. When $\rho_h = 1$ the surface elevation is minimized using the horizontal acceleration only. The container is only tilted for $s_{max} = 0.004$ m when the surface elevation cannot be reduced using the horizontal acceleration. This gives a horizontal acceleration that is close to the minimum time acceleration references

derived in Section 4.4. As ρ_h is increased more tilting action is used to reduce the surface elevation. When $\rho_h = 10^4$ the horizontal acceleration is almost equal for all values of s_{max}. When $s_{max} = 0.012$ m the surface elevation constraint is not active and the solution is the pure minimum energy solution.

Figure 6.2 shows the numerical solution for $b_2 = 25 \cdot 10^{-6}\omega$ which corresponds to a rotational axis positioned 4 cm below the surface, see Table 3.3. The behavior is similar as for $b_2 = 0$ except that when $\rho_h = 10^4$ the rotational acceleration is used to control the surface elevation and not only tilting the container to counteract the oscillation. This results in that the surface elevation constraint is active also for $s_{max} = 0.012$ m.

The numerical solution when $b_2 = -25 \cdot 10^{-6}\omega$ is shown in Figure 6.3, this corresponds to a rotational axis positioned 2 cm below the surface. The solution is similar as for the previous cases except when $\rho_h = 10^4$. For $\rho_h = 10^4$ the surface elevation is controlled using mostly the rotational acceleration which results in that the surface elevation constraint is inactive for $s_{max} = 0.012$ m and $s_{max} = 0.008$ m.

The numerical solutions show that the balancing between horizontal and rotational acceleration in the cost function is very important. If the cost for horizontal acceleration is too small the horizontal acceleration reference will tend to the minimum time acceleration reference before any tilting action is invoked as s_{max} is decreased. A suitable choice of ρ_h seems to be between 10^2 and 10^4. The numerical solutions also show that the solutions for $\rho_h = 1$ and 10^2 are very similar for all values of b_2.

The resulting maximum tilting angle for $s_{max} = 0.004$ m are 6.9° with $\rho_h = 1$, 8.2° with $\rho_h = 10^2$ and 11.7° with $\rho_h = 10^4$ when $b_2 = 0$. The maximum tilting angle is slightly smaller for $b_2 = 25 \cdot 10^{-6}\omega$ and slightly larger for $b_2 = -25 \cdot 10^{-6}\omega$.

As a comparison the minimum movement time when the container is not tilted is also calculated. With $s_{max} = 0.008$ m the minimum movement time is 0.47 s and the smallest movement time when the surface elevation constraint is inactive is 0.58 s. With $s_{max} = 0.004$ m the corresponding movement times are 0.64 s and 0.89 s. The smallest movement time when the surface elevation constraint is inactive is interesting because the resulting horizontal acceleration reference has proved to work well in practice. This shows that the movement time can be reduced considerable if s_{max} is small by tilting the container.

Experimental evaluation

The experimental evaluation is performed in the experimental setup presented in Chapter 2 using a container with a width of 7 cm and a liquid depth of 20 cm. The movement time is 0.5 s and the movement distance is 0.1 m. The experiments are performed with three different vertical po-

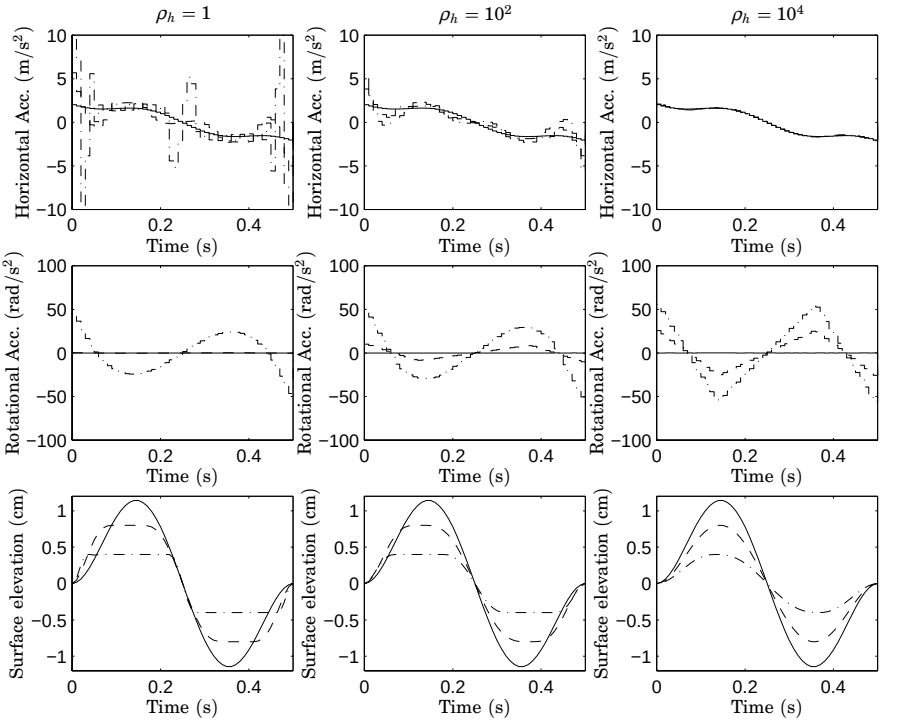

Figure 6.1 The numerical solution to (6.1) and simulated surface elevation with $\rho_r = 1$, $b_2 = 0$ and ρ_h as given in the figure. The problem is solved for $s_{max} = 0.012$ m (solid), $s_{max} = 0.008$ m (dashed) and $s_{max} = 0.004$ m (dash dotted). For $\rho_h = 1$ the horizontal acceleration tends to the minimum time acceleration reference as s_{max} is decreased. When ρ_h is increased more tilting action is used and the horizontal acceleration becomes smoother as well as the simulated surface elevation.

sitions of the rotational axis, $y_r = [-2, -3, -4]$ cm which corresponds to approximately $b_2/\omega = [-25 \cdot 10^{-6}, 0, 25 \cdot 10^{-6}]$. The oscillation frequency in the model is modified to $\omega = 20.5$ rad/s and the damping is set to $\zeta = 0.01$ to reduce the amount of residual slosh in the same way as in Section 4.7.

Experiments are performed for the same values of ρ_h, ρ_r and s_{max} as in the numerical solutions in the previous section. Each movement is performed twice, one forwards and one backwards, to obtain measurements of the surface elevation on both sides of the container. The results of the experiments are shown in the figures 6.4, 6.5 and 6.6.

Figure 6.4 shows the experimental results when $y_r = -3$ cm and $b_2 = 0$. The figure shows that the resulting maximum surface elevation

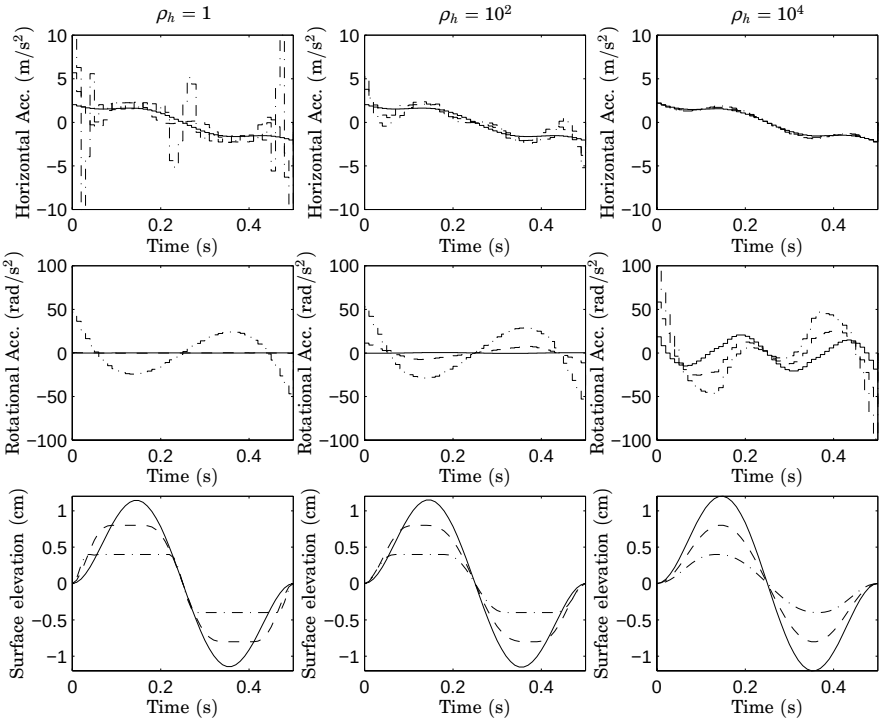

Figure 6.2 Same as Figure 6.1 but with $b_2 = 25 \cdot 10^{-6}\omega$. Compared to Figure 6.1 the rotational acceleration is also used to control the surface elevation when $\rho_h = 10^4$ and the rotational acceleration becomes less smooth and the container is also tilted when $s_{max} = 0.012$ m.

decreases as s_{max} is decreased except when $\rho_h = 1$. The poor performance with $\rho_h = 1$ was expected since the horizontal acceleration reference tends to the minimum time acceleration reference as s_{max} decreases. The minimum time acceleration reference only works for very small maximum amplitudes of the inputs as shown in Section 4.4. When $\rho_h = 1$ and $s_{max} = 0.004$ m liquid splashed out of the container.

For $\rho_h = 10^2$ and $\rho_h = 10^4$ the performance is similar but the maximum surface elevation is slightly smaller for $\rho_h = 10^4$. The residual slosh increases slightly as s_{max} is decreased due to the increased tilting action. Compare the experimental data with the simulations from the numerical solution shown in Figure 6.1.

In Figure 6.5 the experiments with $y_r = -4$ cm and $b_2 = 25 \cdot 10^{-6}\omega$ and in Figure 6.6 the experiments with $y_r = -2$ and $b_2 = -25 \cdot 10^{-6}\omega$ are

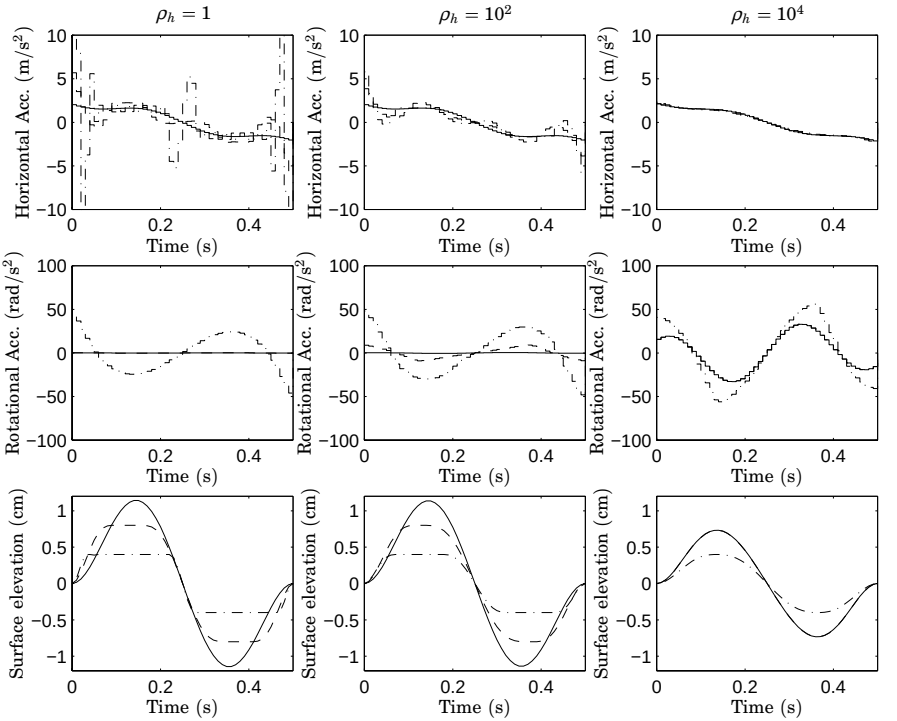

Figure 6.3 Same as Figure 6.1 but with $b_2 = -25 \cdot 10^{-6}\omega$. Compared to Figure 6.1 the rotational acceleration is also used to control the surface elevation when $\rho_h = 10^4$. Since b_2 is negative the rotational acceleration also counteracts the oscillation and the solution for $s_{max} = 0.012$ and 0.008 is equal.

shown. The figures show similar results as for $y_r = -3$ cm and $b_2 = 0$ shown in Figure 6.4.

In the same way as in Section 4.7 the parameters in the model are modified to increase the performance. The performance is measured using the residual slosh defined in Definition 4.2 and the maximum surface elevation relative to the container wall. The parameters $\omega = 20.5$ rad/s and $\zeta = 0.01$ are fixed and the gain from rotational acceleration to surface oscillation b_2 is varied. Only measurements on the backward side of the container are used. The movement time is 0.5 s, the movement distance is 0.1 m, the maximum allowed surface elevation is $s_{max} = 0.004$ m and the cost parameters are $\rho_h = 10^4$ and $\rho_r = 1$. The experiments are performed for three different vertical positions of the rotational axis, $y_r = [-2, -3, -4]$ cm.

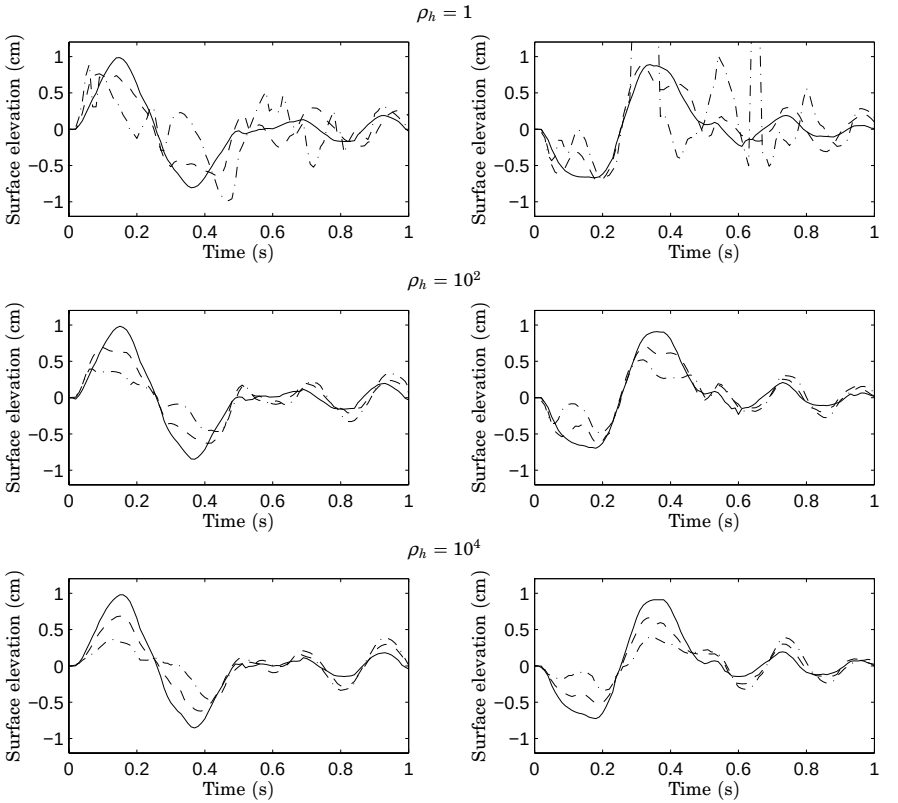

Figure 6.4 Experimental results for acceleration references from the solution of (6.1) with $y_r = -3$ cm, $b_2 = 0$, $\rho_r = 1$ and ρ_h as indicated in the figure. Both the surface elevation on the backward (left) and on the forward side (right) are shown. Experiments are made for $s_{max} = 0.012$ m (solid), $s_{max} = 0.008$ m (dashed) and $s_{max} = 0.004$ m (dash dotted). The experiments show that the performance is very poor when $\rho_h = 1$ and s_{max}=0.004 and that the surface elevation becomes smoother as ρ_h is increased. It can also be seen that the residual slosh increases slightly as more tilting action is invoked.

Figure 6.7 shows the performance measure R, see Definition 4.2, and the maximum measured surface elevation relative to the container. The figure shows that the minimizing b_2 depends on the vertical position of the rotational axis. The minimum of R and the maximum measured surface elevation occur for the same value of b_2 for each position of the rotational axis. With $y_r = -2$ cm, $b_2 = -40 \cdot 10^{-6}\omega$ gives the minimum R and the minimum maximum measured surface elevation, with $y_r = -3$ cm

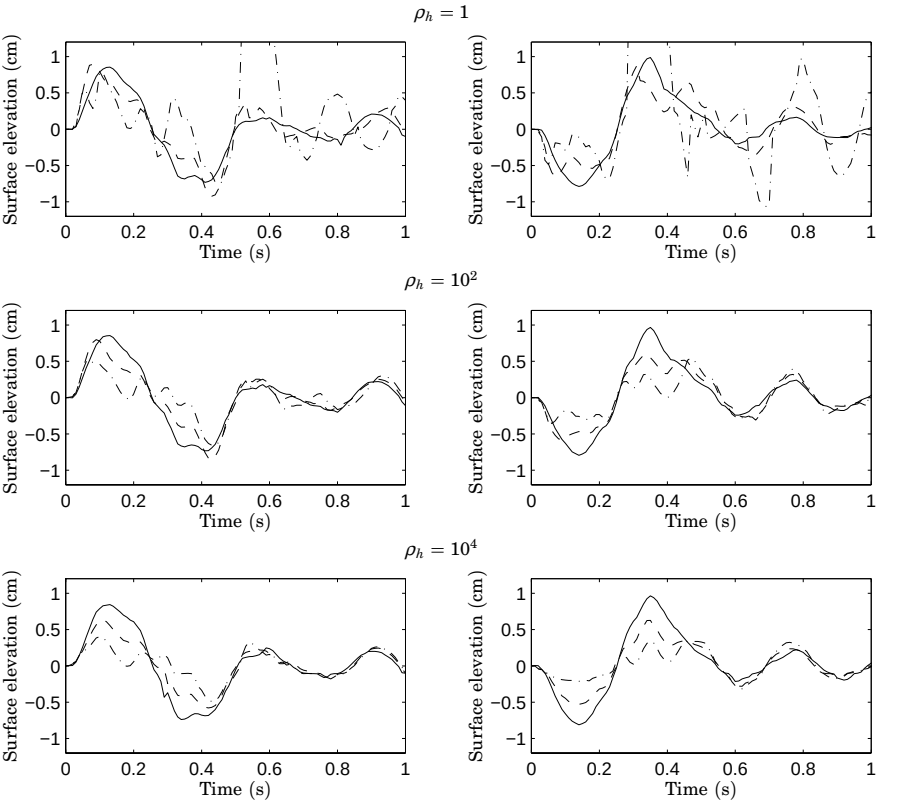

Figure 6.5 Same as Figure 6.4 but with $y_r = -4$ cm and $b_2 = 25 \cdot 10^{-6}\omega$.

$b_2 = -5 \cdot 10^{-6}\omega$ is obtained and for $y_r = -4$ cm, $b_2 = 25 \cdot 10^{-6}\omega$ is the minimizer.

This shows that the performance can be increased by finding the right value of b_2. Another way to increase the performance is to use iterative learning control. Both methods presented in Chapter 5 can easily be modified to find both horizontal and rotational acceleration references.

6.3 Conclusions

In this chapter methods to reduce the surface elevation relative to the container wall using rotation of the container has been explored. Two methods were presented: one based on direct calculation of the tilt angle

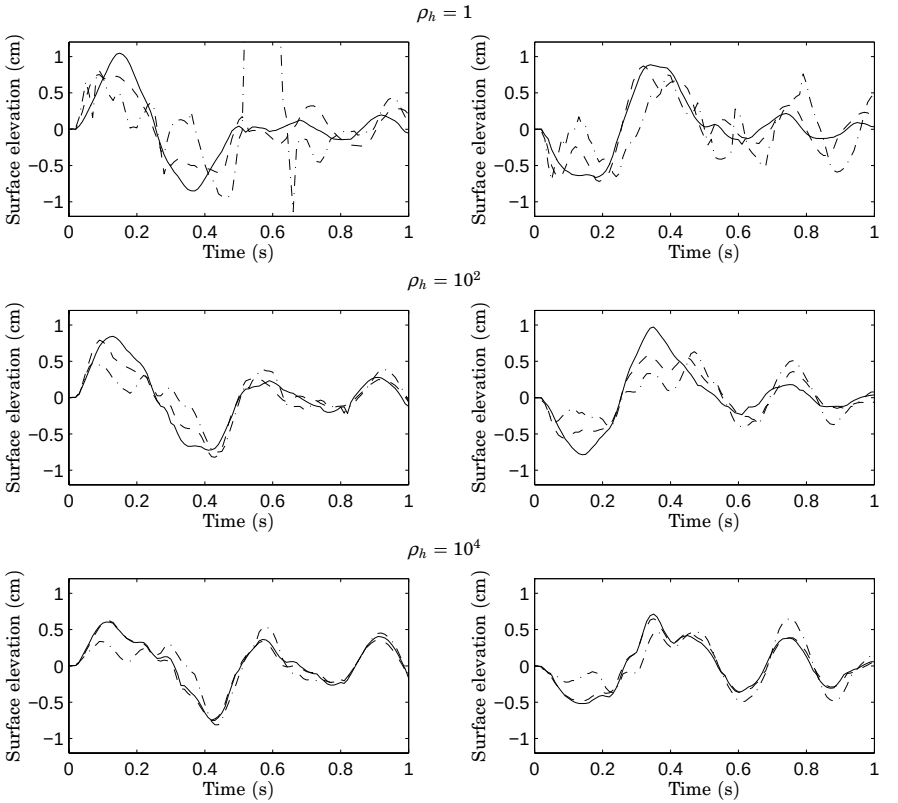

Figure 6.6 Same as Figure 6.4 but with $y_r = -2$ cm and $b_2 = -25 \cdot 10^{-6}\omega$.

to counteract the surface oscillation and one based on optimal control and the model 3.40 presented in Section 3.5 that simultaneously synthesizes the horizontal and rotational acceleration reference.

In Section 6.1 a method to directly calculate the rotational acceleration reference given an horizontal acceleration reference is presented. The method is very simple but can only be used if the rotational acceleration does not cause any surface oscillation.

Section 6.2 presents a method using optimal control and a linearization of the simple model in (3.40) that simultaneously gives the horizontal and rotational acceleration reference. The optimal control problem is a minimum energy problem with a maximum allowed amplitude of the acceleration references and the surface elevation relative to the container wall. The optimal control problem is discretized using zero-order-hold of

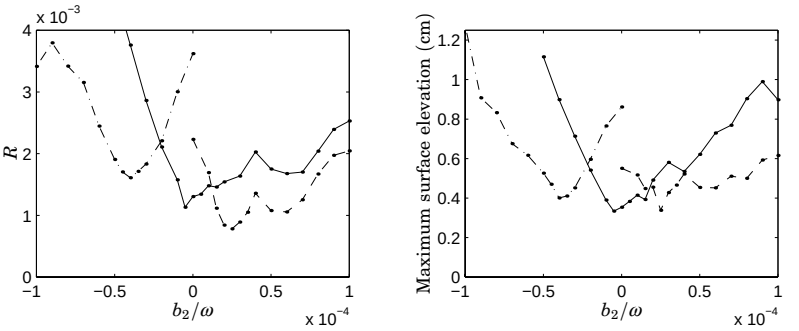

Figure 6.7 The performance measure R in Definition 4.2 and the maximum measured surface elevation for different values of b_2/ω for $y_r = -2$ cm (dash dotted), $y_r = -3$ cm (solid) and $y_r = -4$ cm (dashed). The minimizing b_2/ω is different for the the different values of y_r. The value b_2/ω which minimizes R and the maximum measured surface elevation respectively coincides for each value of y_r.

the acceleration references and formulated as a quadratic program.

The problem was solved numerically for different values of the cost for horizontal acceleration, maximum allowed surface elevation and the different values of the gain from rotational acceleration to surface oscillation which corresponds to different positions of the rotational axis. The numerical solution showed that the balancing of the cost for horizontal and rotational acceleration is very important. If the cost for horizontal acceleration is too small compared to the cost for rotational acceleration then the horizontal acceleration reference will tend to the minimum time acceleration reference as the maximum allowed surface elevation is decreased and the container will only be tilted if the surface elevation cannot be reduced any further using the horizontal acceleration.

Evaluation of the proposed method in the experimental setup showed that the method works well when the cost for horizontal acceleration is large. This was expected since the horizontal acceleration tend to the minimum time acceleration when the maximum allowed surface elevation is decreased which only work for small values of the maximum acceleration as showed in Section 4.4.

Experience from other experiments not presented here have also shown that if the maximum surface elevation is too large, about 2.5 cm, without tilting. Then the model in (3.40) is not valid and the rotation if applied will only cause more oscillation. Therefore this method is only applicable if the maximum allowed surface elevation is small, about 0.5 cm in the cases studied here.

7

Concluding remarks

In this thesis an industrially relevant problem has been described where an open container with liquid should be moved without excessive slosh. The major constraint is to keep the slosh below a certain level during the movement. The problem has been solved by first deriving a simplified mathematical model of the slosh phenomenon and then applying optimal control techniques and iterative learning control to determine the appropriate acceleration reference.

This chapter contains a summary of the conclusions given in previous chapters in Section 7.1. Section 7.2 describes how the work presented in this thesis has been applied in industry. Possible extensions and continuation of this work is presented in Section 7.3.

7.1 Conclusions

The slosh measurement problem is discussed in Chapter 2 and several different methods are evaluated. The evaluations show that the slosh measurement problem is not easy. The only measurement methods that work satisfactorily are the infrared displacement sensor and the computer vision based system. The computer vision based system does not give an online measurement of the surface in this configuration. But this is no restriction here since the measurement is only used for performance evaluation and not for direct feedback.

In Chapter 3 it is shown that it is possible to derive a linear model for the surface elevation above one point using fluid dynamics. In the derivation it is assumed that the surface elevation is small and that the surface is moving slowly. It is also assumed that the liquid is inviscid, incompressible and that the flow is irrotational. The resulting model consists of an infinite number of oscillators with increasing oscillating frequencies and decreasing gains. The slosh phenomenon is examined in experiments

showing that it exhibits two nonlinear phenomena: amplitude dependent oscillation frequency and asymmetric oscillation. The experiments also show that the slosh can be modeled by a second order linear system when the oscillation amplitude is small both when the container is accelerated horizontally and rotationally. The chapter is concluded by presenting a simple second order linear model that can easily be used when solving optimal control problems.

Methods for calculation of horizontal acceleration references are presented in Chapter 4. The methods are based on optimal control and use the simple linear model presented in Section 3.5 to describe the slosh. Both minimum time and minimum energy problems are studied and solved both numerically and analytically. Experimental evaluation of the resulting acceleration references shows that the minimum time references work well only for long movement times with a small maximum surface elevation and small maximum acceleration. The minimum energy acceleration references proved to work well for fast movements if the model parameters were modified to compensate for the amplitude dependent oscillation frequency. This shows that the simple linear model can be used if the surface oscillation is small when solving a minimum time problem or if the control is cautious as when solving a minimum energy problem. The acceleration references calculated are all functions in continuous time which need to be discretized to enable implementation. A simple method for discretization of acceleration references that conserves the motion constraints was presented. Direct calculation of a discrete time acceleration reference was made by solving a discrete time minimum energy problem using quadratic programming.

Two methods based on Iterative Learning Control (ILC) were presented in Chapter 5. The learning signal in both methods is the horizontal acceleration reference. This makes it hard to use the traditional formulation of ILC which uses time invariant linear filters to calculate the new control since there are constraints on the terminal velocity and terminal position. Both methods use the simple linear model of the system to predict the output in the next iteration based on the obtained data.

The first method called Constrained Iterative Learning Control (CILC) formulates the learning algorithm as a quadratic optimization problem with two equality constraints, the terminal position and velocity, that minimizes the control error and the control signal. The optimization problem was solved analytically and the resulting update law is structured similarly as for traditional ILC but the linear filters are time varying. The method tries to make the surface elevation follow a reference calculated using a model of the slosh. If there are modeling errors then the reference will be non-optimal and even infeasible.

To avoid the problem with infeasible references another method called

Iterative Optimal Control (IOC) was derived. The IOC method solves the discrete time minimum energy problem using experimental data in an iterative manner. The algorithm consists of a quadratic program that minimizes the control signal and the residual slosh on both sides of the container subject to constraints on the maximum control, maximum surface elevation, terminal velocity and terminal position. The inequality constraints on the control signal and surface elevation were removed and the quadratic program was solved analytically which resulted in an update law that consisted of three time varying linear filters similarly as the CILC algorithm.

Both algorithms were analyzed for the case when the process is described by a linear system. The eigenvalues of the iterative process were calculated numerically for different parameter values of the process model showing that the robustness is larger when the control cost is high and that the CILC algorithm is more robust than the IOC algorithm to parameter mismatch. Numerical calculation of the stationary solutions of the iteration process shows that the control error and residual slosh decrease as the control cost is decreased but with the CILC algorithm the control signal exhibits chattering if the control cost is too small. The noise variance in the output and in the control signal was calculated numerically showing that the control signal variance becomes very large if the control cost is small using the CILC algorithm and that the output variance decreases as the control cost decreases. Both methods were evaluated using simulations with both a linear and a nonlinear process model with measurement noise. The simulations show that both methods are successful but the weighting matrices in the CILC algorithm needed to be modified to handle the infeasibility of the reference with the nonlinear process model. The experimental evaluation showed that both algorithms are successful in reality.

The possibility to reduce the maximum surface elevation at the wall of the container by tilting of the container was explored in Chapter 6. It is shown how the tilt angle and corresponding rotational acceleration can be calculated directly for any horizontal acceleration reference if it is assumed that the rotation does not cause any surface oscillation. To handle the case when the rotation causes surface oscillation a discrete time minimum energy problem was solved using quadratic programming that simultaneously calculates the horizontal and rotational acceleration satisfying the constraints. The quadratic program was solved numerically which showed that the balancing of the cost between the horizontal and the rotational acceleration is very important. If the cost for rotation is too large then the container will only be tilted when the surface elevation cannot be further minimized by the horizontal acceleration. This leads to a horizontal acceleration that is close to the minimum time acceleration.

Experimental evaluation of the method for different positions of the rotational axis showed that the method works well if the maximum allowed surface elevation is small and the horizontal acceleration is smooth and not too large. Compared to movement without tilting the movement times can be decreased about 20% for the same maximum surface elevation.

The main conclusion is that it is possible to find open-loop acceleration references for movement of the packages using a very simple model of the slosh phenomenon and optimal control. The robustness to modeling errors is achieved by minimizing the control effort and either tuning of the model parameters or iterative learning control.

More detailed conclusions can be found in the summary of each chapter given in the sections 3.5, 4.10, 5.8 and 6.3.

7.2 Industrial application

The calculations of the minimum energy acceleration reference have been implemented in an Excel spreadsheet to enable easy use by the development engineers at Tetra Pak Research & Development AB.

The method has mainly been used in the development phase of new machines, where it has proven to be very useful and given the development engineers a tool to accurately predict the movement times given a certain configuration without extensive testing. This has simplified the development and enabled evaluation of several different machine configurations during the development. This has made it possible to include the control design in the machine design which enables further optimization of the machine with respect to production cost and production rate.

The movement time in one existing machine has also been decreased by 7.4% using the minimum energy acceleration reference and increased the range of possible filling times. The minimum energy method has also been used to show that the movement time cannot be decreased any further in another machine.

7.3 Future work

There are many possible future extensions of this work both theoretically and practically.

The main theoretical extension is to refine the slosh model such that it captures some of the most important nonlinear behavior encountered in the experiments. With a more elaborate model it might be possible to calculate acceleration references that work without adjusting the model

parameters. It is also possible that the solution of the minimum time problem with a better model gives acceleration references that work for larger maximum slosh. Using a better model of the slosh it is also possible to analyze the properties of the iterative methods in a more realistic setting.

It would also be interesting to evaluate the developed strategies in practice with different package geometries, different liquids and when the motion is along a curved path. The iterative methods can also be applied to the case when the container is tilted. Further exploration on the use of tilting is needed to for instance determine the optimal horizontal position of the rotational axis. It is also of interest to design simple experiments that can be used to estimate the model parameters of the simple linear model for different oscillation amplitudes.

8

Bibliography

Armenio, V. (1992): *Dynamic behavior of free surface liquids on ships*. PhD thesis, Department of Naval Architecture, Ocean and Environmental Engineering, University of Trieste, Trieste, Italy.

Armenio, V. and M. La Rocca (1996): "On the analysis of sloshing of water in rectangular containers: Numerical study and experimental validation." *Ocean Engineering*, **23:8**, pp. 705–739.

Baldock, G. R. and T. Bridgeman (1981): *The Mathematical Theory of Wave Motion*. Ellis Horwood Limited.

Bien, Z. and J.-X. Xu (1998): *Iterative learning Control: Analysis, Design, Integration and Applications*. Kluwer Academic Publishers.

Bryson, A. E. (1994): *Control of Spacecraft and Aircraft*. Princeton University Press.

Bryson, A. E. and Y. Ho (1975): *Applied Optimal Control: Optimization, Estimation and Control*. Hemisphere Publishing Corporation, New York. Revised Printing.

Coulson, C. A. (1955): *Waves*, 7 edition. University Mathematical Texts. Interscience Publishers.

Crawley, E. F., R. J. Hansen, and L. D. Peterson (1989): "Nonlinear fluid slosh coupled to the dynamics of a spacecraft." *AIAA Journal*, **27:9**, pp. 1230–1240.

Dietze, S. and F. J. Schmidt (1997): "Entwurf zur optimalsteuerung offener behälter zum förden von fluiden in verarbeitungsmaschinen." Technical Report MATH-NM-13-1997. Technische Universität Dresden, Dresden, Germany.

Dubois, F., N. Petit, and P. Rouchon (1999): "Motion planning and nonlinear simulations for a tank containing a fluid." In *Proceedings of the 1999 European Control Conference*. Karlsruhe, Germany.

Feddema, J. T., C. R. Dohrmann, G. G. Parker, R. D. Robinett, V. J. Romero, and D. J. Schmitt (1997): "Control for slosh-free motion of an open container." *IEEE Control Systems*, **17:1**, pp. 29–36.

Frueh, J. A. and M. Q. Phan (1998): "Linear optimal learning control (LQL)." In *Proceedings of the 37th IEEE Conference on Decision and Control*. Tampa, Florida USA.

Graham, E. W. and A. M. Rodriguez (1952): "Characteristics of fuel motion which affect airplane dynamics." *Applied Mechanics*, **19**, pp. 381–388.

Grundelius, M. (1998): *Motion Control of Open Containers with Slosh Constraints*. Lic Tech thesis ISRN LUTFD2/TFRT--3222--SE, Department of Automatic Control, Lund Institute of Technology, Lund, Sweden.

Grundelius, M. (2000): "Iterative optimal control of liquid slosh in an industrial packaging machine." In *Proceedings of the 39th IEEE Conference on Decision and Control*. Sydney, Australia.

Grundelius, M. and B. Bernhardsson (1999a): "Control of liquid slosh in an industrial packaging machine." In *Proceedings of the 1999 IEEE International Conference on Control Applications and IEEE International Symposium on Computer Aided Control System Design*. Kohala Coast, Hawaii.

Grundelius, M. and B. Bernhardsson (1999b): "Motion control of open containers with slosh constraints." In *Proceedings of the 14th IFAC World Congress*. Beijing, P.R. China.

Grundelius, M. and B. Bernhardsson (2000): "Constrained iterative learning control of liquid slosh in an industrial packaging machine." In *Proceedings of the 39th IEEE Conference on Decision and Control*. Sydney, Australia.

Gunnarsson, S. and M. Norrlöf (1999): "Some aspects of an optimization approach to iterative learning control." In *Proceeedings of the 38th IEEE Conference on Decision and Control*. Phoenix, Arizona USA.

Gustafsson, T. (1995): "Modelling and control of a rotary crane." In *Proceedings of the 3rd European Control Conference*. Rome, Italy.

Kelkar, K. M. and S. V. Patankar (1997): "Numerical method for the prediction of free surface flows in domains with moving boundaries." *Numerical Heat Transfer, Part B: Fundamentals*, **31:1**, pp. 387–399.

Lamb, H. (1945): *Hydrodynamics*, 6 edition. Dover Publications.

Lannegren, H. (1999): "Motion control with slosh suppression." Master thesis ISRN LUTFD2/TFRT--5634--SE. Department of Automatic Control, Lund Institute of Technology, Lund, Sweden.

Lee, H., S. Cho, and J. Cho (1997): "A new anti-swing control of overhead cranes." In *Proceedings of the IFAC International Workshop on Automation in the Steel Industry*. Kyongju, Korea.

Miles, J. W. (1976): "Nonlinear surface waves in closed basins." *Fluid Mechanics*, **75**, pp. 419–448.

Moore, K. L. (1993): *Iterative Learning Control for Deterministic Systems*. Springer Verlag.

Mårtensson, K. (1972): *New Approaches to the Numerical Solution of Optimal Control Problems*. PhD thesis, Department of Automatic Control, Lund Institute of Technology, Lund, Sweden.

Roberts, P. D. (1993): "An algorithm for optimal control of nonlinear systems with model-reality differences." In *Proceedings of the 12th IFAC World Congress*. Sydney, Australia.

Romero, V. J. and M. S. Ingber (1995): "A numerical model for 2-D sloshing of pseudo-viscous liquids in horizontally accelerated rectangular containers." In Brebbia *et al.*, Eds., *Boundary Elements XVII*, pp. 567–583. Computational Mechanics Publications, Southampton, England.

Sankar, S., R. Ranganathan, and S. Rakheya (1992): "Impact of dynamic fluid slosh loads on the directional response of tank vehicles." *Vehicle System Dynamics*, **21:6**, pp. 385–404.

Schwartz, A. L. and E. Polak (1996): *RIOTS: A Matlab Toolbox for Solving Optimal Control Problems Version 1.0*. University of California Berkeley, Berkeley, California.

Shen, S. S. (1993): *A Course on Nonlinear Waves*. Kluwer Academic Publishers.

Venugopal, R. and D. S. Bernstein (1996): "State space modeling and active control of slosh." In *Proceedings of the 1996 IEEE International Conference on Control Applications*, pp. 1072–1077. Dearborn, Michigan.

Yano, K., S. Higashikawa, and K. Terashima (1999): "Active liquid container transfer for complete sloshing-suppression." In *Proceedings of the 1999 European Control Conference*. Karlsruhe, Germany.

Yano, K., T. Yoshida, M.Hamaguchi, and K. Terashima (1996): “Liquid container transfer considering the suppression of sloshing for the change of liquid level.” In *Proceedings of the 13th IFAC World Congress*. San Francisco, California.

Young, N. (1988): *An introduction to Hilbert space*. Cambridge University Press.